Injectable Degradable Composite Materials for Bone Repair and Drug Delivery

Xin Zhao

under supervision of

Dr. Anne Young, Prof. Irwin Olsen and Dr. Vehid Salih

Submitted for the award of Doctor of Phylosophy in Biomaterials and Tissue Engineering at Eastman Dental Institute, University College London.

Declaration

I herewith declare that I autonomously carried out the PhD-thesis entitled “Injectable Degradable Composite Materials for Bone Repair and Drug Delivery”.

The following third party assistance has been enlisted:

1 Nuclear magnetic resonance (NMR) spectra were collected with assistance of Dr Geoff Kelly at the NMR Centre of National Institute for Medical Research.

2 X-ray diffraction spectra were collected with assistance of Prof. Jonathan Knowles at the Eastman Dental Institute, University College London (UCL).

3 Chick embryo chorioallantoic membrane assay was performed with assistance of Dr Paul Buxton at the Eastman Dental Institute, UCL.

4 Statistical evaluations were performed with assistance of Ms Aviva Petrie at the Eastman Dental Institute, UCL.

The thesis has not been submitted elsewhere for an exam, as thesis or for evaluation in a similar context.

I hereby affirm the above statements to be complete and true to the best of my knowledge.

Acknowledgement

First of all, my sincere gratitude goes to my superior, Dr. Anne Young, for her support, patience and tolerance over the past four years. Her energy and enthusiasm in research has motivated all her students, including myself. As a result, research life has been smooth and rewarding for me.

I was delighted to interact with Prof. Irwin Olsen and to have him as my co-supervisor. He sets an example of a world-class researcher for his rigor and passion on research. Input and advice in cell biology from Dr. Vehid Salih, my co-supervisor, is also much appreciated.

I would like to thank Dr. Jonathan Pratten as my postgraduate tutor, Prof. Jonathan Knowles for his assistance with X-ray diffraction analysis, Dr. Geoff Kelly for the NMR analysis, Dr. Paul Buxton for the chick embryo chorioallantoic membrane assay and Ms Aviva Petrie for the statistical evaluation.

My deepest gratitude goes to my family for their unflagging love and support throughout my life; this dissertation would simply have been impossible without them.

I would also like to thank Prof. Robert Schroter for his constant encouragement throughout my graduate study.

Last but not least, special thank goes to the Engineering and Physical Sciences Research Council for granting me the Dorothy Hodgkins Postgraduate Award. Without this support, my ambition to undertake a PhD study within a top university in the world could not have been realised.

Abstract

The aim of this project was to develop injectable materials to repair damaged bone and, to simultaneously release antibacterial drugs and genes in a controllable manner. Fluid poly (propylene glycol -*co*- lactide) dimethacrylate (PGLA-DMA) was first synthesised and then filled with varying levels of β-tricalcium phosphate (β-TCP) and monocalcium phosphate monohydrate (MCPM) to fabricate composite materials.

For all formulations (including polymer and composites), full methacrylate conversion was found to occur within 200 s of exposure to blue light. The initial dry polymer modulus was enhanced three-fold by increasing total filler content to 70%. After composite immersion in water, β-TCP and MCPM was found to react and re-precipitate within the set materials as dicalcium phosphate (DCP, i.e. brushite and monetite). At higher MCPM levels there was an increase in DCP formation, composite degradation rate, release of both calcium and phosphate ions and buffering of acidic polymer degradation products. Additionally, bone-like MG-63 cells were found to attach, spread and proliferate on both the polymer and the composite surfaces and, composites implanted into chick embryo femurs demonstrated close apposition to the host tissue.

To examine the potential value for drug delivery, both the polymer and the composites were prepared containing 10% of the antibacterial chlorhexidine (CHX). The drug was found to be released from material via diffusion, which increased along with antibacterial activity when the filler content was raised.

PGLA-DMA polymer was additionally prepared containing complexes of the commercial cationic lipid Metafectene^{TM} Pro and green fluorescent protein plasmid DNA. Initial studies demonstrated that the components released from the materials were capable of gene transfection into human bone-forming mesenchymal stem cells *in vitro*.

These studies thus demonstrate that the injectable, rapidly settable PGLA-DMA materials produced here might have clinical potential as both bone adhesives and drug delivery devices.

TABLE OF CONTENTS

LIST OF TABLES

CHAPTER 1

CHAPTER 2

CHAPTER 3

CHAPTER 4

CHAPTER 5

LIST OF FIGS.

CHAPTER 1

CHAPTER 2

CHAPTER 3

CHAPTER 5

Chapter 1

Background Review

Abbreviations

In alphabetical order

BMP	bone morphogenetic protein
CDHA	calcium-deficient hydroxyapatite
CHX	chlorhexidine
CPC	calcium phosphate cement
GAM	gene activated matrix
GFP	green fluorescent protein
HA	hydroxyapatite
hMSC	human mesenchymal stem cell
LA	lactide
MA	methacrylate
MCPM	monocalcium phosphate monohydrate
MSC	mesenchymal stem cell
PAH	polyanhydride
PEG	poly(ethylene glycol)
PGLA-DMA	poly(propylene glycol -*co*- lactide) dimethacrylate
PMMA	polymethylmethacrylate
POE	polyorthoester
PPF	poly(propylene fumarate)
PPG	poly(propylene glycol)
PPP	polyphosphazene
TCP	tricalcium phosphate
TTCP	tetracalcium phosphate

The background review first gives a brief introduction in bone structure and fracture healing. In addition, a general review and description of bone-repair materials and drug delivery is presented. Lastly, the aims and objectives of this project are discussed.

1.1. Bone

Bone performs several key functions within the body, including provision of structural support, protection for many organs and metabolism of minerals such as calcium. In addition, it protects the bone marrow which is the primary site for the synthesis of blood cells.

1.1.1. Bone structure and composition

Bone is covered by a connective tissue membrane called the periosteum. Bone itself consists of a smooth, dense, and continuous external layer called compact or cortical bone, composing cylindrical units called osteons (Haversian systems) (Fig. 1.1) (Silver 2006;Olszta *et al*. 2007). Each osteon is composed of concentric lamellae (layers) of hard, calcified matrix. Osteocytes (bone cells) are lodged in lacunae (spaces) between the lamellae. By cellular extensions, these bone cells are connected to each other and to the central canal (containing blood vessels and nerves). Compact bone facilitates bone's main functions: to support the body, to protect organs, and to store and release chemical elements such as calcium and phosphorous (Silver 2006;Olszta *et al*.2007). The interior layer of bone, a network of interlocking plates and spicules, is called spongy or trabecular bone. Like osteons, trabeculae also have osteocytes in lacunae that lie

between calcified lamellae. The enclosing cavities or the hollow centre of a bone shaft are filled with blood vessels and marrow. Spongy bone protects the marrow (Silver 2006; Olszta *et al.* 2007).

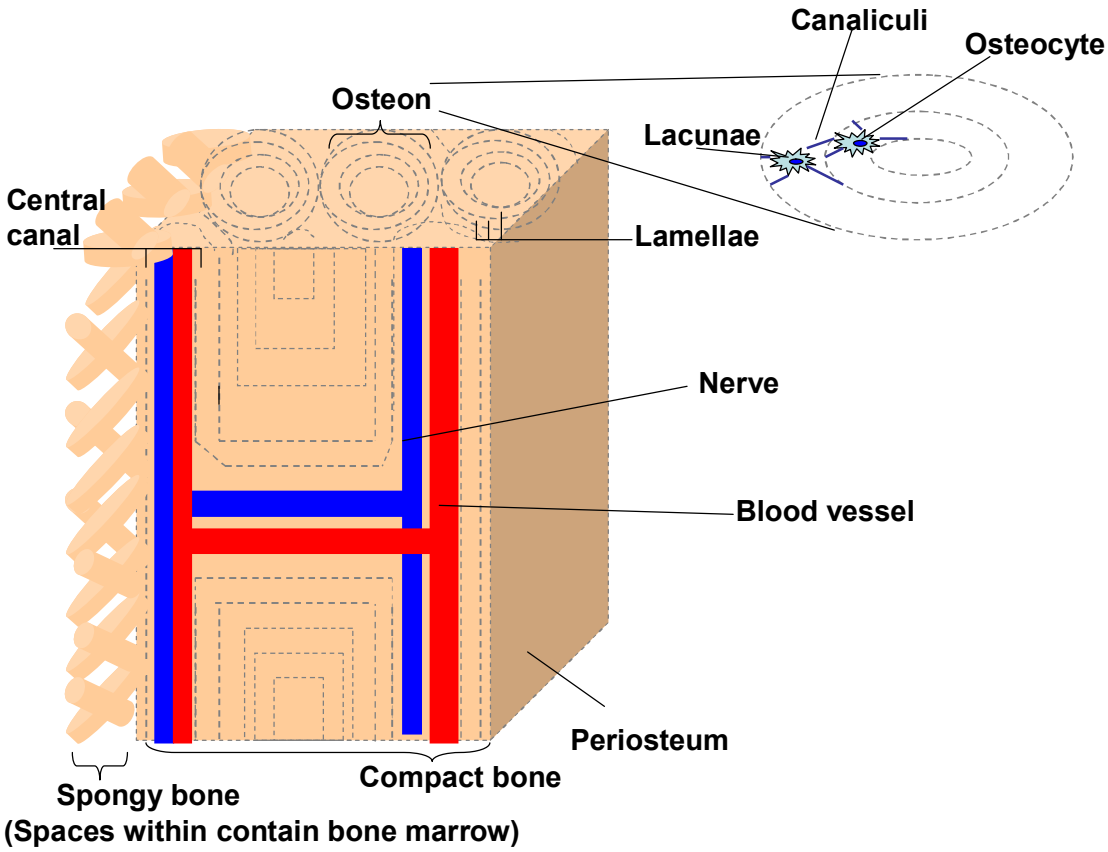

Fig. 1.1. Microscopic organisation of compact and spongy bone.

Bone is a natural composite material. Around 30% of bone is composed of organic compounds including collagen type I fibres (approximately 95%), proteoglycans and numerous non-collagenous proteins (5%). 70% of bone is made up of the inorganic mineral hydroxyapatite (HA). The organic matrix, when calcified (strengthened by deposits of HA crystals), embeds osteocytes (osteoblasts and osteoclasts) which participate in the maintenance and organisation of bone (Olszta *et al.* 2007;Taton 2001).

1.1.2. Bone healing

Bone can be fractured due to trauma or damaged by bone diseases such as osteoporosis. Osteoporosis can lead to weakening of the bone and increased fracture susceptibility. When bone is fractured, fracture healing occurs to restore the tissue to its original physical and mechanical properties. Fracture healing includes three distinct but overlapping stages: 1) early inflammatory stage, 2) repair stage, and 3) late remodeling stage (Fig. 1.2) (Baroli 2009;Doll *et al.* 2008;Schindeler *et al.* 2008).

In the inflammatory stage, a haematoma develops within the fracture site during the first few hours and days (Fig. 1.2.A). Inflammatory cells such as macrophages, monocytes and lymphocytes and fibroblasts infiltrate the bone, resulting in the formation of granulation tissue, ingrowth of vascular tissue and migration of mesenchymal stem cells (MSC). The MSC, recruited from the bone marrow and the periosteum, will then proliferate and differentiate into osteoblasts (Arifin *et al.* 2006;Doll and Hollinger 2008;Schindeler and Little 2008).

During the repair stage, fibroblasts lay down a stroma that helps support vascular ingrowth. As vascular ingrowth progresses, a collagen matrix is laid down when osteoblasts secrete osteoid which is subsequently mineralised by calcium phosphate deposited from blood, resulting in the formation of a soft callus around the repair site (Fig. 1.2.B.i). The soft callus is usually very weak in the first 2 to 3 weeks of the healing process. It then ossifies between 4 and 16 weeks (formation of hard callus), building a bridge of woven bone between

the fracture fragments (Fig. 1.2.B.ii) (Baroli 2009;Doll and Hollinger 2008;Schindeler and Little 2008).

Remodeling of the bone occurs slowly. The bone can eventually be restored to its original shape, structure, and mechanical strength. This is typically achieved in six months and beyond (Fig. 1.2.C) (Baroli 2009;Doll and Hollinger 2008;Schindeler and Little 2008).

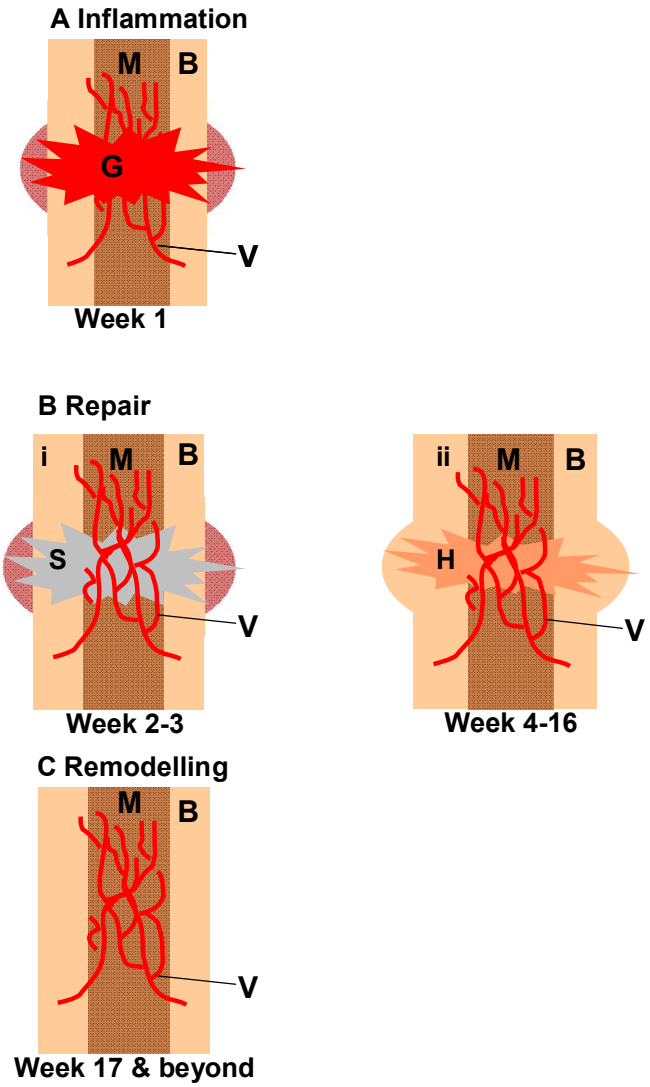

Fig. 1.2. Three stages of bone fracture healing including inflammation (A), repair (B) and remodelling (C). i and ii represent, respectively, soft and hard callus formation during the repair stage. B: bone; M: bone marrow; G: granuation tissue; V: blood vessels; S: soft callus; H: hard callus.

However, natural healing can be problematic in non - union bone defects in the long bones or in the case of massive bone loss. In this context, medical intervention aiming to facilitate bone repair is required (Verettas *et al.* 2002).

1.2. Bone - repair materials

Currently, the number of people who suffer from bone fracture problems is huge and the cost for the treatment of bone fracture is considerable. For example, as estimated by the World Health Organisation, osteoporotic fracture affects 33% (500,000) of women and 12.5% (140,000) of men over the age of 50 in the European Union (Baroli 2009). Moreover, it is expected that a cost for the treatment of osteoporosis-related hip fractures will reach € 31.8 billion by 2025 (Baroli 2009).

Thus, materials able to aid bone repair could be valuable to improve the life of patients who suffer from bone fracture and to reduce healthcare expenses (Baroli 2009).

1.2.1. Natural bone-repair materials

In order to induce bone to regenerate itself, growth factors, e.g., bone morphogenetic proteins (BMP) have been applied into the fractured or diseased site (Vaibhav *et al.* 2007). These proteins have been shown to modulate MSC differentiation and to stimulate bone formation. Genes which can express BMP have also been delivered to transfect local cells, stimulate BMP expression level and enhance bone regeneration (Kishimoto and Watanabe 2009). In addition, gene-modified stem cells have been injected

into fractured sites to augment bone growth. This approach exploits the ability of adult stem cells to express a transgene that can promote bone formation (Hou *et al*. 2009). None of these therapeutic options, however, provide an ideal solution to the problem of massive bone defect repair, especially for load bearing sites that require immediate mechanical support.

Massive bone defects can be treated via graft transplantation (autologous or allogeneic) (Betz 2002). Autografting is regarded as the 'gold standard' as it is based on the patient's own tissue. However, the popularity of this approach has been restricted due to the inadequate amount of bone that can be safely harvested. Furthermore, to expand and grow the patients' tissue takes time (approximately three weeks) (Baroli 2009;Barriga *et al.* 2004;McCann *et al.* 2004). Allografting uses material stored within regulated bone banks and may circumvent these difficulties. With allograft materials, however, disease transfer is of concern (Baroli 2009;Barriga *et al.* 2004).

Other therapies include the use of natural polymers. Natural polymers can be protein based (e.g. collagen, albumin or gelatin) or polysaccharide based (alginate, cellulose, or hyaluronate). They can also be synthesised naturally, e.g., polyhydroxyalkanoate is generated by micro-organisms under nutrient stress (Sabir *et al.* 2009). These natural polymers are generally biodegradable and have excellent biocompatibility (Nuss and von Rechenberg 2008). However, they may be immunogenic or suffer from restricted availability and their chemical composition is usually difficult to control (Allcock 2006;Dusseault *et al.* 2006).

1.2.2. Synthetic bone-repair materials

Synthetic products that can provide structural support and enhance bone repair are under increasing demand due to their greater availability, reduced concerns of immunogenicity and raw material source reliability (Papisov 1999). Currently used synthetic bone-repair materials can be divided into three major classes: metals, polymers and ceramics. They can be used either alone or in combinations. Metals, e.g., titanium, usually have the major advantage of high fracture toughness. They may suffer, however, from several disadvantages, such as cytotoxicity of any released ions as well as wear debris, or high Young's modulus which may lead to stress shielding (Kokubo 2009). Polymers such as polymethylmethacrylate (PMMA) generally have controllable chemical, physical and biological characteristics that depend on the repeating units of the polymer chains. Ceramics (e.g., bioactive glasses, calcium phosphates, etc) are a large family of inorganic biomaterials with a wide range of characteristics (e.g., density, porosity, solubility, etc) that strongly depend on the processing method used (Nuss and von Rechenberg 2008).

1.2.2.1. Required properties

Current surgical trends are tending towards more minimally invasive surgery. These favour materials with injectability and controllable setting. Additional requirements to be satisfied include mechanical properties, degradability and biocompatibility.

A. Injectability

Injectability (e.g., through needles) enables a material to fill defects of varying morphology. Injection of the materials can be achieved either directly underneath the skin or via small surgical incisions, thereby avoiding complex surgery. After injection, the materials should ideally set forming a solid of exactly the required dimensions *in situ*. This process should also enable material adhesion to the surrounding tissue by micromechanical interlocking (Temenoff and Mikos 2000).

B. Settability

The injected material should ideally set from liquid to solid in a few minutes to minimise the length of the procedure and enable the material to provide early mechanical support to the surrounding tissue, whilst still allowing surgeons ample time for placement before hardening (Xu *et al.* 2007).

C. Mechanical properties

The materials should provide sufficient mechanical support without causing stress shielding (Temenoff and Mikos 2000). To achieve this, their mechanical properties should be as close as possible to those of the tissue to be regenerated. For compact bone, an implant's Young's modulus should be around 3 - 30 GPa and strength 20 - 200 MPa (Keller *et al.* 1990). For trabecular bone, the modulus should be around 20 - 500 MPa (Agrawal and Athanasiou 1997;Bergsma *et al*. 1995) and strength 2 - 15 MPa (McCalden *et al.* 1997*)*.

Various mechanical properties should be considered for materials used in orthopaedics, including under compression, tension and torsion. Tensile properties are particularly important upon replacement of compact bone while compressive properties are most relevant for trabecular bone (Yaszemski *et al.* 1996).

D Degradability

Degradability enables the new bone to progressively integrate and ultimately replace the grafted material, eliminating the need for device removal surgery. Gradual degradation of the materials can avoid long-term toxicity problems as small amounts of degradation products can be readily disposed of by tissue elimination routes. The degradation rate of the material should be coupled to that of tissue formation so that slow transfer of mechanical load to the healing bone or damage site is facilitated (Temenoff and Mikos 2000). It has been suggested that an implant should degrade within 12 weeks as the natural bone healing signal appears to disappear about 7 to 12 weeks after injury (Ekholm *et al.* 1995). With longer degradation, a fibrous tissue scar can be the result, which may inhibit integration between the implant and the bone.

E Biocompatibility

Biocompatibility means that the implanted material itself and its degradation products do not cause severe cell death/tissue necrosis, or disrupt the normal

biological function of the target cells (Gerhart *et al.* 1998;Temenoff and Mikos 2000).

There are a wide variety of procedures used to assess biocompatibility. *In vitro* cell-attachment and cell-proliferation tests are widely used to determine whether the materials are deleterious to cells (Teixeira *et al.* 2008), since these aspects have been shown to be closely associated with cell survival, cell differentiation, matrix mineralisation and, therefore, new bone formation (Garcia and Reyes 2005). *In vivo* assessment includes examination of the tissue response to the implanted materials. Positive short-term indications can include the presence of osteoblasts as a marker of bone formation at the interface between the material and the bone, along with the absence of inflammation or other adverse tissue reaction (Wang *et al.* 2007). Positive long-term results can include osteointegration, i.e., the intimate and direct contact of the bone and the implanted material and absence of soft tissue. Osteointegration is indicative of a rigid and biologically compatible fixation of the implant in the bone during functional loading (Wang *et al.* 2007).

1.2.2.2. Different synthetic bone-repair materials

A. Polymers

I. Polymethylmethacrylate

PMMA (molecular structure shown in Fig. 1.3) is frequently used in orthopaedics (Lewis 2008). It is commonly used as an aid in securing implants for total hip or knee replacement. Additionally, PMMA beads have been

impregnated with antibiotics before being packed into wound cavities for the treatment of chronic bone infections (Nandi *et al.* 2009).

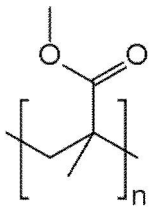

Fig. 1.3. Molecular structure of polymethylmethacrylate (PMMA). n is the number of the repeating monomer units.

PMMA is typically synthesised from methyl methacrylate using benzoyl peroxide as initiator. This semi-liquid material can be injected *in situ*, then continues to harden over several minutes, adhering to surrounding tissue via micromechanical interlocks. Tissue damage, however, may occur due to the high temperature achieved during the curing of PMMA (Lewis 2008). PMMA modulus can be varied via adjusting the material porosity and initiator concentration. Being non-degradable, PMMA may act as a barrier to bone ingrowth and potentially could limit blood flow. Its monomer is considered to be cytotoxic, release of which may cause tissue irritation or inflammation (Lewis 2008).

II. Polylactide, polyglycolide and poly (lactide-co-glycolide)

Polylactide, polyglycolide and their copolymers, poly (lactide-*co*-glycolide) are also frequently used in orthopaedics. Polylactide and poly (lactide-*co*-glycolide) are generally used as fixation plates and screws while polyglycolide is mainly used as biodegradable sutures (Sabir *et al.* 2009). Their molecular structures are shown in Fig. 1.4. They can be synthesised by ring-opening

polymerisation of the respective cyclic monomers using antimony or zinc as catalysts (Sabir *et al.* 2009). They are usually viscous liquids or solid materials and are not readily injectable unless used as micro- or nano-particles (mainly for drug delivery applications) (Herrero-Vanrell and Molina-Martinez 2007). Mechanical properties and degradation rates of these polymers can be manipulated to some extent by controlling their molecular weight and crystallinity. With poly (lactide-*co*-glycolide), these properties can additionally be adjusted by the unit ratio of lactide (LA) to glycolide (Sabir *et al.* 2009). They can be degraded via hydrolytic or enzymatic degradation. Their degradation products, lactic acid or glycolic acid, are natural metabolism products and can be incorporated in the tri-carboxylic acid cycle and excreted by the lungs as carbon dioxide and water (Sabir *et al*. 2009). Potential problems with these polymers may include acid production during degradation. The produced acid may reduce the local pH and further induce polymer degradation (auto-catalysis). This may eventually cause catastrophic degradation leading to sudden loss of structural support and localised acid accumulation resulting in tissue damage (Sabir *et al*. 2009).

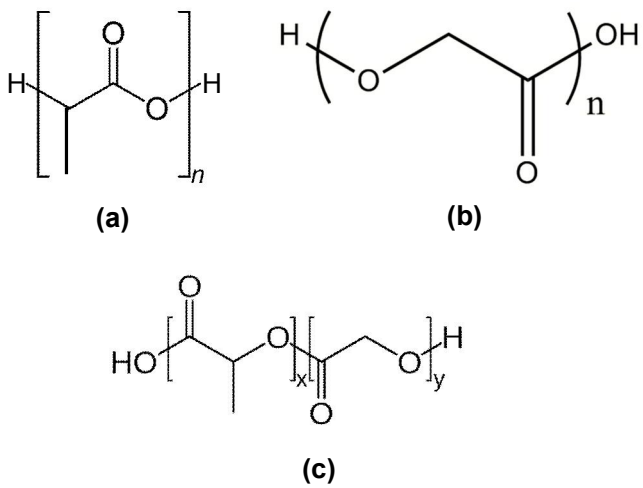

Fig. 1.4. Molecular structure of polylactide (a), polyglycolide (b) and poly (lactide-*co*-glycolide) (c). n, x and y are the number of the repeating monomer units.

Synthetic polymers with both injectability and degradability include various poly (ether-*co*-ester)s, polyanhydrides (PAH) and poly(propylene fumarate) (PPF) (Nair and Laurencin 2007),etc.

IV. Poly (ether- co- ester)s

Poly (ether-*co*-ester)s are copolymers of polyether and polyester (molecular structure shown in Fig. 1.5). Polyesters are generally not injectable but using polyethers as initiator for ring-opening polymerisation of cyclic esters, fluid, relatively short chain poly (ether-*co*-ester)s can be produced (Ho and Young 2006;Kim *et al.* 2009). Insertion of ester linkages allows the system to be degradable, whereas pure long chain polyethers are not. End-capping of the polymer units with acrylate or methacrylate (MA) groups enables crosslinking (Ho and Young 2006).

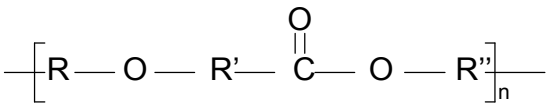

Fig. 1.5. Molecular structure of poly(ether-*co*-ester)s. R, R' and R'' represent different functional groups and n is the number of the repeating monomer units.

The polyether, poly (ethylene glycol) (PEG) is frequently used to increase polyester biocompatibility and to modulate its degradation (Goraltchouk *et al.* 2005). Commonly used polyesters include PLA, polyglycolide, poly (lactide-*co*-glycolide) and poly (ε-caprolactone) (PCL) (Sabir *et al.* 2009). Photo-polymerisable ester-PEG-ester hydrogels (e.g., dimethacrylated LA-PEG-LA) have been successfully formulated in the last decade (Quick and Anseth 2004). Setting times of these polymers are variable depending on the repeating units of the polymer. Degradation times can vary from days to months depending on the crosslinking density, polymer molecular weight and the employed ester types (Hubbell 1998). These PEG based materials can offer excellent biocompatibility and controllable degradation rates. Unfortunately, they often suffer from low mechanical properties due to their high water sorption (arising because of the hydrophilicity of PEG) and may undergo catastrophic degradation.

Formulations containing less hydrophilic polyethers have therefore been developed. For example, fluid poly (propylene glycol-*co*-lactide) dimethacrylates (PGLA-DMA) have been synthesised. Poly (propylene glycol) (PPG) (a commonly used excipient in pharmaceutical formulations) has a similar molecular structure to PEG but more methyl groups which endow a

higher degree of hydrophobicity. These dimethacrylated materials are not only injectable and set rapidly, but are also likely to swell to a lesser extent in water and degrade and release acid more slowly because of their higher hydrophobicity compared with their PEG counterparts. These materials, however, are of relatively low modulus and their biological reactivity with bone-related cells and tissue is not yet known (Ho and Young 2006).

V. Polyanhydride

PAH (molecular structure shown in Fig. 1.6) can be synthesised by the dehydration of a dicarboxylic acid or a variety of aromatic and aliphatic dicarboxylic acids via melt condensation (Sabir *et al.* 2009). It contains one of the most reactive functional groups (-COO-) for hydrolytic degradation, ensuring surface-eroding and fast-degrading characteristics. Because these polymers are surface-eroding, they are expected to maintain bulk mechanical properties while undergoing degradation (Sabir *et al.* 2009). The fast-degradation property also allows the material to be used for drug delivery. Depending on the monomers (R group in Fig. 1.6) used, the mechanical properties as well as degradation time can be varied. For example, PAH can be formed from monomers of sebacic acid with addition of monomers of 1,3-bis(*p*-carboxyphenoxy) propane or 1,6-bis (*p*-carboxyphenoxy) hexane. The acrylated or methacrylated PAH can be set rapidly, within several minutes. These polymers can have mechanical properties similar to those of trabecular bone. The degradation rates of these polymers can be controlled, spanning from days to months, by changing the ratio of sebacic acid and other monomers in the structure (Sabir *et al.* 2009). Degraded aliphatic monomers

such as sebacic acid are likely to participate in the β-oxidation pathway for energy production. Degraded aromatic monomers can be eliminated without further metabolic transformation (Sabir *et al.* 2009). Minimal inflammatory response to sebacic acid/ 1,3-bis(*p*-carboxyphenoxy) propane / 1,6-bis (*p*-carboxyphenoxy) hexane was also observed (Sabir *et al.* 2009). One drawback of PAH is that most of them have to be stored in a frozen state under anhydrous conditions because of the hydrolytic instability of the anhydride bond (Park *et al.* 2005).

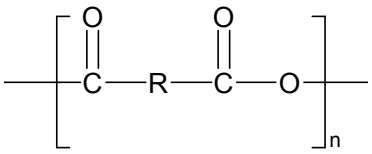

Fig. 1.6. Molecular structure of polyanhydride (PAH). R represents different functional groups and n is the number of the repeating monomer units.

VI. Poly (propylene fumarate)

PPF (molecular structure shown in Fig. 1.7) is a synthetic, unsaturated linear polyester formed by co-polymerisation of fumaric acid and PPG. PPF can be thermal- or photo- crosslinked through its fumarate double bond in 30 minutes. Obtaining PPF of high molecular weight is often difficult owing to the side reactions due to the presence of the backbone double bond. This may make its mechanical properties less than ideal for cortical bone although properties within the range of those of trabecular bone have been achieved. The degradation of PPF can occur by hydrolytic chain scission of its ester groups and is usually of the order of several months. Its degradation products include fumaric acid and PPG. These are of relatively low toxicity and can be excreted directly or after entry and exit from various metabolic pathways. Degradation

rate depends on many factors such as molecular weight, crosslinking density, and also other copolymer or constituent ratio in the PPF networks. *In vivo* tests of these polymers have shown no apparent deleterious long-term response with only an initial mild inflammatory side effects (Sabir *et al.* 2009).

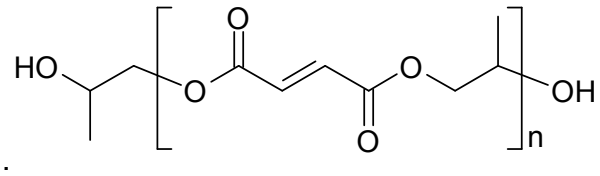

Fig. 1.7. Molecular structure of PPF. n is the number of the repeating monomer units.

VII. Other polymers

Other injectable, degradable polymers under development include polyorthoester (POE) and polyphosphazene (PPP). Their molecular structures are shown in Fig. 1.8. POE is highly hydrophobic and very stable under physiological conditions. They are mainly considered to be potential candidates for drug delivery applications. The mechanical properties of POE can vary over a wide range by the selection of starting materials with different compositions and molecular weights. Their application is limited due to the lack of variability in the degradation kinetics (Sabir *et al.* 2009). POE can induce moderate inflammation in bone.

PPP contains alternating nitrogen and phosphorous with no carbon atoms in their backbone structure. It is feasible to control the mechanical, degradation and biological properties of PPP by precisely controlling the side group's substituents (e.g., R and R' can be amino acid esters, lactic acid or imidazolyl units) (Sabir *et al*. 2009).

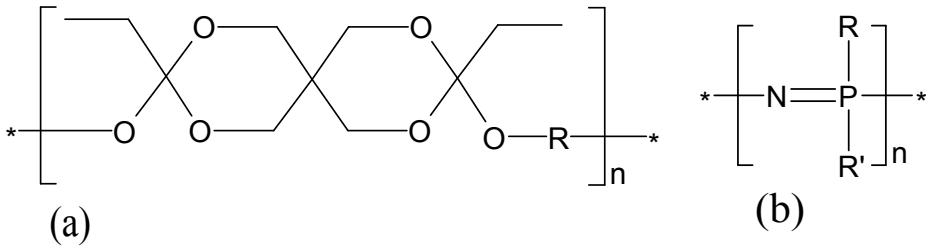

Fig. 1.8. Molecular structure of polyorthoester (POE) (a) and polyphosphazene (PPP) (b). R and R' represent different functional groups and n is the number of the repeating monomer units.

B. Calcium phosphate cements (CPC)

Calcium phosphate cements (CPC) are considered as excellent materials for maxillofacial and craniofacial applications. In addition, they can be used in treating vertebral body compression fractures, femoral neck fractures, distal radius fractures, and reinforcement of pedicle screw fixation (Dorozhkin 2008). Recently, it has been suggested they might compete with the PMMA bone cements and the apatite coatings for fixation of metal endoprostheses in orthopaedics and oral implantology (Muller and Stangl 2006) .

CPC can adapt to local defect sites and then harden without elevation of temperature, although they may lack sufficient cohesion and tend to disintegrate upon early contact with blood or other fluids before they start to set. In general, CPC are formed by mixing calcium phosphate powders (one or more types), with a liquid (usually water or an aqueous solution). The resulting paste will then set and harden after implantation in the body. The cement setting and hardening is a result of dissolution and precipitation processes. Setting time, porosity and mechanical properties of the CPC can

be adjusted by modifying different factors, such as the powder / liquid ratio, the chemical composition of reactants (powder and / or liquid) and the particle size of calcium phosphates (Ambard and Mueninghoff 2006;Larsson and Bauer 2002).

CPC are generally brittle and have low impact resistance and relatively low tensile strength. Porosity is considered to be the major reason responsible for this weakness as micro- and macro- cracks easily run throughout the mass upon loading. CPC are often considered to be degradable, biocompatible and osteoconductive. The overall dissolution of CPC is solution-mediated (the implant dissolves in physiologic solutions) and cell-mediated (phagocytosis). Complete cement resorption and replacement by bone may take months to years. Bone substitution depends on sex, age, and general metabolic health of the recipient and anatomic site, as well as porosity, crystallinity, chemical composition, particle size, and powder / liquid ratio of the cement. The degradation products of calcium and phosphate ions are resorbed as part of the normal ion pool within the body. The release of phosphate and calcium ions is also considered to be biologically beneficial as it stimulates osseous tissue development. The dissolved calcium and phosphate ions can re-precipitate on the surface of the cement as, for example HA, with a high and interconnected micro-porosity, chemically and structurally similar to biological apatites, starting a bone-cement interaction and bonding process. CPC are therefore considered to be more compatible with mineralised tissue and more osteoconductive than polymeric materials (Ambard and Mueninghoff 2006;Larsson and Bauer 2002).

Numerous CPC formulations have been proposed in the last 25 years, but presently there are two major possible end products for CPC reactions: an apatite such as HA ($Ca_{10}(PO_4)_6(OH)_2$) or calcium-deficient HA (CDHA; $Ca_9(HPO_4)(PO_4)_5OH$) and dicalcium phosphate dihydrate (brushite, $CaHPO_4 \cdot 2H_2O$) or the anhydrous form, monetite ($CaHPO_4$).

I. Apatite CPC

HA cements can be produced using the reaction between the basic tetracalcium phosphate (TTCP, $Ca_4(PO_4)_2O$) and the neutral monetite. TTCP and monetite react in water according to the formula below (Bohner 2007):

$$2Ca_4(PO_4)_2O + 2CaHPO_4 \rightarrow Ca_{10}(PO_4)_6(OH)_2 \quad 1.1$$

Most commercial cements are formed using a slightly basic α-tricalcium phosphate (α-TCP, $\alpha\text{-}Ca_3(PO_4)_2$), which can be converted via dissolution-precipitation to a slightly basic CDHA according to (Bohner 2007):

$$3\alpha\text{-}Ca_3(PO_4)_2 + H_2O \rightarrow Ca_9(HPO_4)(PO_4)_5OH \quad 1.2$$

Conventionally, the mixing of apatite CPC powders with aqueous solution takes place during surgery and the setting time of the apatite CPC is generally too long (Bohner 2007). Recently, puttied premixed CPC pastes were therefore prepared (Apelt *et al.* 2004). For example, Xu *et al.* have developed a premixed CPC whose powder phase consisted of TTCP and monetite and liquid phase comprised of PEG with hydroxypropyl methylcellulose as gelling agent, and tartaric acid as the hardening accelerator. The CPC can be set in < 10 min in physiological solution, possesses comparable strength with human

cancellous bone and has good osteoblast compatibility (Xu *et al.* 2007). Advantages of these premixed CPC include: (i) avoid powder – liquid mixing during surgery thereby shortening the surgical time; (ii) will harden rapidly in an aqueous environment or physiological solution and no harden in the package or in a syringe.

However, apatite cements are of low solubility at physiological pH and therefore would be very slow to resorb in the body. Consequently, the apatite cements woud be unlikely to provide sufficient calcium and phosphorous required for bone regeneration (Ambard and Mueninghoff 2006;Bohner 2000).

II. Brushite CPC

Brushite CPC are normally resorbed faster than apatite CPC as brushite is more soluble than apatite at physiological pH (Bohner 2001). Brushite CPC have been developed using mixtures of monocalcium phosphate monohydrate (MCPM, $Ca(H_2PO_4)_2.H_2O$) and β-TCP. These two phosphates can rapidly react to form lower density brushite according to the equation below (Bohner 2007):

$$\beta\text{-}Ca_3(PO_4)_2 + Ca(H_2PO_4)_2 \cdot H_2O + 7H_2O \rightarrow 4CaHPO_4 \cdot 2H_2O \qquad 1.3$$

During this process, the MCPM particles dissolve in water and re-precipitate, thereby solidifying the cement and forming brushite crystallites and/or the anhydrous dicalcium phosphate, monetite. Previously brushite CPC have also been produced using β-TCP or HA with phosphoric acid or using TTCP with polyphosphoric acid (Bohner 2007).

Setting of brushite CPC can sometimes be too rapid (e.g., within ten seconds) (Bohner 2007). In order to increase the setting period and hence provide sufficient time to the surgeon for safe CPC placement, use of less soluble reagents (e.g. HA instead of β-TCP) has been suggested. This can increase the setting period but only to a limited extent (Bohner 2007). Recently, puttied premixed CPC pastes were prepared by combining cement liquids comprised of glycerol or PEG with CPC powders that consisted of β-TCP and MCPM. Setting time of these premixed CPC was raised to between 10 and 30 minutes. The mechanical properties of these cements, however, were less than ideal (Han *et al.* 2009).

C. Composite materials

Table 1 summarises different properties of the above mentioned polymers and CPC and their main disadvantages. To overcome various problems, polymers and CPC may be combined. As mentioned above (section 1.1.1), natural bone is made of an organic collagen matrix and HA crystals. Polymer-ceramic composite materials therefore imitate well natural bone. PMMA, PLA, polyglycolide, poly (lactide-*co*-glycolide), poly (ether-*co*-ester), PAH and PPF can act as the organic phase whereas HA and brushite can act as the mineral part in the formulation of composites for bone replacement.

Ceramic particles have been incorporated into injectable polymers as fillers to modify their mechanical and degradation properties as well as biocompatibility (Cai *et al.* 2009). The incorporated calcium phosphate fillers can also act in degradable polymer systems as internal buffers to neutralise the local pH and

inhibit any autocatalytic degradation (Peter *et al.* 1998). However, there are still some limitations in these polymer-calcium phosphate composites. Firstly, the filler may not have a strong interaction or bond with the polymer matrix and this interface can be a point of material weakness. Secondly, filler addition to unsaturated polymer may reduce the light-activated polymerisation rate in thicker samples, due to scattering effects (Berthomieu and Hienerwadel 2009).

1.3. Delivery of therapeutic agents for bone repair

Tissue engineering involves the use of materials as structural support for regenerating tissue. Incorporation of drugs into these materials can endow them with therapeutic properties (e.g., resistance to bacterial infections, induction of osteogenesis). Such materials can thus act as local delivery devices. Major advantages of using controlled delivery systems include the maintenance of a desired drug concentration at a specific site for long period of time without reaching a toxic level or dropping below the minimum effective level (Arkfeld and Rubenstein 2005). Additionally, such systems may eliminate the need for repeated administrations.

Drugs used in bone tissue engineering include antibacterial drugs (to reduce infections), anti-inflammatory drugs (to treat inflammatory conditions), anti-cancer agents (to treat tumors), hormones (to treat osteoporosis) and growth factors or their genes (to facilitate wound healing) (Malafaya *et al.* 2002).

Table 1.1. Summary of different properties of polymers and calcium phosphate cements (CPC).

	Type of biomaterial	Injectability	Setting rate	Young's modulus	Tensile/ compressive strength	Degradation rate	FDA approval	Main disadvantages
Polymers	PMMA	√	√	√	√	~~√~~	√	Non-degradable
	Polylactide	-	-	√	√	√	√	Non injectable unless in the form of micro- or nano-particles;
	Polyglycolide	-	-	√	√	√	√	
	Poly(lactide-*co*-glycolide)	-	-	√	√	√	√	Catastrophic degradation
	Poly(ether-*co*-ester)	√	√	√	√	√	-	Dependant upon particular formulation
	PAH	√	√	√	√	√	√	Low storage stability
	PPF	√	~~√~~	√	√	√	-	Slow setting and low modulus
CPC	HA	√	√	√	√	~~√~~	√	Low resorption rate
	Brushite	√	√	√	~~√~~	√	-	Low mechanical strength

PMMA = polymethylmethacrylate; PAH = polyanhydride; PPF = poly (propylene fumarate); CPC = calcium phosphate cements; HA = hydroxyapatite. '√' and '~~√~~' mean that the corresponding material can or cannot meet a desirable criterion respectively; '-' = not applicable.

1.3.1. Considerations in drug delivery

Successful drug delivery requires formulation and sterilisation methods that do not damage the pharmacologic actions of the drug. For example, when using synthetic degradable polymers for drug delivery, drugs may undergo thermal damage due to elevated temperatures during polymer setting (i.e., crosslinking) or acid degradation due to acidic breakdown products of the crosslinked polymer (del Valle *et al.* 2009). Other potential problems also include initially delayed or burst release (Young and Ho 2008). In addition, drugs may interact chemically or physically with the polymer or its degradation products, possibly limiting their release (Young and Ho 2008), while incorporated drug may affect the degradation rate of the polymer matrix itself (Tang and Singh 2008). With CPC, the setting reaction of the CPC itself can be significantly modified by drug introduction into either the powder or liquid phase. As a result, the physico-chemical and mechanical properties can change (Takechi *et al.* 1998). In other cases, modification of CPC properties can result from chemical interactions between the drug and the cement, e.g., tetracycline can chelate calcium atoms (Ratier *et al.* 2001). Drug release rates can be too rapid due to the high porosity of CPC (Bohner *et al.* 1997), or it can be inhibited due to the decreasing porosity of the CPC upon formation of a dense HA layer on the CPC surface (Otsuka *et al.* 1997). Moreover, drugs of high molecular weight, e.g., proteins, may not be released due to the entrapment in nanopores on the CPC surface (Ruhe *et al.* 2003).

1.3.2. Antibacterial drug delivery

Bacterial infections are a major problem affecting the service life of medical implants, and need to be prevented to allow wound healing processes to take place. Such implant-associated infections are the result of bacterial adhesion and subsequent bio-film formation at the implantation site, so that inhibiting adhesion is often regarded as a critical step in preventing infection (Mourino and Boccaccini 2009). Antibacterial drugs are therefore incorporated into the bone-repair materials to resist bacterial adhesion and infections.

1.3.2.1. Antibacterial drugs to treat bone infections

Gentamicin and tetraycline (Kim *et al.* 2004) are commonly employed antibiotics in treating trauma, and widely used for the treatment of osteomyelitis (bone infection) because of their broad-spectrum characteristics. Other antibiotics including vancomycin, polymyxin B, gatifloxacine, ciprofloxacin and ampicillin have also been used for this purpose. However, bacteria may develop antibiotic resistance (Mourino and Boccaccini 2009). Therefore, other antibacterial drugs such as chlorhexidine (CHX) have been incorporated into bone fillers or bone cements in order to inhibit bacterial growth (Leung *et al.* 2005;Young *et al.* 2008;Young and Ho 2008). CHX has been chosen as the antibacterial drug due to its broad spectrum of activity against both Gram-positive and Gram-negative bacteria and very low incidences of resistance development (Harris *et al.* 2006).

1.3.2.2. Antibacterial drug activated matrix

Biomaterials containing antibacterial drugs are defined as antibacterial drug activated matrices. Local drug release profiles should exhibit a high initial release rate in order to respond to the elevated risk of infection from bacteria introduced during an initial shock. This should then be followed by sustained release at an effective level for inhibiting the re-occurrence of latent infection (Zilberman and Elsner 2008).

Young *et al.* have investigated the use of injectable degradable PGLA-DMA for CHX delivery (Young and Ho 2008). Early CHX release was consistent with diffusion and the drug release rate increased with raised PPG and LA unit length. However, interactions between the positively charged CHX ions and the large negatively charged bulk acidic degradation products may have inhibited sustained drug release. Young *et al.* have also investigated CHX release from brushite CPC using MCPM and β-TCP as reactants (Young *et al.* 2008). Most of the CHX was released in one day and the total amount of CHX was released within ten days. CHX release in this case is considered to be too rapid, possibly due to the high CPC porosity.

1.3.3. Gene delivery

Growth factors such as BMP have been incorporated into bone-repair materials with the aim of improving or increasing the osteoinductive capacity of the material (Ohura *et al.* 1999). An alternative approach for delivering growth factors is to deliver their corresponding genes. Since the gene rather than a degradable protein is being delivered, this technique may result in

more constant levels of protein production (Nussenbaum and Krebsbach 2006), and, most importantly, an inherently stable DNA which is available and potentially active over a prolonged period of time (Bonadio 2000).

1.3.3.1. Genes to enhance bone formation

Major classes of gene products relevant to bone tissue engineering include growth factors (e.g., BMP), transcription factors (e.g., LIM mineralisation protein-1, which was shown to induce expression of BMP), cytokines (e.g., interleukin 1-receptor antagonist, which was observed to reduce bone resorption), and angiogenic factors (e.g., vascular endothelial cell growth factor, which was found to induce formation of blood vessels) (Salvay and Shea 2006).

1.3.3.2. DNA delivery techniques

Naked plasmid DNA does not readily enter or express inside cells possibly due to its negative charge and susceptibility to nuclease degradation (Liu and Huang 2002). A number of techniques to facilitate DNA transfer intracellularly and expression by target cells have therefore been developed. These techniques can be classified into three general types: 1) mechanical and electrical techniques; 2) vector - assisted delivery; and 3) gene activated matrix (GAM).

A. Mechanical and electrical techniques

Mechanical and electrical strategies of introducing naked DNA into cells include microinjection, particle bombardment, and electroporation.

Microinjection transfers DNA into one cell at a time. This procedure is efficient but highly time consuming. Particle bombardment involves transfer of DNA - gold micro-particles using equipment such as a gene gun. Its application is restricted in the dermis and muscle as direct exposure of target tissues is required. Electroporation uses high - voltage electrical current to facilitate DNA transfer but it often results in high cell mortality (Luo and Saltzman 2000).

B. Vector-assisted DNA delivery

Vector-assisted DNA delivery systems can be classified into two types: biological viral DNA delivery systems and chemical non-viral delivery systems.

I. Viral delivery vectors

Viruses can readily transfer DNA molecules into cells. High transfection efficiency can be achieved using this approach in many types of tissues such as kidney, heart, etc. Considerable progress for the treatment of a wide range of diseases, such as AIDS and cancer has been made using gene therapy with viral systems (Luo and Saltzman 2000). However, there are several concerns over the use of these vectors. These include 1) the toxicity of the viruses, 2) the potential to generate an immune response and 3) the potential to inhibit expression of normal cellular genes or to activate oncogenes (Favre *et al*. 2001;Raper *et al.* 2003).

II. Non-viral delivery vectors

Commonly used non-viral vectors can be classified into two major types: 1)

calcium phosphate precipitation and 2) cationic polymers or lipids. The technique of calcium phosphate precipitation for *in vitro* transfection relies on the formation of ionic complexes of divalent metal cations, such as Ca^{2+}, Mg^{2+}, Mn^{2+} and Ba^{2+} with the phosphate backbones of helical DNA (Truong-Le *et al.* 1999), followed by transport across the cell membrane via endocytosis (Truong-Le *et al.* 1999). This technique is usually simple and inexpensive and has minimal cellular toxicity. The low level of transgene expression, however, has prompted the development of other techniques, e.g., cationic polymers or lipids as DNA carriers (Luo and Saltzman 2000).

Cationic polymers or lipids complex with anionic DNA molecules, interact with the negatively charged cell surface and deliver DNA into cells (Hwang and Davis 2001;Patil *et al.* 2005). Diversity of physicochemical properties and ease of manipulation are also important advantages of polymer or lipid gene carriers. Commercially available cationic polymer or lipid based gene transfection reagents include Lipofectamine™ (Invitrogen), Effectene™ (Qiagen), Tranfectam™ (Promega) and Metafectene™ (Biontex) (Kang *et al.* 1999;Oliveira *et al.* 2009). However, cytotoxicity is the major concern regarding these delivery vectors, while, the transfection efficiencies of non-viral cationic polymers or lipids vectors are not as high as those of viral vectors (Hwang and Davis 2001;Patil *et al.* 2005).

C. Gene activated matrix

DNA (with or without a chemical non-viral delivery vector) incorporated into bone-repair materials, give a gene activated matrix (GAM). Ideally, the GAM

should provide a controllable long-term supply of the gene to the target tissues, thereby increasing the chance of continuing uptake, intracellular function and successful gene therapy. DNA release in this case generally occurs through a combination of surface desorption, drug diffusion and material degradation (Jang *et al.* 2004;Quick *et al.* 2004;Quick and Anseth 2004). Varying the matrix density, porosity, hydrophilicity and degradation rate can control the DNA release rate.

GAM shows improved activity if the genes loaded inside are incorporated together with delivery vectors rather than as naked DNA alone (Endo *et al.* 2006;Huang *et al.* 2005;Itaka *et al.* 2007;Quick *et al.* 2004;Quick and Anseth 2004). This increased activity may be due to the vectors protecting the DNA, e.g., from polymer degradation and photo-polymerisation (Quick *et al.* 2004;Quick and Anseth 2004). For example, Quick *et al.* produced a surface-eroding, photo-crosslinkable PAH which was able to deliver DNA plasmids into *Escherichia coli* DH 5α. The DNA coated by alginate could continually transform the bacteria for four days whereas the naked DNA was only active for one day (Quick *et al.* 2004). However, the 4-day DNA transformation period was still too short for use in bone regeneration. Quick *et al.* have also developed photo-polymerised di-methacrylated LA-PEG-LA macromers as a bioerodible hydrogel platform for delivering plasmid DNA (Quick and Anseth 2004). The DNA, protected by cationic peptide protamine sulfate, could be released for 6 - 100 days with high biological activity. The DNA release rate can be controlled by varying hydrogel crosslinking density and degradation

rates. However, the hydrogel could not provide sufficient mechanical support due to its hydrophilicity.

Poly (lactide-*co*-glycolide) scaffolds have also been used to deliver genes encoding BMP-4 (condensed by the cationic polymer, polyethylenimine) in rat cranial defects (Huang *et al.* 2005). Bone formation was observed after 15 weeks of implantation. Histomorphometric analysis revealed a significant increase in total bone formation and bone density within the scaffolds incorporating condensed DNA, relative to scaffolds incorporating uncondensed DNA. This study has suggested that delivery of condensed DNA would be more effective to enhance bone regeneration, compared to that of uncondersed DNA. However, these poly(lactide-*co*-glycolide) scaffolds suffered from lack of injectability and therefore required surgical incision.

In summary, the GAM previoiusly investigated suffered from two major difficulties: 1) the DNA delivery period was too short (Itaka *et al.* 2004) and / or 2) the GAM themselves had low mechanical properties or are not injectable (Huang *et al.* 2005;Quick and Anseth 2004).

1.4. Aim and objectives

1.4.1. Aim

Current materials for bone repair with minimally invasive surgery are limited by problems such as slow setting rates, poor mechanical properties and slow degradation rates. In addition, drug release from such materials, particularly DNA, usually occurs as a burst which lasts only for a short period. The aim of

this study is therefore to develop novel materials that are injectable, rapid setting, of comparable mechanical properties with bone, degradable and biocompatible. Moreover, these new materials would be capable of releasing, locally and in a controllable manner, therapeutic reagents such as antibacterial drugs to treat bone infections and genes to improve osteogenic responses.

The materials selected for this study consisted of fluid PGLA-DMA filled with MCPM and β -TCP powders (reactants of brushite CPC). The reagents to be delivered were CHX and plasmids encoding green fluorescent proteins (GFP), a model DNA for gene therapy. The properties considered relevant to this study include injectability, polymerisation rate, mechanical properties, degradation rate, biocompatibility, CHX release rate, antibacterial activity and DNA transfection efficiency.

1.4.2. Objectives

1. To synthesise and identify PGLA-DMA of defined chemical structure.
2. To investigate the setting rate, mechanical properties, degradation and biocompatibility (*in vitro* and *in vivo*) of systematically varying PGLA-DMA based composite materials.
3. To quantify CHX release from the PGLA-DMA based composite materials and its subsequent antibacterial activity.
4. To examine gene transfection in hMSC upon release of condensed GFP plasmids from the set PGLA-DMA.

Chapter 2
Polymer Synthesis and Preparation

Abbreviations

In alphabetical order

FTIR	Fourier transform infrared
LA	lactide
MA	methacrylate
MAC	methacryloyl chloride
NMR	Nuclear magnetic resonance
PPG	poly (propylene glycol)
PGLA	poly (propylene glycol -*co*- lactide)
PGLA-DMA	poly (propylene glycol -*co*- lactide) dimethacrylate
TEA	triethylamine
TEA·HCl	triethylamine·hydrochloride
SD	standard deviation

2.1. Introduction

This project used fluid degradable poly (propylene glycol -*co*- lactide) dimethacrylate (PGLA-DMA) as the organic component of the composite materials (see details in Chapter 3) for bone repair and drug delivery. The PGLA-DMA (see molecular structure in Fig. 2.1) consisted of poly (propylene glycol) (PPG) of low molecular weight to which degradable lactide (LA) units were attached each end. These were then terminated with polymerisable methacrylate (MA) groups. The rationale of using PPG lies in that: (1) It is biocompatible. PPG has been evaluated as potential lubricous coatings for various medical products (Kim *et al.* 2000). PPG of low molecular weight, can be eliminated from the body by excretion (He *et al.* 2001); (2) It is hydrophobic and anticipated to produce more hydrophobic backbones to provide a means of reducing water sorption rates. LA is used to facilitate degradation and its degradation products are natural metabolites in the body (An *et al.* 2000;Gunatillake and Adhikari 2003). The MA end groups will enable the monomers to polymerise and crosslink using either light or chemical cure means.

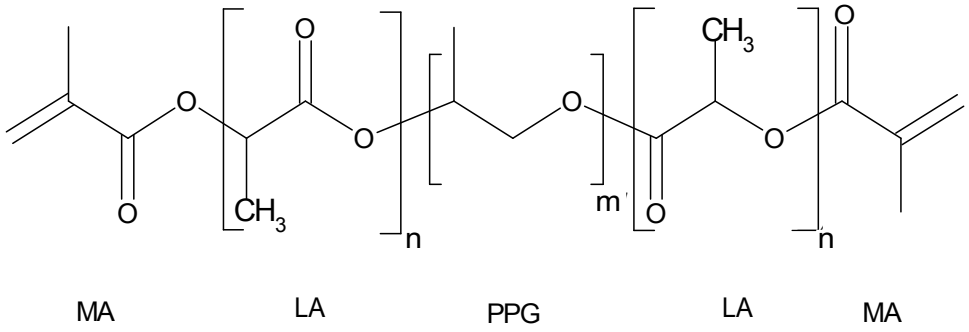

Fig. 2.1. Molecular structure of PGLA-DMA. PPG = poly (propylene glycol); LA = lactide; MA = methacrylate. m and n are the unit length of PPG and LA respectively.

Synthesis of PGLA-DMA with systematically varying the unit length of PPG and LA has been reported previously (Ho and Young 2006). The formulation with 17 units of PPG and 4 units of LA was selected in this study because of its fluidity and stability (Ho and Young 2006).

In previous work, problems in preparation of these monomers included: 1) low efficiency of end-capping MA to PGLA (~ 80%); 2) low reaction yield of PGLA-DMA synthesis (~ 60%) and 3) high level of difficult to remove impurities (i.e., crystals of triethylamine· hydrochloride (TEA·HCl)) (Ho and Young 2006).

High methacrylation efficiency is desirable as this property of a monomer strongely affects crosslinking density after polymerisation. A monomer with vinyl groups at both ends will form a densely crosslinked polymer network. Those with one vinyl group will however form linear chains, which may make the polymer weak and pliable (Muggli *et al.* 1998) thereby preventing the polymer from matching mechanical properties of any bone tissue it will replace. High reaction yield is also advantageous due to improved time and cost effectiveness. In addition, TEA·HCl impurities may lower monomer clarity and thus light catalysed polymerisation rate. They may also affect the physical, chemical or biocompatibility properties of the polymer (e.g., accelerate the polymer degradation). As much as possible of the TEA·HCl crystals should therefore be removed.

The aim of this study was therefore to increase the MA end-capping efficiency and reaction yield of PGLA-DMA synthesis by varying synthesis conditions

and to improve the purification level (removal of TEA·HCl) using different solvents.

2.2. Materials and methods

2.2.1. Synthesis of monomer

PGLA-DMA was synthesised in two steps: 1) LA attachment to PPG to produce PGLA and 2) methacrylation of PGLA to produce PGLA-DMA. The synthesis procedure primarily used a method described by Ho *et al*. (Ho and Young 2006). As shown by Ho *et al*., synthesis of PGLA is reproducible with high reaction yield (>95%) whereas synthesis of PGLA-DMA is problematical (i.e., low methacrylation efficiency and reaction yield and high impurity level). In an attempt to improve methacrylation efficiency and reaction yield, in the following three reaction conditions were modified or varied. These include 1) change in addition order of methacryloyl chloride (MAC) and triethylamine (TEA) to PGLA (as suggested by Shen *et al*. (Shen *et al.* 2007)), 2) variation in PGLA concentration in dichloromethane and 3) variation in molar ratio of MAC to PGLA (see details in section 2.2.1.2.A). Furthermore, additional purification steps used by Shen *et al*. (Shen *et al.* 2007) have been applied to improve TEA.HCl removal (see details in section 2.2.1.2.B).

2.2.1.1. Synthesis of poly (propylene glycol -*co*- lactide) (PGLA)

PPG (0.04 mol, information regarding all reagents and their suppliers is provided in Appedix A, *sic passim*) was reacted with 0.16 mol of D,L-LA (within a 250 ml one-neck round-bottom flask equipped with a magnetic stirrer) at 150 °C in a nitrogen atmosphere for 6 h, using stannous octoate (0.05 wt.

% of PPG) as a catalyst. Using a Carousel 6 place reaction station (Radleys Discovery Technologies, Essex, UK), 6 batches of product could be produced at one time.

The resultant products were then cooled to room temperature, 100 ml propan-2-ol added into each flask and the mixtures vacuum filtered to remove any unreacted solid LA. The propan-2-ol was finally removed by rotary evaporation at 45 ˚C for 2 h (Rotary evaporator RE200B, Bibby Sterilin Ltd., Pontypridd, UK).

2.2.1.2. Synthesis and purification of poly (propylene glycol -*co*- lactide) dimethacrylate (PGLA-DMA)

A. Synthesis of PGLA-DMA under different reaction conditions

Purified PGLA was dissolved in 50 ml dichloromethane at concentrations of 0.1 or 0.2 mol /L. To end-cap both ends with MA units, MAC and TEA (used as catalyst) were added whilst maintaining the temperature at 0 °C. The molar ratio of MAC to TEA was fixed at 1 but MAC to PGLA set as 2 or 4 (for details see Table 2.1). Synthesis of PGLA-DMA was repeated six times for each reaction condition to address synthesis reproducibility.

All reactions were performed in 250 ml three-neck round-bottom flasks equipped with a magnetic stirrer using a cooled Carousel 6 place reaction station (Radleys Discovery Technologies, Essex, UK). Two necks of each flask were fitted with a dropping funnel: one contained MAC and the other TEA (each dissolved in 25 ml dichloromethane). Both solutions were added

dropwise and simultanesouly into the PGLA / dichloromethane solution at a dripping rate of approximately 15ml/h. This was contrary to the previous report by Ho *et al*. in which MAC was added after all the TEA (Ho and Young 2006).

After complete addition of MAC and TEA, the reaction mixture was stirred for 2 h at 0 °C and then at room temperature (approximately 20 ˚C) for 24 h. A simplified synthesis procedure is shown in Fig. 2.2.

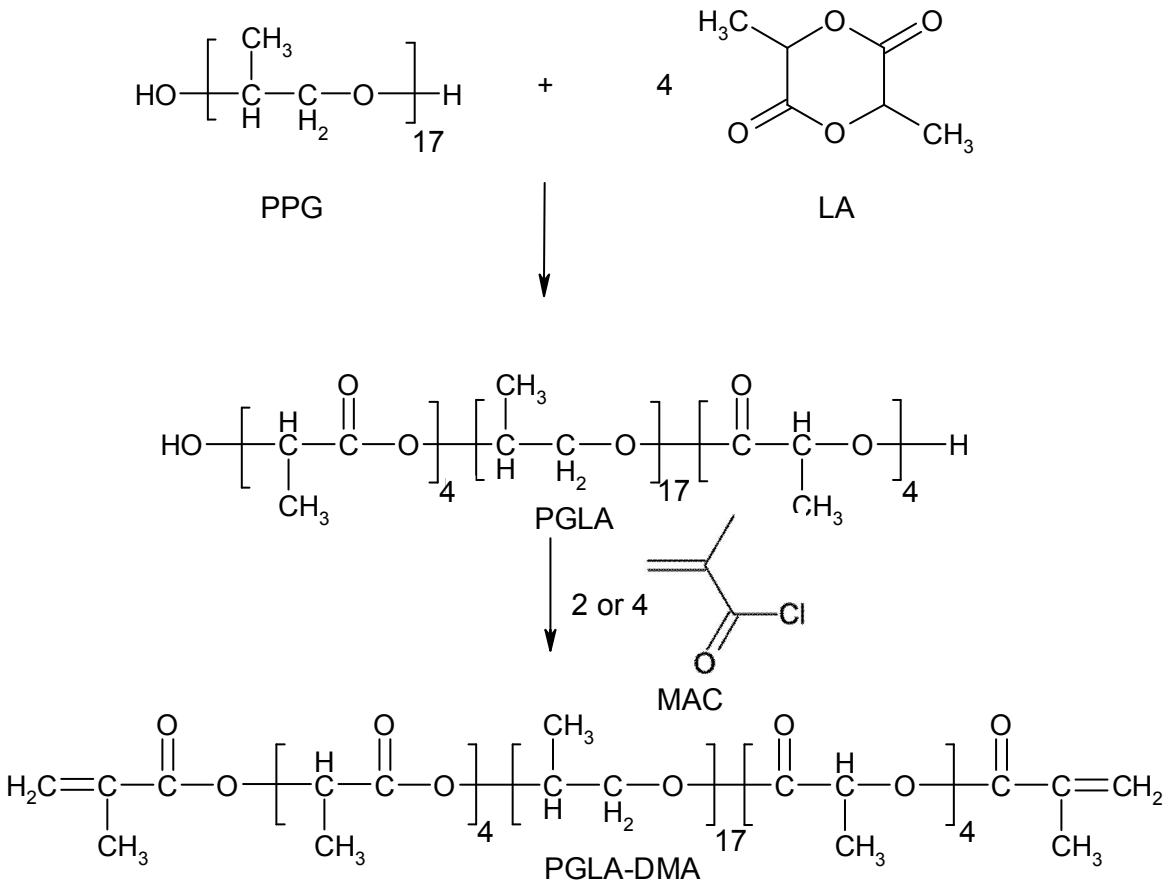

Fig. 2.2. Two-step synthesis of PGLA-DMA. PPG: poly (propylene glycol); LA: lactide; PGLA: poly (propylene glycol -*co*- lactide); MAC: methacryloyl chloride; PGLA-DMA: poly (propylene glycol -*co*- lactide) dimethacrylate.

B. Purification of PGLA-DMA

I. Primary purification using organic solvents

The mixture of PGLA-DMA and dichloromethane was filtered under vacuum to remove any large white crystals of TEA·HCl. Rotary evaporation at 45 ºC under vacuum for 15 - 20 min produced further TEA·HCl crystals that were removed. The filtrate was dissolved in 100 ml acetone, rotary evaporated at 45 ºC under vacuum for 15 - 20 min and filtered again. This acetone addition / filtration step was repeated three times. After the last wash, the mixture of PGLA-DMA with residual acetone was kept in a fume hood overnight to allow slow formation of TEA·HCl crystals of larger size for easier filtering. The mixture of PGLA-DMA and acetone was finally condensed via rotary evaporation under vacuum at 45 ºC for 2 h to remove residual acetone.

II. Further purification using aqueous acid and base

The following second additional stage was used by other goups (Shen *et al*. 2007), but not used in previous studies of PGLA-DMA synthesis (Ho and Young 2006). The resultant PGLA-DMA (40 g) was dissolved in 200 ml dichloromethane and then washed with 200 ml dilute HCl (0.1 mol/L). Aqueous HCl and PGLA-DMA in dichloromethane were separated using a separating funnel: the upper layer consisted of HCl solution with dissolved TEA·HCl and the bottom layer was a mixture of PGLA-DMA and dichloromethane. The bottom layer was washed several more times using 200 ml HCl until the pH of the upper layer was close to 7 (TEA·HCl solution was alkaline). The bottom layer was then washed using 200 ml $NaHCO_3$ (0.1 mol/L) two times to remove residual HCl. Finally, the mixture was washed with

200 ml double distilled H_2O twice to remove traces of $NaHCO_3$. Dichloromethane was finally removed by rotary evaporation under vacuum at 45 °C for 24 h.

2.2.2. Identification of synthesised monomers

The synthesised PGLA and PGLA-DMA were characterised using Fourier transform infrared (FTIR), Raman (see Appedix B for more details) and ^{1}H-nuclear magnetic resonance (NMR) spectroscopy. Peak assignment was aided by comparing spectra of the intermediates (PGLA) and the final products (PGLA-DMA) with those of the starting materials PPG, D,L-LA and MAC. FTIR, Raman and NMR were used to confirm the presence of different chemical groups in the synthesised products. NMR was additionally used to gain quantitative information on the chemical structure of PGLA and PGLA-DMA, i.e., the length of LA segments and the efficiency of MA attachment.

2.2.2.1. Fourier transform infrared (FTIR) spectroscopy

FTIR spectra were obtained using a Perkin Elmer series 2000 FTIR spectrometer with Spectrum software v 5.0.1 (Perkin-Elmer, Beaconsfield, UK) using resolution at 4 cm^{-1}, wavenumber between 500 and 4000 cm^{-1} and four scans per spectrum. All spectra were normalised using the PPG 'C-O' peak at 1088 cm^{-1}. The peak intensities due to other chemical groups then provided an indication of the level of that group relative to PPG.

2.2.2.2. Raman spectroscopy

Raman spectra were recorded using a Raman spectrometer fitted with a 633 nm laser (LabRAM HR, Horiba Jobin Yvon Ltd., Stanmore, UK). The instrument filter was set at 100%, hole at 300, slit at 150, grating at 1800 and microscope objective ×50. Exposure times for all samples were 10 s and the accumulation number set at 6. Background subtraction, normalisation and smoothing were performed using the Labspec software. All spectra were normalised using the 'C-H' peak at 1447 cm^{-1}. The peak intensities due to other chemical groups then provided an indication of the level of that group within the molecule.

2.2.2.3. Nuclear magnetic resonance (NMR) spectroscopy

NMR spectra were recorded using a 600 MHz Varian Unity INOVA spectrometer (Palo Alto, CA, USA) at 25 ºC using WILMAD® NMR tubes of diameter of 5 mm with deuterated chloroform ($CDCl_3$) or deuterated water (D_2O) as solvent. All spectra were normalised using the PPG 'CH_3' peak at 1.13 ppm. The peak areas due to other chemical groups then provided an indication of the level of that group within the molecule. NMR spectra were collected with assistance from Dr. Geoff Kelly.

2.2.3. Determination of methacrylation efficiency of PGLA-DMA synthesis

NMR spectra were used to quantify the methacrylation efficiency of PGLA-DMA synthesis. Peaks were first assigned to different chemical groups in an

NMR spectrum and then relative number of a chemical group R determined using:

$$R = \frac{A}{n} \qquad 2.1$$

where A is the areas assigned to a chemical group and n is the number of hydrogen atoms in that chemical group. For example any peak areas due to CH_3 groups were divided by 3.

Subsequently the number of LA molecules attached per molecule (m) was calculated using:

$$m = 17 \times \frac{R_{LA}}{R_{PPG}} \qquad 2.2$$

where LA and PPG represent any peak associated with LA or PPG groups respectively. The number 17 arises because this is the average number of propylene glycol units in PPG of 1000 g/mol molecular weight.

The MA end-capping efficiency (E_{MA}, %) was subsequently calculated using:

$$E_{MA} = \frac{17R_{MA}}{2R_{PPG}} \times 100 \qquad 2.3$$

2 is the optimal number of MA groups per molecule. Results of methacrylation efficiency were presented as the means ± standard deviation (SD), n=6. T-test was used to determine if effects of different synthesis conditions on methacrylation efficiency were statistically significant (SPSS 14.0 for Windows, SPSS, Inc., Chicago, Ill., USA). Statistical evaluation was performed with assistance from Ms Aviva Petrie (*sic passim*).

2.2.4. Determination of reaction yield of synthesised monomers

The reaction yield of PGLA (Y_1) and PGLA-DMA (Y_2) and overall synthesis yield (Y) were calculated using:

$$Y_1 \text{ or } Y_2 = \frac{M_{obt}}{M_{exp}} \times 100 \quad 2.4$$

$$Y = \frac{Y_1 \times Y_2}{100} \quad 2.5$$

where M_{obt} and M_{exp} are the obtained and expected mass of the product at each stage.

2.3. Results

The obtained intermediate product PGLA and final product PGLA-DMA were both colourless and “oil” like. The results of synthesised PGLA-DMA under different reaction conditions shown below are products after double purification. The difference in purity of products after primary and after further purification is presented in section 2.3.3.

2.3.1. Chemical structure of synthesised monomers

The FTIR spectra of PPG gave absorption peaks at 1447 and 1372 cm^{-1} due to ‘C-H’ groups and at 1088 cm^{-1} due to ‘C-O’ groups (see example in Fig. 2.3 and see PPG molecular structure in Fig. 2.2).

In the spectra of PGLA, these peaks remained and additional peaks at 1744 cm^{-1} due to LA ‘C=O’ groups and peaks at 1268 and 1184 cm^{-1} due to LA ‘C-O’ groups were present (see example in Fig. 2.3 and see PGLA molecular structure in Fig. 2.2). In addition, reduction in ‘O-H’ peak height at 3500 cm^{-1},

compared to PPG, was consistent with LA attachment to the PPG. The LA attachment to PPG was further confirmed by comparison of the NMR spectra of starting D,L-LA with those of PGLA. This is because the linear LA peaks in the PGLA NMR spectra are clearly separated from the PPG and are at high intensity (see below).

All spectra of PGLA-DMA were similar to those of PGLA with the exception of additional small peaks at 1719 and 1678 cm^{-1} due to MA 'C=O' groups, at 1640 cm^{-1} attributed to MA 'C=C' groups (see example in Fig. 2.3 and see PGLA-DMA molecular structure in Fig. 2.2). This was consistent with attachment of MA groups to PGLA.

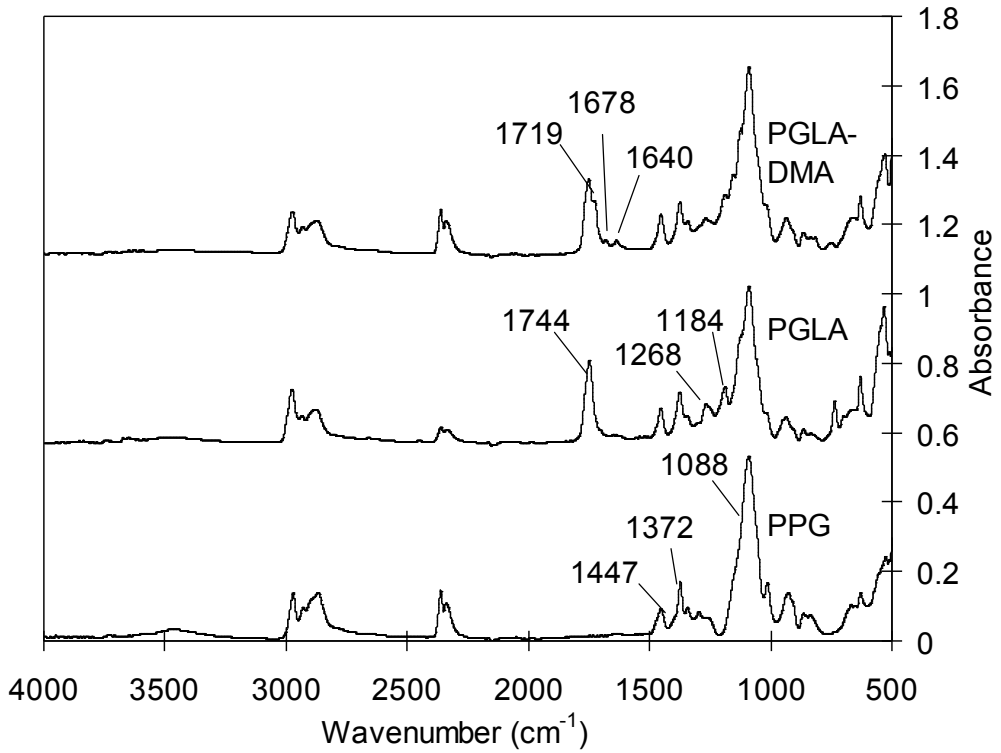

Fig. 2.3. FTIR spectra of PPG, PGLA and PGLA-DMA. PPG: poly (propylene glycol); PGLA: poly (propylene glycol -*co*- lactide); PGLA-DMA: poly (propylene glycol -*co*- lactide) dimethacrylate. The PGLA-DMA shown was synthesised under condition 'F4' (PGLA/dichloromethane of 0.2 mol/L and molar ratio of MAC to PGLA of 4 mol/mol, see Table 2.1 for details). Note the additional peaks at 1184, 1268 and 1744 cm^{-1} of PGLA and peaks at 1640, 1678 and 1719 cm^{-1} of PGLA-DMA indicating respectively attachment of LA to PPG and MA to PGLA.

Raman spectra of PPG, PGLA and PGLA-DMA also demonstrated attachment of LA to PPG and MA to PGLA (see example in Fig. 2.4). In the Raman spectra of PPG, the three main peaks at ~3000 cm^{-1} (i.e. 2975, 2940 and 2875 cm^{-1}) and the peak at 1447 cm^{-1} corresponded to 'C-H' groups. The spectra of PGLA were similar to those of PPG except for the presence of the peak at 1744 cm^{-1} due to LA 'C=O' group.

In all spectra of PGLA-DMA, additional peaks were present upon methacrylation. These included peaks at 1719 and 1678 cm^{-1} (both due to MA 'C=O' groups) and at 1640 cm^{-1} (due to MA 'C=C' groups).

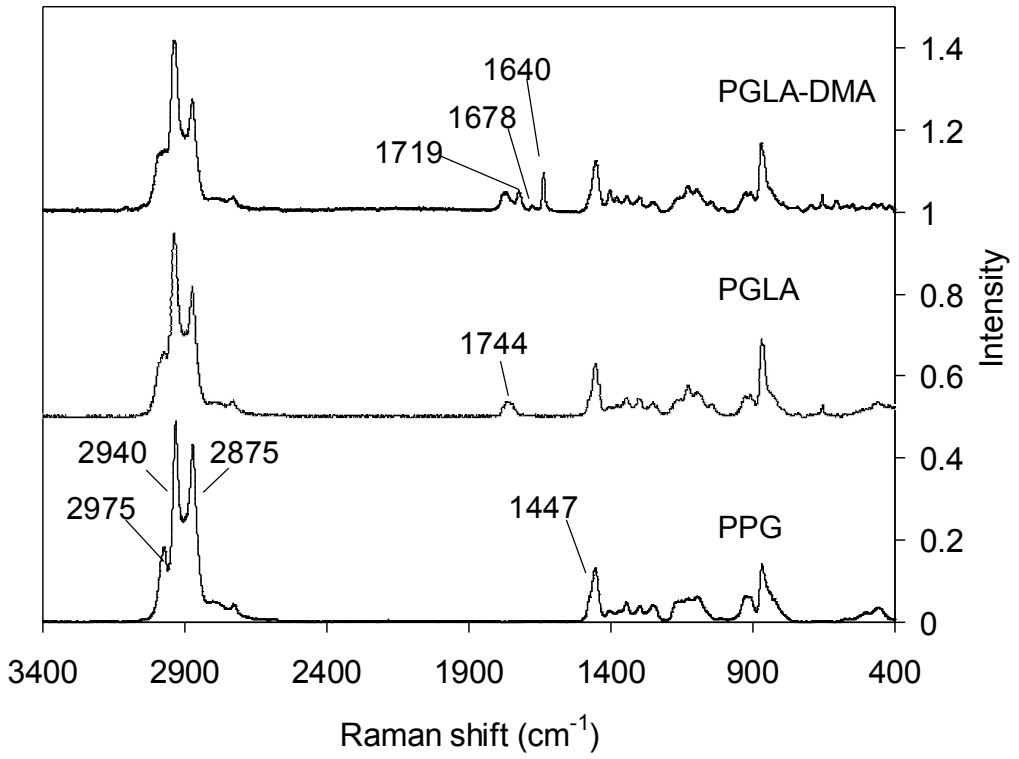

Fig. 2.4. Raman spectra of PPG, PGLA and PGLA-DMA. PPG: poly (propylene glycol); PGLA: poly (propylene glycol -*co*- lactide); PGLA-DMA: poly (propylene glycol -*co*- lactide) dimethacrylate. The PGLA-DMA shown was synthesised under conditions 'F4' (PGLA/dichloromethane of 0.2 mol/L and molar ratio of MAC to PGLA of 4 mol/mol, see Table 2.1 for details). Note the additional peaks at 1744 cm^{-1} of PGLA and peaks at 1640, 1678 and 1719 cm^{-1} of PGLA-DMA indicating respectively attachment of LA to PPG and MA to PGLA.

NMR spectra of PPG, PGLA and PGLA-DMA additionally provided evidence for attachment of LA to PPG and MA to PGLA (see example in Fig. 2.5.A).The PPG NMR spectra exhibited a broadened peak at 3.54* ppm caused by both

'CH' and 'CH_2' protons and a multiple peak at 1.13 ppm due to 'CH_3' protons. Peaks marked with '*' were used for NMR calculations.

In the PGLA spectra, new multiplets at 5.11* ppm (assigned to linear LA 'CH' protons in the chains) and at 4.35* ppm (assigned to LA 'CH' protons adjacent to the terminal 'OH' groups) appeared (see example in Fig.2.5.A). There are also new peaks at 1.54 ppm arising from the presence of linear LA 'CH_3' groups. Unreacted cyclic LA has a quartet at 5.09 ppm due to 'CH' protons and a doublet at 1.65 ppm due to 'CH_3' protons (Fig. 2.5.B). The difference in the spectra between liner LA and cyclic LA has suggested that the cyclic ring of LA has been opened and attached to the PPG.

All final PGLA-DMA spectra showed three additional peaks to those observed for the PGLA. Those at 6.21* and 5.64* ppm could be assigned to the protons attached to the MA 'C=C' bonds and those at 1.95 ppm to MA 'CH_3' protons. The NMR peaks of starting MAC have been slightly shifted, consistent with its attachment to LA (compare Fig. 2.5.B and A).

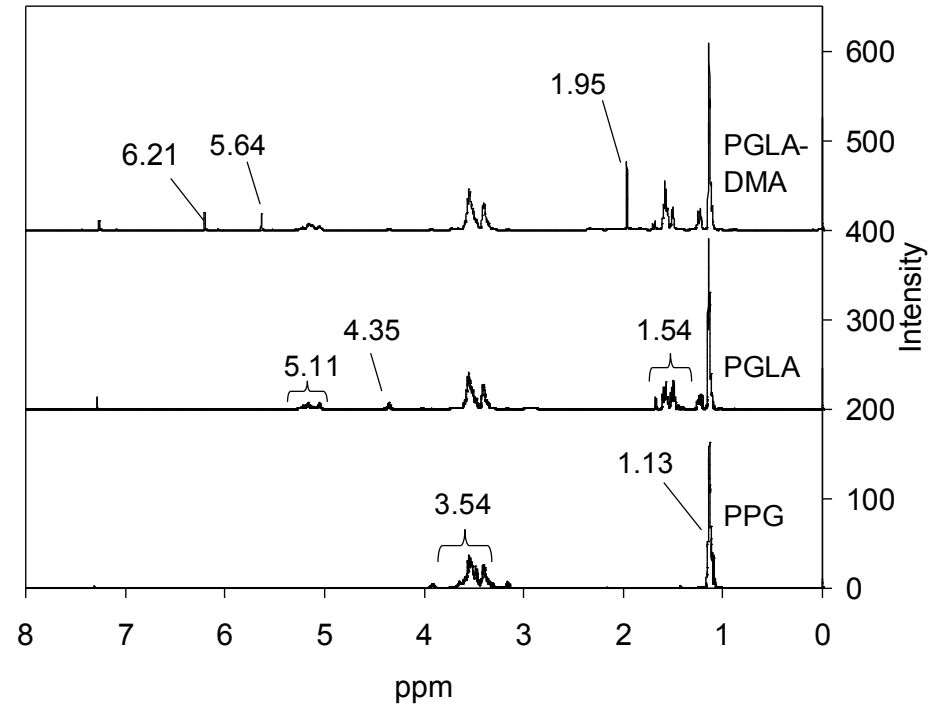

A

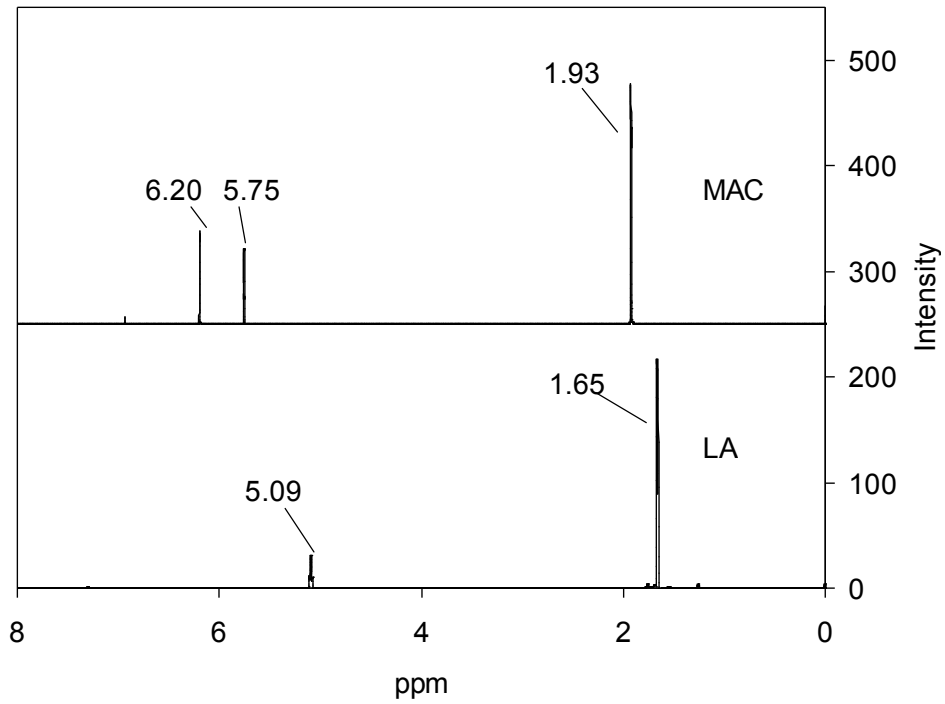

B

Fig. 2.5. A: NMR spectra of PPG, PGLA and PGLA-DMA. The PGLA-DMA shown was synthesised under conditions 'F4' (PGLA/dichloromethane of 0.2 mol/L and molar ratio of MAC to PGLA of 4 mol/mol, see Table 2.1 for details). B: NMR spectra of starting reagents D,L-LA and MAC. PPG: poly (propylene glycol); PGLA: poly (propylene glycol -*co*- lactide); PGLA-DMA: poly (propylene glycol -*co*- lactide) dimethacrylate; LA: lactide; MAC: methacryloyl chloride. Note the additional peaks around 1.54, 4.35 and 5.11 ppm of PGLA and peaks at 1.95, 5.64 and 6.21 ppm of PGLA-DMA indicating respectively attachment of LA to PPG and MA to PGLA.

2.3.2. Effect of reaction conditions on PGLA-DMA synthesis

2.3.2.1. Effect of reaction conditions on methacrylation efficiency

In order to improve methacrylation efficiency, two reaction variables (i.e., PGLA concentration in dichloromethane and molar ratio of MAC to PGLA) were investigated. PGLA concentration in dichloromethane had no experimentally significant effect on FTIR, Raman or NMR spectra (data not shown). Increase in the molar ratio of MAC to PGLA, however, clearly resulted in higher 'C=C' content per PGLA-DMA molecule (see example in Fig. 2.6, comparing F4 and F2 (with MAC/PGLA of 4 and 2 mol/mol respectively). FTIR spectra were not highly sensitive to 'C=C' group attachment (see example in Fig. 2.6.A). Raman spectra, however, were more sensitive in detecting 'C=C' group, and have demonstrated substantial increase in peak intensity at 1640 cm^{-1} (due to 'C=C') when the molar ratio of MAC to PGLA was increased from 2 to 4 mol/mol (see example in Fig. 2.6.B). Furthermore, NMR spectra of PGLA-DMA synthesised with higher molar ratio of MAC to PGLA showed obviously increased peak intensity at 5.64 and 6.21 ppm (due to 'C=C') (see example in Fig. 2.6.C).

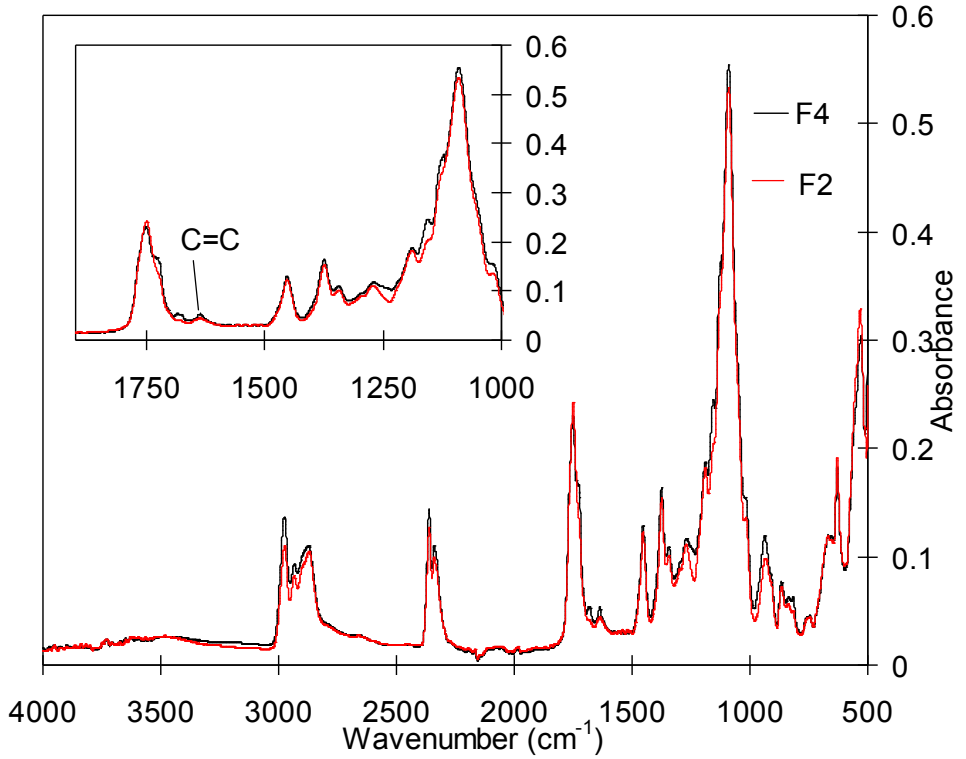
C=C
F4
F2
Absorbance
Wavenumber (cm-1)

A

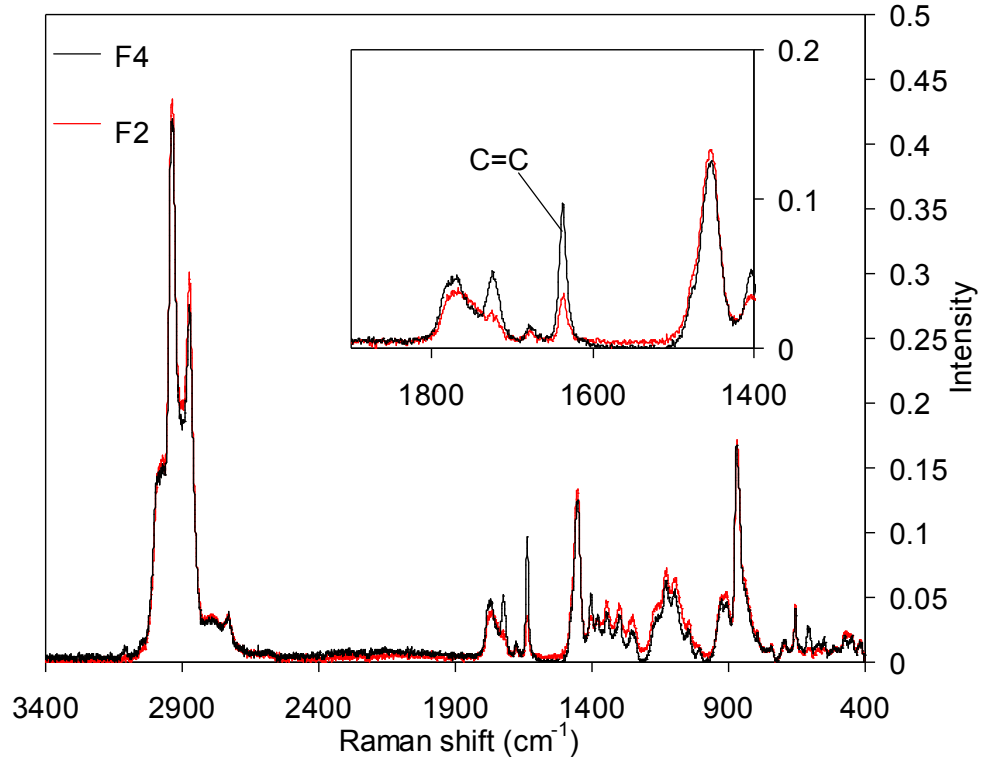
F4
F2
C=C
Intensity
Raman shift (cm-1)

B

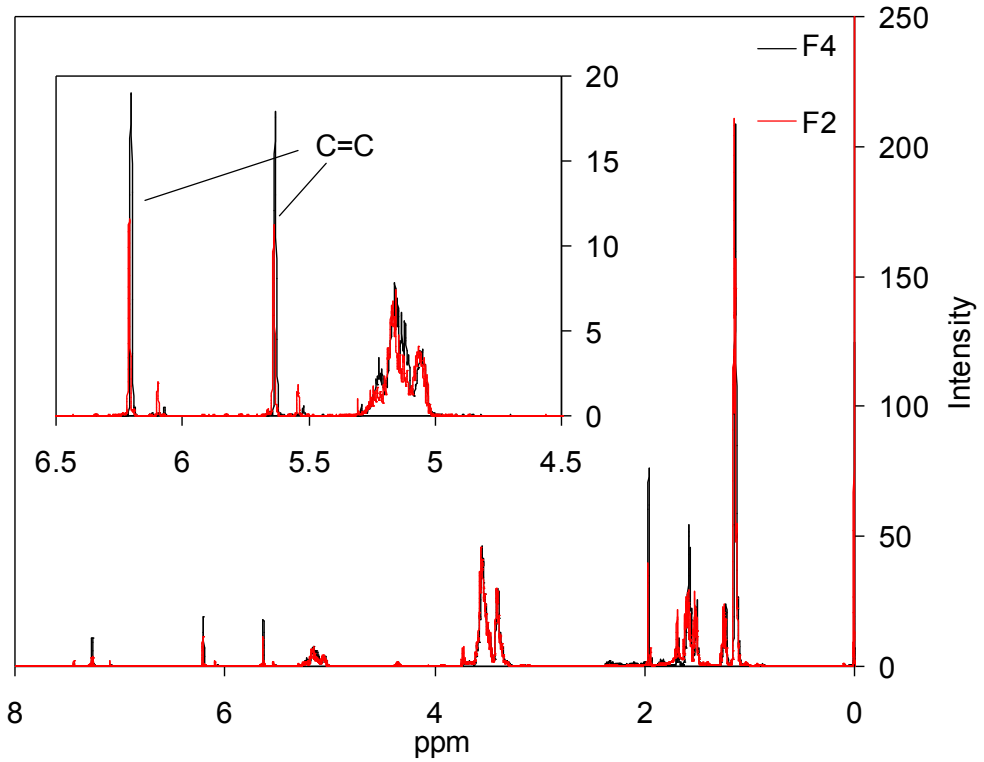

Fig. 2.6. FTIR (A), Raman (B) and NMR (C) spectra of PGLA-DMA synthesised under different reaction conditions. F2 = PGLA/dichloromethane of 0.2 mol/L and MAC/PGLA of 2 mol/mol; F4 = PGLA/dichloromethane of 0.2 mol/L and MAC/PGLA of 4 mol/mol. This figure illustrates how FTIR is less sensitive than Raman and NMR in detecting the 'C=C' group. Note the increase in the 'C=C' peak intensity with increase in the molar ratio of MAC/PGLA.

To quantify the effect of different reactions conditions on methacrylation efficiency, NMR calculations were used to determine the number of LA and MA groups in each PGLA-DMA molecule. It was found that the number of LA goups per PGLA-DMA molecule was 3.9, close to the expected value of 4 (Table 2.1.A). The number of MA groups per PGLA-DMA molecule varied depending on the synthesis conditions. The average number of MA groups attached to PGLA increased in the order: F1, F2 (1.3) < F3, F4 (1.9) (Table 2.1.A). There was no significant difference in the methacrylation efficiency

when the PGLA concentration in dichloromethane was 0.1 or 0.2 mol/L (Table 2.1.B). However, the methacrylation efficiency substantially increased when the molar ratio of MAC to PGLA increased from 2 to 4 mol/mol ($p<0.05$) (Table 2.1.B).

2.3.2.2. Effect of reaction conditions on reaction yield

The reaction yield for the synthesis of PGLA was as high as 96 %, as reported by Ho and Young (Ho and Young 2006). The reaction yield for the synthesis of PGLA-DMA was lower, between 65 and 78%. The overall yield therefore ranged between 63 and 75% (Table 2.1.A). The yield of PGLA-DMA synthesis significantly increased when the PGLA concentration in dichloromethane increased from 0.1 or 0.2 mol/L ($p<0.05$) (Table 2.1.B). The molar ratio of MAC to PGLA however had no measurable effect on the yield of PGLA-DMA (Table 2.1.B).

Table 2.1.A. Effect of reaction conditions on methacrylation efficiency and reaction yield of PGLA-DMA synthesis.

Formulations	Synthesis conditions		m_{LA}	m_{MA}	E_{MA} (%)	Observed formula	Y_1 (%)	Y_2 (%)	Y (%)
	PGLA in dichloromethane (mol/L)	MAC/PGLA (mol/mol)							
F1	0.1	2	3.9	1.3±0.1	65±5	$PPG_{17}LA_{3.9}MA_{1.3}$	96	70±4	67±4
F2	0.2	2	3.9	1.2±0.1	60±5	$PPG_{17}LA_{3.9}MA_{1.2}$	96	78±5	75±4
F3	0.1	4	3.9	1.9±0.1	95±5	$PPG_{17}LA_{3.9}MA_{1.9}$	96	65±5	63±4
F4	0.2	4	3.9	1.9±0.1	95±5	$PPG_{17}LA_{3.9}MA_{1.9}$	96	75±5	72±4

m_{LA} and m_{MA} are the number of LA and MA groups per PGLA-DMA molecule (see Eq. 2.2). E_{MA} is the methacrylation efficiency (see Eq. 2.3). The expected PGLA-DMA formula was $PPG_{17}LA_4MA_2$. Y_1 and Y_2 are the reaction yield of synthesis of PGLA and PGLA-DMA respectively (see Eq. 2.4). Y is the overall reaction yield (see Eq. 2.5). Data are presented as the means ± SD, n=6.

Table 2.1.B. Statistical evaluation in methacrylation efficiency and reaction yield of PGLA-DMA synthesis under different reaction conditions.

	Methacrylation efficiency					Reaction yield			
Reaction conditions	F1	F2	F3	F4	Reaction conditions	F1	F2	F3	F4
F1			*	*	F1		*		*
F2			*	*	F2	*		*	
F3	*	*			F3		*		*
F4	*	*			F4	*		*	

*significant difference between the values of corresponding formulations.

2.3.3. Effect of different solvents on PGLA-DMA purification

NMR spectra of PGLA-DMA after primary purification using organic solvents alone showed a quartet at 3.05 ppm (due to 'CH_2') and a triplet at 1.24 ppm (due to 'CH_3') attributed to residual TEA·HCl ($(CH_3CH_2)_3N$·HCl) crystals (see example in Fig. 2.7). These peaks could also be observed in the NMR spectra of PGLA-DMA after secondary purification (using aqueous acid and base) but at much lower intensity (see example in Fig. 2.5, PGLA-DMA). These results have demonstrated that the concentration of TEA·HCl in further purified PGLA-DMA was reduced compared to that in the primary purified PGLA-DMA.

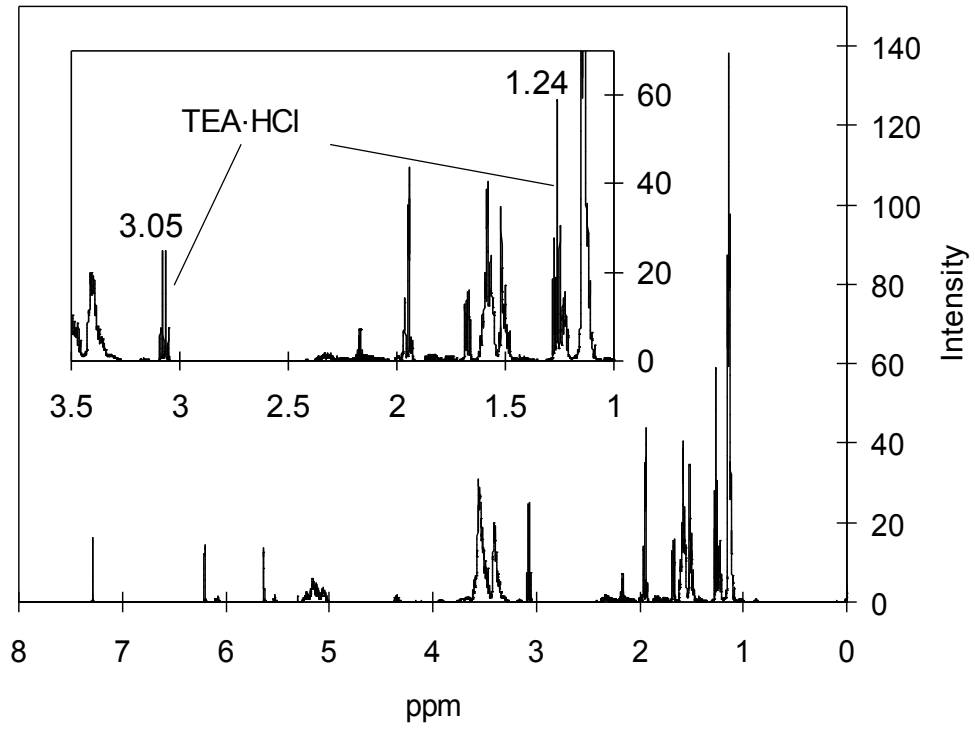

Fig. 2.7. NMR spectrum of an example PGLA-DMA after primary purification. TEA·HCl: triethylamine hydrochloride. Note the presence of TEA·HCl (impurity).

2.4. Discussion

The synthesis procedure used in this project was found to be successful in attaching LA to PPG and MA to PGLA. Effects of different reaction conditions on PGLA-DMA synthesis and effects of different solvents on PGLA-DMA purification were analysed.

2.4.1. Effect of reaction conditions on PGLA-DMA synthesis

2.4.1.1. Effect of reaction conditions on methacrylation efficiency

This study increased the methacrylation efficiency of PGLA from 80 (see previous report (Ho and Young 2006)) to >90%. The major difference in the synthesis procedure in the current study compared with the previous work was the order of addition of MAC and TEA. Previously TEA was added prior to MAC whereas in this new study, the two reagents were added at the same time. The reason for the increased methacrylation efficiency is unclear but might be because of the reduction of some side reactions between MAC and TEA (found in other studies, data not shown). If TEA was added first, its high concentration might enhance its ability to form by-products with MAC thereby lowering the probability of MA attachment to PGLA.

In addition, PGLA concentration in dichloromethane was found to have no measurable effect on the methacrylation efficiency. However, increase in the molar ratio of MAC to PGLA from 2 to 4 mol/mol markedly improved the methacrylation efficiency from 63 to 95%. This indicates that an excess of MAC and TEA is required in order to gain good MA attachment efficiency. The

high monomer methacrylation efficiency will enable higher crosslinking density upon polymerisation and thus potentially improved mechanical properties.

2.4.1.2. Effect of reaction conditions on reaction yield

This study had also increased the average reaction yield of PGLA-DMA synthesis from 60 (see previous report (Ho and Young 2006)) to 75%. The higher reaction yield might be a partial consequence of changing the order of MAC and TEA addition. The two reagents were added at the same time in the present study, which might reduce the probability of side reactions between MAC and TEA, thereby increasing the reaction yield (see section 2.4.1.1 for more details).

In addition, the reaction yield of PGLA-DMA synthesis increased with the increase in PGLA concentration in dichloromethane. The high reaction yield is advantageous due to improved time and cost effectiveness. Molar ratio of MAC to PGLA however had no effect on the reaction yield.

2.4.2. Effect of different solvents on PGLA-DMA purification

The primary purification using organic solvents could remove the bulk of the produced TEA·HCl crystals, as reported previously (Ho and Young 2006). Additional washing with dilute HCl, $NaHCO_3$ solution and double distilled water, however, was found to improve removal of small crystals of TEA·HCl.

In summary, the optimal preparation procedure to synthesise and purify PGLA-DMA is illustrated below:

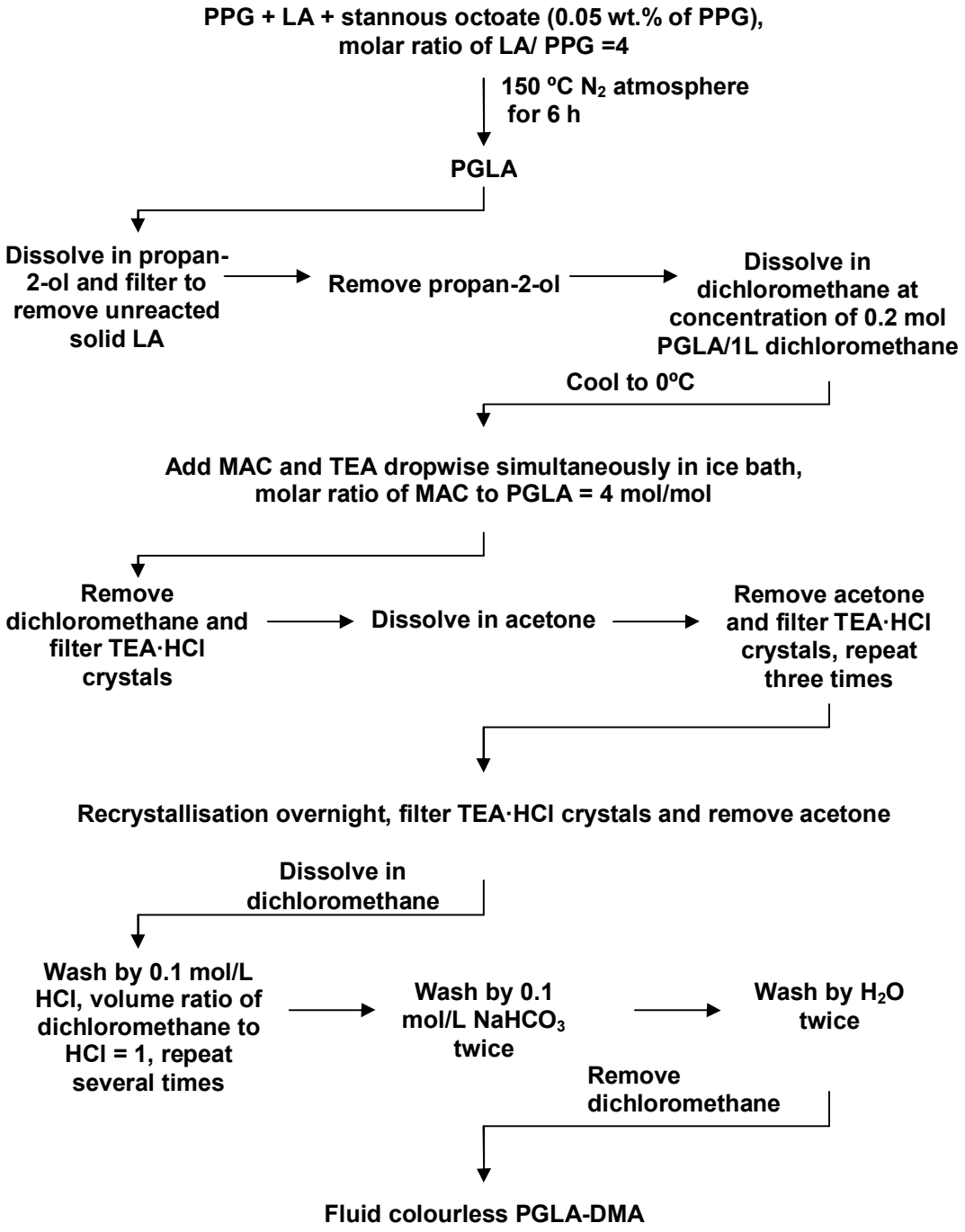

Fig. 2.8. Flow chart of preparation of PGLA-DMA. PPG: poly (propylene glycol); LA: lactide; PGLA: poly (propylene glycol -*co*- lactide); TEA·HCl: triethylamine·hydrochloride; PGLA-DMA: poly (propylene glycol -*co*- lactide) dimethacrylate.

2.5. Conclusion

The PGLA-DMA synthesised in this study was fluid and colourless with chemical structure as expected. Methacrylation efficiency and reaction yield were improved via varying synthesis conditions. Purification level was also enhanced by using aqueous acid and base in addition to organic solvents.

Chapter 3

Composite Preparation and Characterisation

Abbreviations

In alphabetical order

CAM	chorioallantoic membrane
CPC	calcium phosphate cement
CQ	camphorquinone
DCP	dicalcium phosphate
DMA	dynamic mechanical analyser
DMEM	Dulbecco's modified Eagle's medium
DMPT	*N,N*-dimethyl-*p*-toluidine
EDAX	energy dispersive X-ray analysis
FBS	fetal bovine serum
FTIR	Fourier transform infrared
F%	filler content
HA	hydroxyapatite
HEMA	hydroxyethyl methacrylate
IC	ion chromatography
MCPM	monocalcium phosphate monohydrate
M_d	MCPM particle size
PBS	phosphate buffered saline
PGLA-DMA	poly (propylene glycol -*co*- lactide) dimethacrylate
SD	standard deviation
SEM	scanning electron microscope
SQRT	square root
TCP	tricalcium phosphate
T/M	molar ratio of β-TCP/MCPM
XRD	X-ray diffraction

3.1. Introduction

Synthetic poly (propylene glycol -*co*- lactide) dimethacrylates (PGLA-DMA) are fluid and rapidly photo-polymerisable (Ho and Young 2006). The set materials, however, have a relatively low modulus as well as a slow degradation rate, and produce acid during degradation. These characteristics may, respectively, cause concerns of insufficient functional support, impedance of new tissue growth (Rizzi *et al.* 2006) and potential inflammatory response *in vivo* (Walton and Cotton 2007), if PGLA-DMA is used as bone adhesives (used to connect fractured bone) or fillers (used to fill bone defects).

In the present study, β-tricalcium phosphate (β-TCP) and monocalcium phosphate monohydrate (MCPM) particles were incorporated into PGLA-DMA as fillers to fabricate composite materials. Although addition of filler particles may reduce the rate and level of PGLA-DMA polymerisation (Xia and Cook 2003), it was expected that the composite materials could have improved mechanical, degradation, acid production and biological properties over the unfilled polymer (Cai *et al.* 2009;Peter *et al.* 1998).

β-TCP and MCPM are reactants of brushite forming calcium phosphate cement (CPC) (Bohner 2007). It was felt that the water-induced setting of β-TCP and MCPM directly within the polymer might increase the homogeneous dispersion of the particles throughout the polymer and improve the material mechanical properties. Reactants that produce brushite rather than hydroxyapatite (HA) were

used due to the higher aqueous solubility of brushite at physiological pH (7.2 ~ 7.4) (Bohner 2001). Brushite therefore dissolves faster than HA providing higher phosphate and calcium concentration in solution (Agrawal and Athanasiou 1997). These phosphate and calcium ions are essential for bone re-mineralisation (Bohner 2000;Bohner *et al.* 2005;Hofmann *et al.* 2009), and can also buffer acid produced (Linhart *et al.* 2001). Furthermore, the much faster setting of brushite CPC compared with that of HA CPC is likely to be beneficial in a set polymer within which reaction kinetics will be substantially hindered.

The first aim of this study was therefore to examine any possible deleterious effect on photo-polymerisation due to the filler addition and to characterise any water-sorption induced changes in the filler chemistry. Additionally, the effect of filler addition on material modulus, degradation, phosphate and calcium ion release as well as acid release (indicative of buffering capacity of filler) were investigated. Finally, biocompatibility (*in vitro* and *in vivo*) of the PGLA-DMA based composite materials was assessed. These results were combined to determine whether these composite materials have potential to be used as bone adhesives or fillers. Parts of this work were published in *Acta Biomaterialia* in 2010 (Zhao *et al.* 2010).

3.2. Materials and methods

3.2.1. Fabrication of composite materials

The organic phase of the composite materials consisted of PGLA-DMA (90 wt.%), camphorquinone (CQ, 1 wt.%, as photo-initiator), *N,N*-dimethyl-*p*-toluidine (DMPT, 1 wt.%, as accelerater to enable photo-polymerisation) and hydroxyethyl methacrylate (HEMA, 8 wt.%, to aid dispersion of CQ and DMPT). The inorganic phase (i.e. filler) was a mixture of β-TCP and MCPM. There were three variables in the filler type including filler content (F%, 70, 60 or 50 wt.%), molar ratio of β-TCP to MCPM (T/M, 4, 2 or 1) and MCPM particle size (M_d, 90, 60 or 30 μm) (see Table 3.1 for details of different formulations). Variation in F% could have influence on the material polymerisation rate (Xia and Cook 2003) and mechanical properties (Iisaka 1976;Lee *et al.* 2007;Witt and Cizek 1954). Change in T/M could result in different chemical composition of calcium phosphates after reaction and thus degradation, phosphate and calcium ion release, pH compensation capability and biocompatibility. Alteration in M_d could affect the material mechanical properties (Iisaka 1976;Lee *et al.* 2007;Witt and Cizek 1954). Factorial analysis was used in this study to determine the level of effect of each of these variables on different material properties including photo-polymerisation, modulus, degradation, pH compensation ability and biocompatibility (see section 3.2.4 for details). This was undertaken to aid material optimisation.

The organic phase was then mixed with the filler and the resulting composite mixtures moulded using steel rings, with top and bottom surfaces covered by acetate sheets (3M AF 4301, Manchester, UK). These were then cured in a light box (Triad® 2000™ visible light cure system, Dentsply Trubyte, Palo Alto, USA) using blue light exposure (100 mW/cm^2) for 12 min, to produce solid discs (12 mm diameter, 2 mm thick, unless otherwise stated). Polymer discs without filler were used as control. Raman spectroscopy was then used to confirm full polymerisation (i.e. no detectable peak at 1640 cm^{-1} due to 'C=C' in PGLA-DMA) (Ho and Young 2006) and the density of the set samples was measured to confirm negligible air incorporation (i.e. the practical density was identical to the calculated theoretical density within experimental error). Each test was performed in triplicate, and the results were expressed as means ± standard deviation (SD).

3.2.2. Characterisation of composite materials

3.2.2.1. Polymerisation kinetics

The unset material was placed on a Golden Gate™ heated diamond top-plate at 37 ºC, within a Perkin-Elmer Series 2000 Fourier transform infrared (FTIR) spectrometer with Timebase software. The paste was confined within a ring of 5 mm diameter and 2 mm depth, and sealed with acetate sheet. FTIR spectra of the lower few microns of the sample in contact with the diamond were generated over the range between 500 and 4000 cm^{-1} at a resolution of 4 cm^{-1} every 8 s for 30 min. At 40 s each mixture was exposed to blue light (400 mW/cm^2) for 120 s using a dental light curing gun (Coltene®, Sussex, UK).

Before and after the 30 min FTIR analysis, all formulations were examined using Raman spectroscopy (LabRam HR Raman spectrometer, Horiba Jobin Yvon, Stanmore, UK). This instrument was equipped with a 633 nm wavelength laser, x 50 objective lens and 1800 grating. All spectra were background subtracted and normalised by the 'C-H' peak at 1447 cm^{-1}. The fraction of the monomer remaining, P, was determined as the ratio of the final to the initial height of the monomer Raman peaks at 1640 cm^{-1}, attributed to 'C=C' stretches of PGLA-DMA (Ho and Young 2006).

The monomer conversion percentage (Q_t) was then quantified using:

$$Q_t = \frac{[\Delta A_t - \Delta A_0]}{[\Delta A_f - \Delta A_0]} \times (1 - P) \qquad 3.1$$

where ΔA_t, ΔA_0, ΔA_f are the difference in the absorbance at 1716 and 1736 cm^{-1}, respectively, at time t, initially and finally. FTIR spectra exhibited maximum spectral change during light curing at 1716 cm^{-1} (absorbance loss) and at 1736 cm^{-1} (absorbance gain) due to the changes in the chemical environment of the methacrylate 'C=O' bond. Polymerisation rate (%/s) was defined as the slope of the linear region of 'Q_t versus light exposure time' curve (Q_t between 20 and 60%).

3.2.2.2. Water induced chemical changes

The light cured composite specimens (12 mm diameter, 2 mm thick) were soaked statically in 10 ml of deionised water (pH = 7, adjusted by 0.01mol/l NaOH) at 37 ºC. Specimens after 24 h and 12 weeks of water immersion were collected and

air dried at room temperature for chemical characterisation by Raman and X-ray diffraction (XRD) spectroscopy. During the 12-week storage period, the solution was changed weekly to avoid saturation of degradation products (e.g., Ca^{2+} and PO_4^{3-}) in the storage solution.

A. Raman

In order to characterise the chemical changes of specimens before and after 24 h and 12 weeks of water immersion, Raman maps (×2) of an area (100 × 100 μm) of the core (transverse section) of each specimen were obtained at a step size of 5 μm, using a 633 nm laser, x 50 objective and 1800 grating. Exposure times for each single-point spectrum were 10 s and the accumulation number set at 6. Each single-point spectrum was recorded and the chemical composition maps were generated using LabRam software. The mean Raman spectra were obtained following background subtraction and normalisation using the polymer 'C-H' peak at 1447 cm^{-1}. The peak intensities due to other components then provide an indication of the level of that component relative to the polymer (Ho and Young 2006;Mehdawi *et al.* 2009). Standard Raman spectra of the polymer, β-TCP, MCPM, brushite and monetite were also recorded for comparison.

B. XRD

XRD was additionally used to identify the presence of different crystalline calcium phosphate in the specimen. The specimens were cut transversely and the new surfaces generated examined. XRD spectra were obtained using a Brüker D8 advance diffractometer (Karlsruhe, Germany), with Ni filtered Cu Kα radiation.

Data were collected from 10° to 100° 2θ with a step size of 0.02° in a count time of 18.9 s using a Bruker Lynx Eye detector. In addition to the International Centre for Diffraction Data database volumes 1, spectra of starting chemicals of β-TCP and MCPM were used to assign peaks of different calcium phosphates. XRD analysis was performed with assistance of Prof. Jonathan Knowles (*sic passim*).

3.2.2.3. Compressive modulus

Specimens (5 mm diameter, 2 mm thick) were analysed before and after placement in 2.5 ml of neutral deionised water at 37 ºC for 24 h, 1, 4 and 7 days and then weekly up to 10 weeks. At each time point, the storage solution was replaced with fresh 2.5 ml of deionised water. The variation of polymer and composite compressive modulus with time was characterised using a dynamic mechanical analyser (DMA 7e, Perkin Elmer Instruments, Bucks, UK, see Appendix B for more information).

In this test, a linearly increasing quasi-static stress was applied to the specimen on a parallel plate incorporating a 10 mm probe. An increasing static force from 10 mN to 8000 mN was applied to the sample at a constant rate of 500 mN/min. The resultant displacement in strain was plotted against the applied stress, and the modulus (E) was calculated as the slope of the initial linear portion (0.1-0.2 MPa) of the stress-strain curve using Pyris TM version 5 software.

3.2.2.4. Hydrolytic degradation

Each set specimen disc (12 mm diameter, 2 mm thick) was placed upright in the conical end of a Sterilin® 30 ml polystyrene container (Sterilin Ltd., Caerphilly, UK) in which 10 ml of neutral deionised water was added. Each specimen was then incubated in the storage solution at 37 °C for 0, 30 min, 1, 2, 4, 8, 24 h, 2, 4, 7 days, 2, 3, 4, 5, 7, 9, 10 and 12 weeks. At each time point, the mass and density of each disc were measured using an electronic balance with a density kit (Mettler Teledo, Osaka, Japan) prior to replacement in fresh storage solution for measurement at the next time point. The storage solution at different time points was also used for the subsequent ion and acid release study (see section 3.2.2.5 for details).

The mass change at time t (ΔW_t) due to combined water sorption and material loss was calculated using:

$$\Delta W_t = \frac{W_{a,t} - W_{a,0}}{W_{a,0}} \times 100 \qquad 3.2$$

where $W_{a,t}$ and $W_{a,0}$ are the wet mass (measured in air) of the specimen at time t and the initial dry mass (prior to water immersion) respectively.

The specimen density at time t, ρ_t, was determined using:

$$\rho_t = \rho_w \times \frac{W_{a,t}}{W_{a,t} - W_{w,t}} \qquad 3.3$$

where ρ_w is the density of water at the operating temperature and $W_{w,t}$ is the wet mass (measured in water) of the specimen at time t.

The volume change (ΔV_t) of the specimen at time t was thus determined using:

$$V_t = \frac{W_{a,t}}{\rho_t} \quad 3.4$$

$$\Delta V_t = \frac{V_t - V_0}{V_0} \times 100 \quad 3.5$$

where V_t and V_0 are the wet volume of the specimen at time t and the initial dry volume (prior to water immersion) respectively.

Additionally, the water content at 24 h, w, and the final mass loss at 12 weeks, m, of the polymer and composites were determined using:

$$w = \frac{W_{s,t} - W_{d,t}}{W_{d,t}} \times 100 \quad 3.6$$

where $W_{s,t}$ and $W_{d,t}$ are the swollen and dry mass of the specimen after 24 h of immersion in water. The dry specimens were obtained after vacuum drying at room temperature to constant mass.

$$m = \frac{W_{a,0} - W_{d,f}}{W_{a,0}} \times 100 \quad 3.7$$

where $W_{a,0}$ is the initial dry mass of the specimen prior to water immersion and $W_{d,f}$ is the final dry mass of the specimen after 12 weeks of immersion in water. The dry specimens were obtained after vacuum drying at room temperature to constant mass.

3.2.2.5. Ion and acid release

Phosphate and calcium release were monitored using ion chromatography (IC, see Appendix B for more information) with Chromeleon® software (Dionex, Surrey, UK). To measure PO_4^{3-} concentration, an ICS2500 system equipped with an AS50 autosampler and an EG50 eluent generator system was used. The mobile phase was a 30 mM KOH solution with a flow rate of 1.5 ml/min and 10 min running time. An ASRS®-300 (4 mm) column mounted in an AS50 thermal compartment and an ASRS suppressor was used. Ca^{2+} was measured on a Dionex ICS1000 system equipped with an AS50 autosampler, using 20 mM methylsulphonic acid as the mobile phase at a flow rate of 1 ml/min with a CSRS ULTRA (4 mm) column and a CAES suppressor. The running time was also 10 min. Calibration was obtained with standard solutions containing 1, 10, 25, 50 and 100 ppm of PO_4^{3-} or Ca^{2+}. An injection loop of 25 µl was used. The pH of the collected solutions was determined using a pH meter (Jenway 3340, Essex, UK).

3.2.2.6. Biocompatibility

A. In vitro biocompatibility

In vitro biocompatibility was examined using the MG-63 osteosarcoma cell line, which has previously been widely employed as an *in vitro* test model for assessing the effects of many types of biomaterials (Lee *et al.* 2003;Price *et al.* 1997). The cells were cultured in polystyrene flasks in Dulbecco's modified Eagle's medium (DMEM) supplemented with 10% fetal bovine serum (FBS), 50 IU/ml of penicillin and 50 µg/ml of streptomycin (termed 'full culture medium') at

37 °C in a humidified atmosphere of 5% CO_2 in air. Sub-confluent cells (70 - 80% confluence) were passaged by using trypsin-EDTA (0.25% (w/v) trypsin, 1 mmol/l EDTA).

In this test, the set polymer and composite discs (13 mm diameter, 2 mm thick) were sterilised under UV light (254 nm) for 30 min and placed into 15 ml NUNC™ centrifuge tubes (Thermo Fisher Scientific, Loughborough, UK) and incubated in 10 ml of 'full culture medium (defined in section 3.2.2.6 A)' at 37 °C for 24 h. This was to eliminate the burst acid release due to the dissolution of acidic MCPM and to remove any possibly deleterious products initially present in the materials (i.e. photo-initiators) (Pagoria *et al.* 2005). This 24-h pretreatment could also allow full reaction of β-TCP and MCPM. The preconditioned discs were then placed into individual wells of 24 well tissue culture plates (Thermo Fisher Scientific, Loughborough, UK). 1 ml of MG-63 cell suspension (1 x 10^4 cells/ml) was then added to each well and incubated at 37 °C.

To determine cell proliferation, after 3 days of culture, 100 µl of alamarBlue™ dye (see Appendix B for more information) was added to each well and incubated for a further 4-h period. Fluorescence measurements (excitation wavelength of 530 nm and emission wavelength of 590 nm) were then made using a Fluroscan Ascent plate reader (Labsystems, Helsinki, Finland). Relative cell viability was calculated as the ratio of the fluorescence intensity of the reduced alamarBlue™ caused by the cells proliferating on the material surface compared with that by

the cells growing on the control Thermanox™ plastic coverslips (NUNC™, Thermo Fisher Scientific, Loughborough, UK), defined as 100%.

In a parallel study, to observe cell and material surface morphology, after 3 days of incubation, the specimens were washed with phosphate buffered saline (PBS) and fixed using 3% (v/v) gluteraldehyde in 0.1 mol/l sodium cacodylate buffer for 24 h. The specimens were finally dehydrated in a graded series of ethanol (50, 70, 95 and 100% x 3) for 10 min each, immersed in hexamethyldisilazane for 2-3 min, air-dried for 3 h, mounted and coated with gold/palladium (Polaron E5000 sputter coater, Quorum Technologies, Sussex, UK). Cell and material surface morphology was then examined by scanning electron microscopy (SEM, JEOL JSM-5410LV, Tokyo, Japan) at an accelerating voltage of 15 kV. Concurrently, elemental analysis of the crystal precipitation on different material surfaces was determined using energy dispersive X-ray analysis (EDAX, Inca 300, Oxford Instruments, UK) combined with SEM. The average P/Ca ratio of the precipitated crystals was obtained from 10 readings.

B. In vivo biocompatibility

The *in vivo* biocompatibility of the set materials was evaluated using a chick embryo chorioallantoic membrane (CAM) model (see Appendix B for more information) as previously described (Groessnerschreiber *et al.* 1992). The composite formulation with F = 50%, T/M =1 and M_d = 30 µm was selected for this test due to its high phosphate and calcium release and buffering capacity

(see section 3.3.5). Additionally, its fluidity facilitates the production of thin films as required for this test. The fully polymerised composite films (100 µm thick) were cut into strips (4 mm long, 1 mm wide) and sterilised using 70% ethanol for 1 min prior to implantation.

Femurs were isolated from fertilised eggs (J.K. Needle and Co., Herts, UK) after 14 days of incubation at 39 ºC. Soft tissue was removed from the femur and a small defect (up to the bone marrow cavity and 4 mm long) was made manually with a tip of a needle (25G, BD Microlance**,** Benelux, Belgium) in the middle of the femur. The periosteum was only disrupted at the defect site. The films were implanted sagittally and gently tapped with forceps into the prepared defect so that the surface of the film and the femur were level. The femur and film was then placed onto the CAM of a 7 day old host egg which had previously been 'windowed' at day 3 (Andacht *et al.* 2004). The windows were sealed with tape and the host eggs incubated at 39 ºC for a further 7 days. Two non-implanted femurs (control) and four test femurs with a strip in each were placed in the host eggs (two femurs per egg).

After 7 days, the femurs were collected and fixed with 4% paraformaldehyde for 24 h, washed with PBS prior to dehydration in ascending concentrations of ethanol (70 x 2, 95 and 100% x 2, each concentration for 1 h), then cleared in xylene for 1 h (x 2) and finally embedded in wax for 80 min. Transverse 8 µm sections were cut, placed on a glass slide and heated on a hotplate at 60 ºC for

10 min to fix the tissue to the glass slide. The samples were then immersed in xylene for 5 min (x 2) to remove wax and rehydrated in descending ethanol concentrations (100 x 2 and 50%, each concentration for 1 min) and water (1 min) and stained with 1% toluidine blue for 1 min.

The slides were then washed with water, dried with blotting paper, immersed in 100% ethanol for 10 s, xylene for 10 s and mounted with cover glass using DPX mounting medium.

To determine any gross cytotoxicity due to the contact between the implant and the CAM, two composite strips were placed directly onto the CAM of a 7 day old host egg (one strip per egg), and incubated at 39 ºC for a further 7 days. Images were finally captured using a Leica DFC320 digital camera attached to a Leica MZ75 binocular microscope (Leica AG, Heerbrugg, Switzerland).

The *in vivo* study was performed with assistance of Dr. Paul Buxton and was approved under the UK Home Office Animals (Scientific Procedures) Act 1986.

3.2.3. Statistical evaluation

The statistical significance of differences between the polymer and the composites in various material properties was evaluated using one-way ANOVA. If the values of a property were homogeneously distributed, the Bonferroni post hoc test would be used. Data were evaluated using SPSS 14.0 for Windows

(SPSS, Inc., Chicago, Ill., USA). The results were expressed as means ± SD, and p values <0.05 were considered statistically significant.

3.2.4. Factorial analysis

Factorial analysis (see details in Appendix C) was used in this study to assess the effect of the three variables (F%, T/M and M_d) on different material properties (P in Eq. 3.8) including photo-polymerisation, compressive modulus, degradation, phosphate and calcium release, pH compensation ability and *in vitro* biocompatibility. An appropriate factorial expression in this case would be (Ho and Young 2006;Young and Ho 2008):

$$\ln P = <\ln P> \pm a_{F\%} \pm a_{T/M} \pm a_{M_d} \qquad 3.8$$

where <lnP> is the average value of lnP for all 8 possible formulation combinations excluding the intermediate formulation (see Table 3.1 for details). The intermediate formulation is used to check the validity of Eq. 3.8. When Eq. 3.8 is valid, the P of intermediate formulation should equal to the geometric mean of P of all 8 formulations. a_i indicates the level of an effect that a variable (e.g., F%) has on a material property (e.g, polymerisation rate). A positive 'a value' means that the property increases with increasing variable and vice versa for negative a_i. Higher values of a_i indicate greater effects of the variable on a property. a_i for each term was determined using:

$$a_i = \frac{1}{2}\ln\left[\frac{P_H}{P_L}\right] \qquad 3.9$$

where P_H and P_L are the geometric means of a property of all samples with the variable, e.g., F%, at its high (H) (e.g., 70%) and low level (L) (e.g., 50%) respectively. Values of a_i were determined in triplicate, and results expressed as means ± SD.

3.3. Results

The unset composites with F% = 50 and 60% were fluid whereas formulations with F% = 70% were thicker and 'paste-like' (did not spread when placed on a flat surface).

3.3.1. Polymerisation kinetics

In all samples, polymerisation began almost immediately when the curing light was turned on (see example in Fig. 3.1). The average polymer polymerisation rate was 1.6 %/s (Table 3.1). The average composite polymerisation rate was 1.7 %/s for composites with F% = 50% (C_{F50}, i.e., formulations 6-9), 1.6 %/s for C_{F60} (formulation 5) and 0.9 %/s for C_{F70} (formulations 1-4), respectively (Table 3.1). There was no significant difference in polymerisation rate between the polymer and the C_{F50} or C_{F60} but high F% (i.e., F% = 70%) resulted in significantly slower polymerisation rate ($p<0.05$). For all samples, over 85% of the monomer could be converted after light curing for 120 s and 100% degree of monomer conversion (i.e. full polymerisation) could be achieved within 200 s (see example in Fig. 3.1). Factorial analysis confirmed that the polymerisation rate was affected strongly and only by F%, with higher F% leading to slower polymerisation rate (Table 3.2).

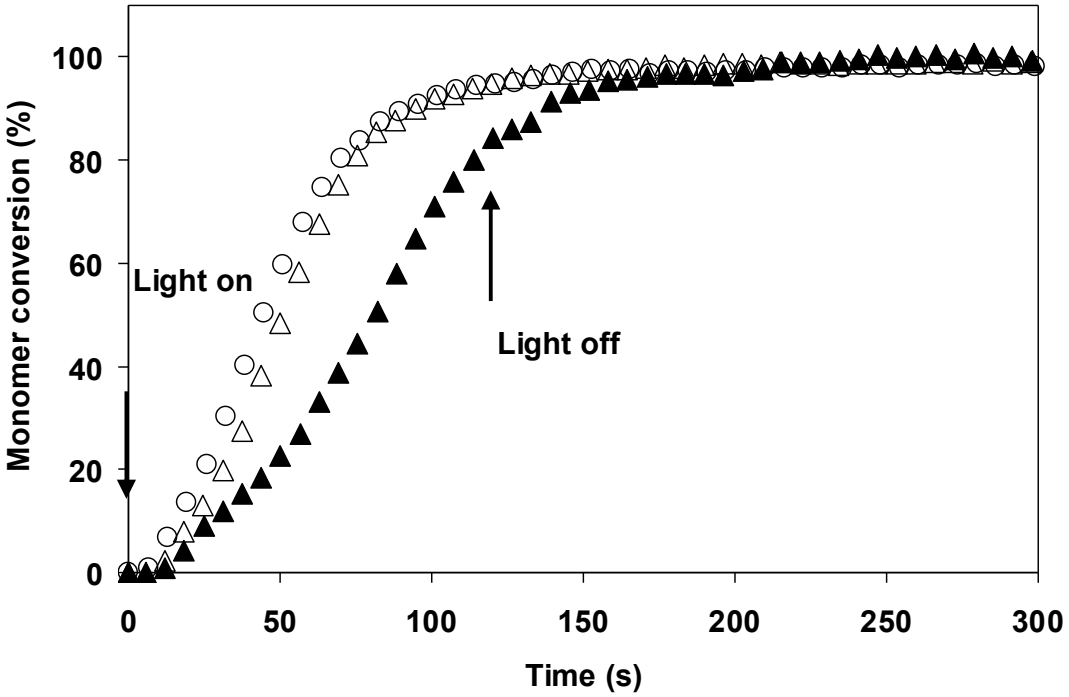

Fig. 3.1. Example polymer and composite monomer conversion versus time. ○ polymer, Δ F% = 50%, T/M =1, M_d = 30 μm, ▲ F% = 70%, T/M =1, M_d = 30 μm. The results demonstrate the decline in rate (gradient of the linear region of the plot between 20 and 60% conversion) with higher filler content.

Table 3.1. Polymerisation rate, compressive modulus, initial water content and final material loss of composites and polymer.

Formulations		F% (%)	T/M	M_d (μm)	q (%/s)	E_0 (MPa)	E_{24} (MPa)	$-\Delta E_{24}$ (%)	E_f (MPa)	w (%)	m (%)
Composites	1	70	4	90	0.9±0.2*	**27 ± 4***	9 ± 1*	67 ± 3*	7 ± 1*	10±1*	4±1
	2	70	4	30	1.0±0.2*	**21 ± 4***	10 ± 1*	52 ± 7*	8 ± 1*	10±1*	4±1
	3	70	1	90	0.9±0.2*	**21 ± 4***	7 ± 1	67 ± 9*	6 ± 1*	16±1*	**12±1***
	4	70	1	30	0.9±0.2*	**27 ± 3***	8 ± 1	70 ± 8*	7 ± 1*	15±1*	**12±1***
	5	60	2	60	1.6±0.2	15 ± 1*	9 ± 1*	40 ± 4*	6 ± 1*	11±1*	6±1*
	6	50	4	90	**1.7±0.3**	12 ± 2*	9 ± 1*	33 ± 4*	5 ± 1*	6±1*	4±1
	7	50	4	30	**1.6±0.3**	15 ± 1*	10 ± 1*	33 ± 3*	7 ± 1*	6±1*	4±1
	8	50	1	90	**1.6±0.3**	12 ± 2*	7 ± 1	42 ± 5*	5 ± 1*	10±1*	**9±1***
	9	50	1	30	**1.7±0.3**	14 ± 3*	8 ± 1	43 ± 9*	6 ± 1*	10±1*	**10±1***
	Polymer				1.6±0.3	9 ± 4	7 ± 1	9 ± 4	3 ± 1	3±1	3±1

F% (filler content), T/M (molar ratio of β-TCP to MCPM) and M_d (MCPM particle size) are three variables involved in the composite filler factorial design. With three variables (F%, T/M and M_d), each at two levels, high (e.g. F%=70%) and low (e.g. F%=50%), plus one intermediate level (e.g. F%=60%), there are nine formulations. Formulation 5 is defined as intermediate formulation (a formulation with all variables (i.e., F%, T/M and M_d) at their intermediate level (i.e., 60%, 2 and 30 μm respectively). q = polymerisation rate; E_0 = initial dry compressive modulus prior to immersion in water; E_{24} = compressive modulus after 24 h of immersion in water; $-\Delta E_{24}$ = reduction in modulus after 24 h of water immersion relative to the original dry compressive modulus; E_f = final wet compressive modulus after 10 weeks of immersion in water; w = water content of specimens after 24 h of immersion in water (see Eq. 3.6); m = final material loss at 12 weeks (see Eq. 3.7). Results = means ± SD (n=3). * significant differences ($p<0.05$) from the control values (i.e. polymer).The best results are marked in bold.

Table 3.2. 'a terms' demonstrating the effect of filler variables on properties of composite materials.

Filler variable / Material property	$a_{F\%}$	$a_{T/M}$	a_{Md}
Polymerisation rate	-0.3±0.1	-	-
Initial dry compressive modulus	0.3±0.1	-	-
Reduction in modulus after 24 h of water immersion	0.2±0.1	-0.1±0.04	-
Initial water content	0.3±0.1	-0.3±0.1	-
Final material loss	0.1±0.04	-0.5±0.1	-
PO_4^{3-} release at 24 h	0.3±0.1	-0.6±0.1	0.1±0.05
Long-term PO_4^{3-} release	0.7±0.1	-0.5±0.1	-
Ca^{2+} release at 24 h	0.1±0.02	-0.5±0.1	0.2±0.1
Long-term Ca^{2+} release	0.6±0.1	-0.3±0.1	-
pH of storage solution between 2 and 24 h	-0.1±0.04	0.1±0.05	-
pH of storage solution between 24 h and 12 weeks	0.1±0.1	-0.1±0.02	-
Relative cell viability	0.1±0.04	0.3±0.1	-

F% (filler content), T/M (molar ratio of β-TCP to MCPM) and M_d (MCPM particle size) are three variables involved in the filler design. The results shown are 'a values' calculated using Eq. 3.9. Results = means ± SD (n=3). The magnitude of the 'a' value and its sign indicate the size and direction of the effect of each variable on a material property. A positive 'a value' means that the property increases with increasing variable and vice versa for negative 'a'. Higher values of 'a' indicate greater effects of the variable on a property. '-' means the effect of a variable on a property is negligible.

3.3.2. Chemical changes before and after water immersion

3.3.2.1. Raman

A. Average Raman spectra

No characteristic 'C=C' peak at 1640 cm^{-1} was observed in any of the polymer and composite Raman spectra, consistent with full monomer conversion after light exposure. Inorganic Raman peaks were easier to distinguish in composites with higher filler content and, due to the relatively small areas (100 x 100 μm) examined, more reproducible with smaller MCPM particle size. The major factor affecting changes in the average Raman spectra with time was T/M.

I. Formulations with excess β-TCP

With T/M = 4, β-TCP peaks (main peaks at 945, 970 and 1045 cm^{-1}) dominated the average Raman spectra before (0 h) and after specimen immersion in water for 24 h and 12 weeks (see example in Fig. 3.2.A). MCPM (main peaks at 903, 915 and 1108 cm^{-1}) was just observable in the 0-h Raman spectra but not detectable in the 24-h and 12-week Raman spectra. Peaks due to dicalcium phosphate (DCP, in its hydrated brushite or anhydrous monetite form) were, however, difficult to detect in the 24-h and 12-week Raman spectra although small regions of DCP could be observed in the Raman maps (see section 3.3.2.1.B). Raman spectra of polymer, β-TCP, MCPM, brushite and monetite standards are shown in Fig. 3.2.C.

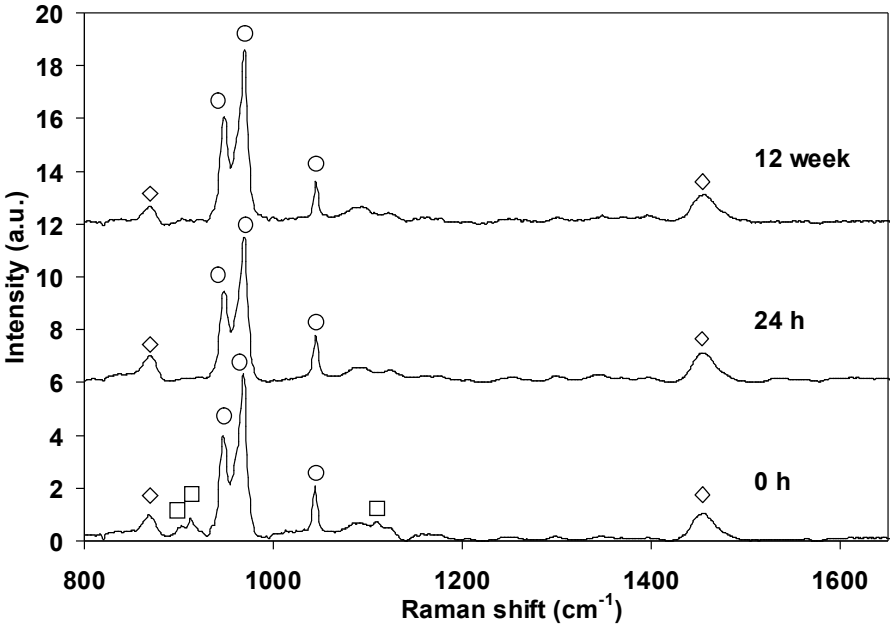
Intensity (a.u.)
Raman shift (cm-1)
12 week
24 h
0 h

A

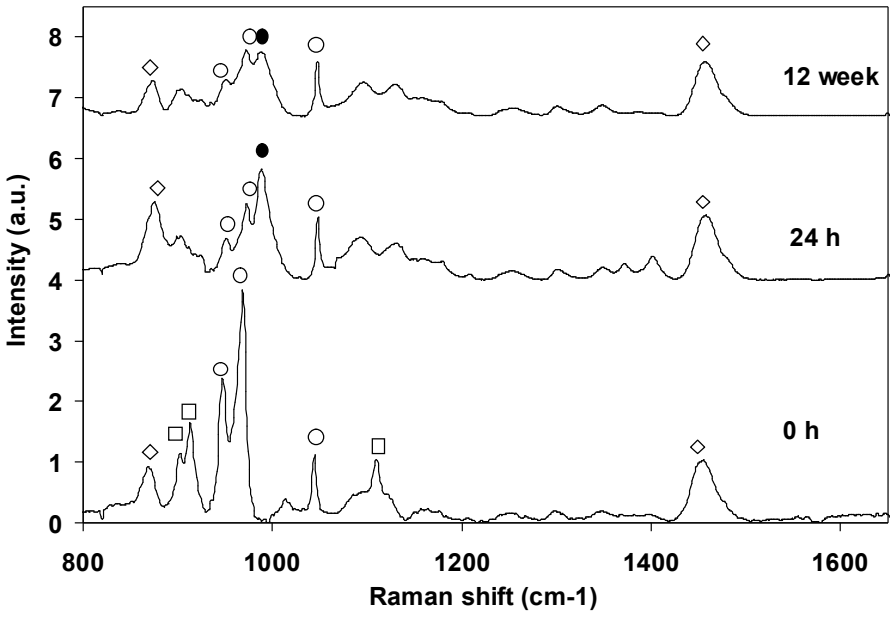
Intensity (a.u.)
Raman shift (cm-1)
12 week
24 h
0 h

B

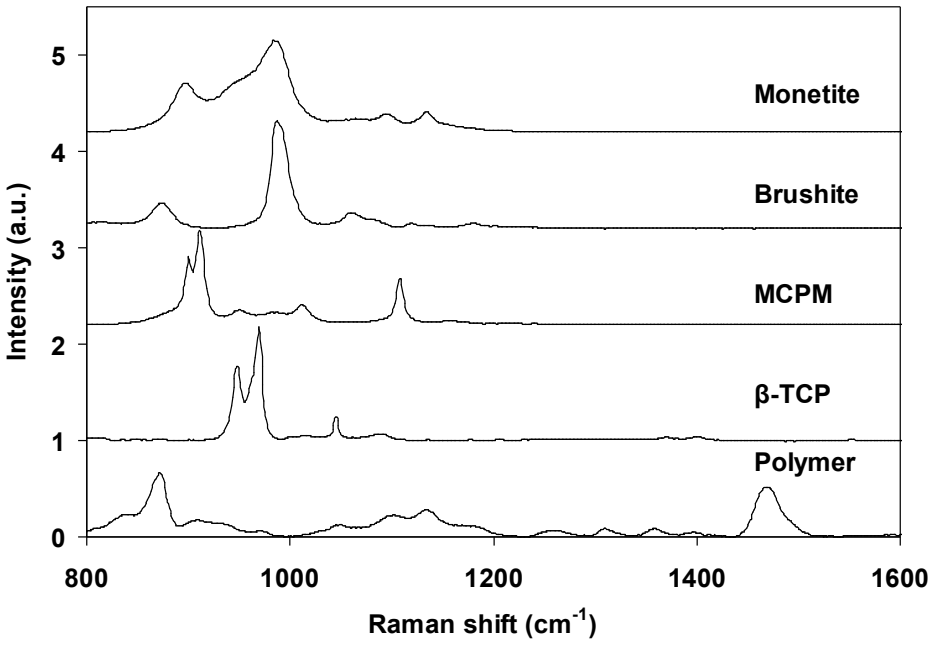

C

Fig. 3.2. Raman spectra of an example composite with F% = 70%, T/M = 4 and M_d = 30 µm (A) and an example composite with F% = 70%, T/M = 1 and M_d = 30 µm (B) before (0 h) and after 24-h and 12-week immersion in water. ◊ polymer, ○ β-TCP, □ MCPM, ● dicalcium phosphate, i.e., hydrated brushite or anhydrous monetite. C: Raman spectra of standards including the set polymer, β-TCP, MCPM, brushite and monetite. Note the absence of MCPM and presence of dicalcium phosphate after composite (T/M=1) immersion in water for 24 h.

ii. Formulations with equimolar β-TCP and MCPM

Conversely, with equimolar β-TCP and MCPM (T/M=1), peaks in the average Raman spectra due to both β-TCP and MCPM could readily be detected in dry samples (see example in Fig. 3.2.B). Following 24-h water immersion, the β-TCP peak intensity reduced dramatically and MCPM peaks vanished. A peak at 980 cm^{-1} attributed to DCP could be observed. In the following 12 weeks little change occurred in the level of β-TCP but the level of DCP was markedly reduced.

The above results have demonstrated that β-TCP and MCPM had reacted and precipitated as DCP, i.e., brushite and monetite in 24 h, with higher initial MCPM amount resulting in greater DCP formation. The resultant DCP had largely dissolved into the sample storage solution after 12 weeks.

B. Raman maps

In Raman maps, different colours indicate different chemical components. When the components are well separated on the micron scale the area occupied by a given colour provides an indication of the amount of the component the colour represents. Raman maps also provide information regarding the dimensions of each chemical component.

I. Formulations with excess β-TCP

Before specimen immersion in water, the β-TCP (red) and MCPM (pink) were dispersed throughout the fully polymerised polymer (blue) and were readily distinguishable in the Raman maps (see example in Fig. 3.3.A.i). The area

occupied by β-TCP was larger than that by MCPM as expected, with the particles size of β-TCP smaller than that of MCPM.

After 24-h storage in water, the β-TCP was still clearly distinguished but the MCPM was not detectable. Additional small areas representing DCP (green), brushite and monetite, were present (see example in Fig. 3.3.A.ii).

After 12-week water immersion, β-TCP was still the major calcium phosphate remaining in the samples but the area occupied by DCP was reduced (see example in Fig. 3.3.A.iii).

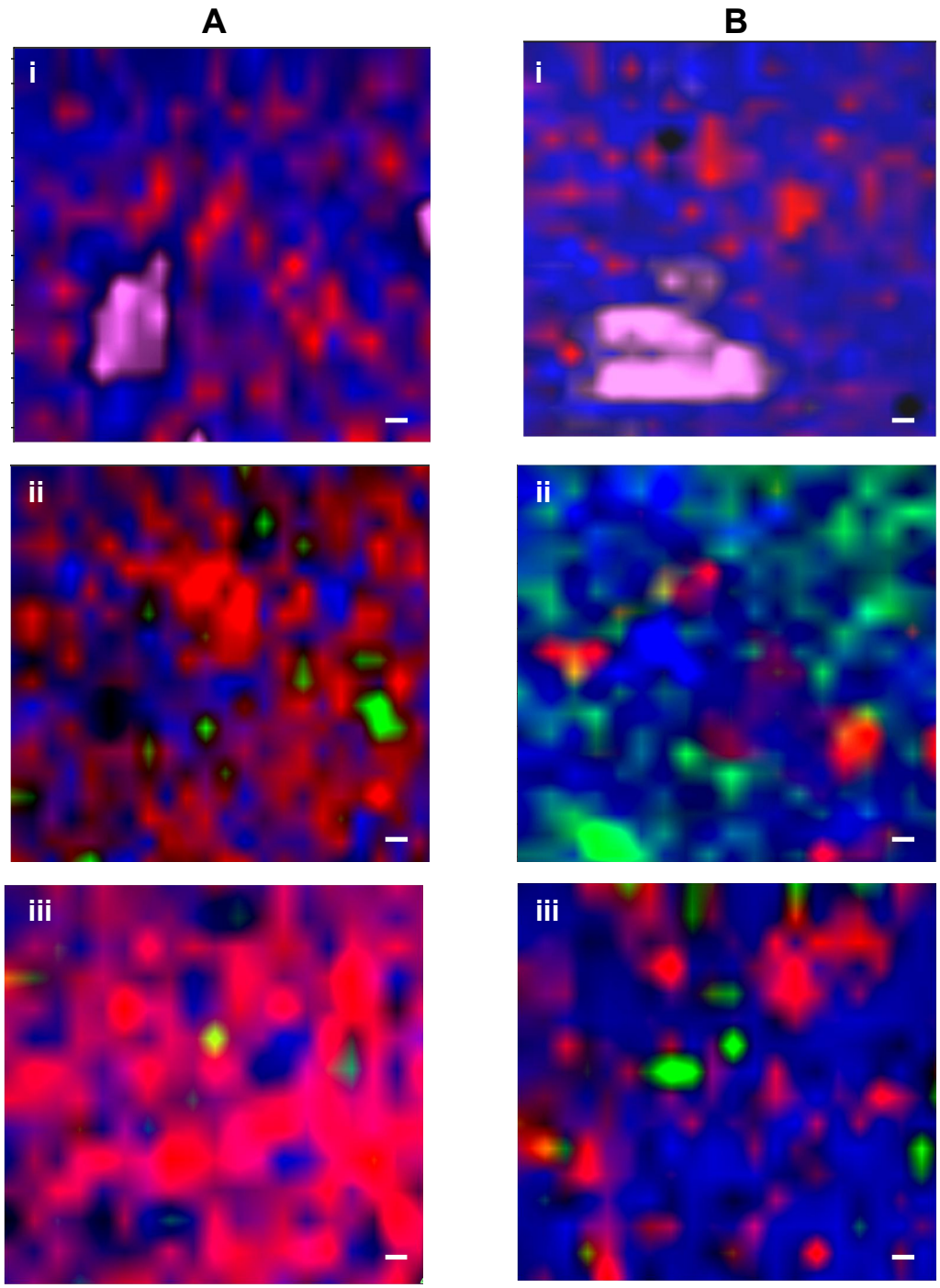

Fig. 3.3. Raman maps of representative composite A: F% = 70%, T/M = 4 and M_d = 30 μm and B: F% = 70%, T/M = 1 and M_d = 30 μm before (0 h, i) and after 24-h (ii) and 12-week (iii) water immersion. Blue stands for polymer, red for β-TCP, pink for MCPM, green for dicalcium phosphate, i.e., brushite and monetite. Scale bars = 5 μm. Note the absence of MCPM and presence of dicalcium phosphate after composite immersion in water for 24 h.

II. Formulations with equimolar β-TCP and MCPM

Before the specimen immersion in water, the β-TCP (red) and MCPM (pink) were dispersed throughout the fully polymerised polymer (blue) and were readily distinguishable in the Raman maps (see example in Fig. 3.3.B.i).

After 24-h immersion in water, the area occupied by β-TCP decreased noticeably and the MCPM had vanished (see example in Fig. 3.3.B.ii). Instead, large amounts of small particles identified as DCP (green) had appeared.

After 12-week water immersion, β-TCP was the major calcium phosphate remaining in the samples. The area indicative of DCP was reduced compared with that in the 24-h Raman maps (see example in Fig. 3.3.B.iii).

The Raman spectra and Raman maps exhibited consistent results although both the average Raman spectra and the Raman maps could not distinguish brushite from monetite clearly because of the overlap of their peaks (see Fig. 3.2.C, compare brushite and monetite peaks). However, brushite and monetite could be distinguished by comparison of each of the point spectrum in a Raman map with the brushite and monetite standards.

3.3.2.2. X-ray diffraction (XRD)

XRD studies were consistent with the Raman data but additionally enabled brushite and monetite to be more readily quantified and distinguished. Moreover, XRD spectra could be more representative as the examination

covered the whole specimen surface whereas Raman maps only covered small areas (100 x 100 μm).

A. Formulations with excess β-TCP

As expected, XRD spectra of the dry formulations were dominated by β-TCP (main peaks at 27.9, 31.2 and 34.5 º2θ) and MCPM (main peaks at 23 and 24.3 º2θ) was just detectable (see example in Fig. 3.4.A). After 24-h immersion in deionised water, the β-TCP peaks remained but the MCPM peaks disappeared. Brushite (main peaks at 12, 21 and 29.4 °2θ) and monetite (main peaks at 26.7 and 30.3 º2θ) became visible in the spectra. After the specimens were placed in water for 12 weeks, β-TCP and monetite peaks remained but brushite peaks vanished. XRD spectra of standards of β-TCP, MCPM, brushite and monetite are shown in Fig. 3.4.C.

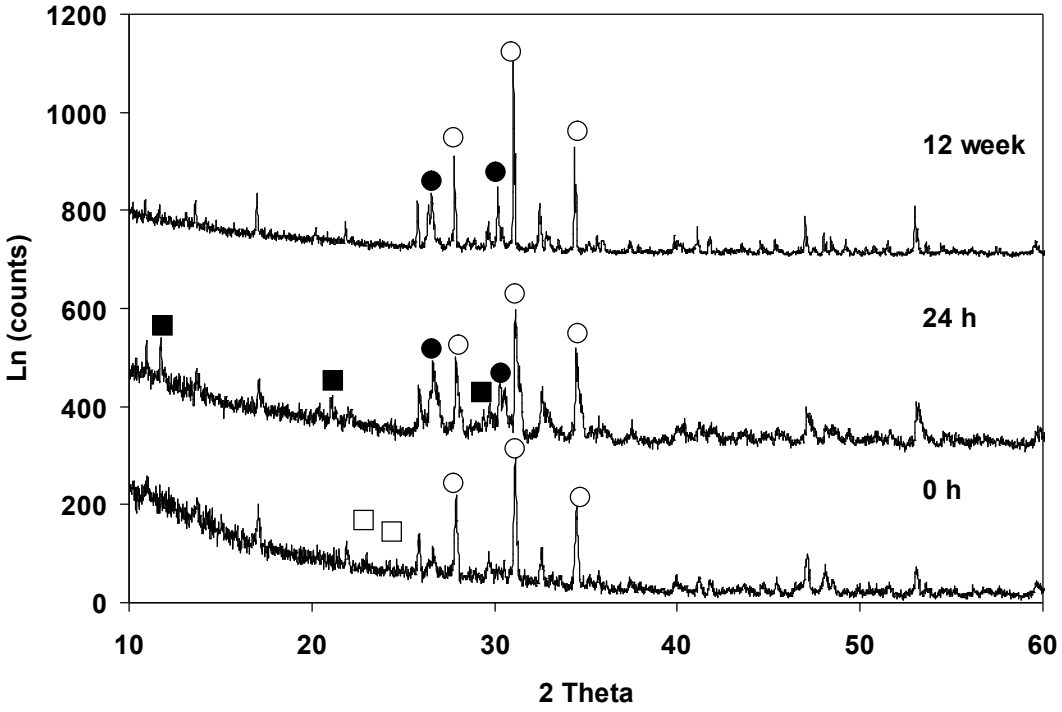
1200
1000
800
600
400
200
0
Ln (counts)
12 week
24 h
0 h
10
20
30
40
50
60
2 Theta

A

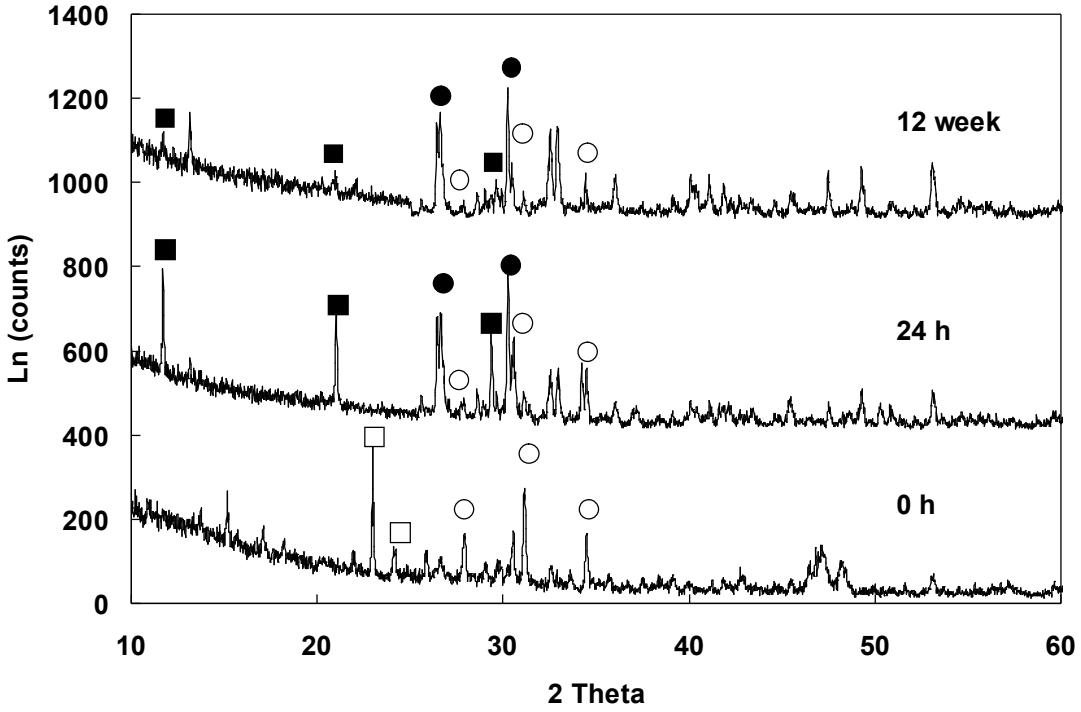
1400
1200
1000
800
600
400
200
0
Ln (counts)
12 week
24 h
0 h
10
20
30
40
50
60
2 Theta

B

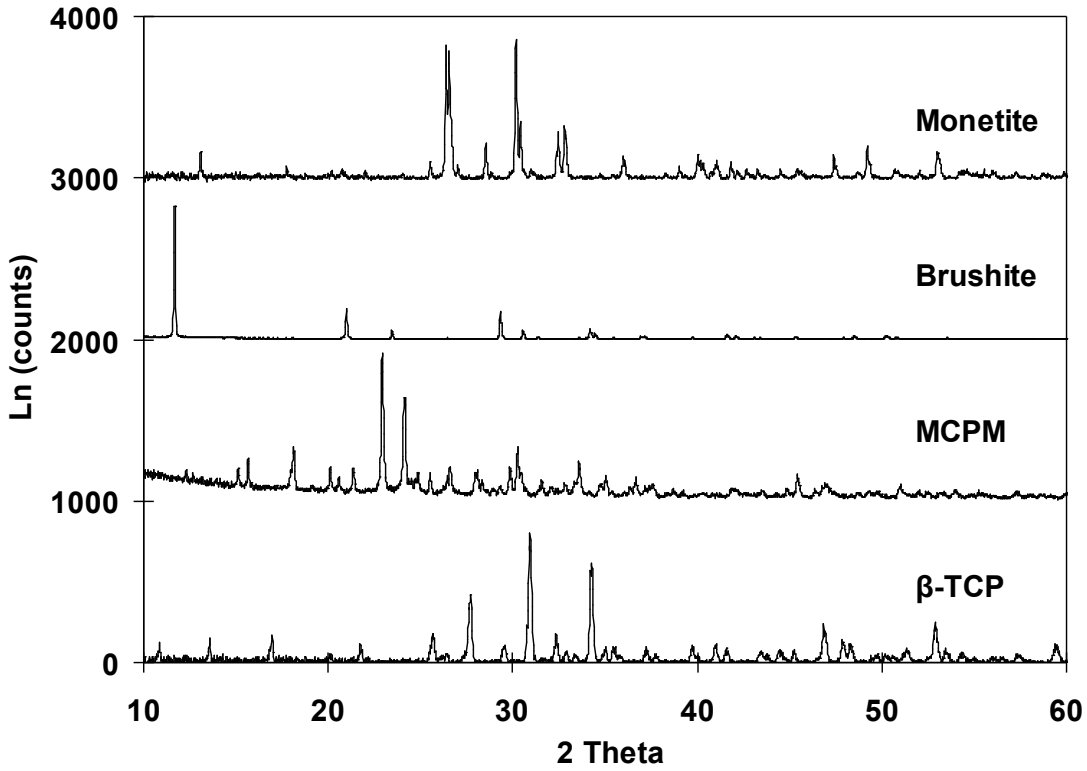

C

Fig. 3.4. XRD spectra of an example composite with F% = 70%, T/M = 4 and M_d = 30 μm (A) and an example composite with F% = 70%, T/M = 1 and M_d = 30 μm (B) before (0 h) and after 24-h and 12-week immersion in water. ○ β-TCP, □ MCPM, ■ brushite, ● monetite. C: XRD spectra of standards including β-TCP, MCPM, brushite and monetite. Note the absence of MCPM and presence of brushite and monetite after composite immersion in water for 24 h.

B. Formulations with equimolar β-TCP and MCPM

β-TCP and MCPM could both be readily detectable in dry samples (see example in Fig. 3.4.B). After 24-h sample immersion in water, the MCPM peaks had vanished and additional peaks due to brushite and monetite became clearly visible. After 12-week specimen immersion in water, β-TCP and monetite peaks remained but the brushite peaks declined greatly.

Presence of different calcium phosphates in all formulations before and after 24-h or 12-week water immersion is summarised in Table 3.3.

3.3.3. Compressive modulus

The average initial dry, 1-day wet and final 70-day wet modulus of the polymer was 9, 7 and 3 MPa respectively (Table 3.1). In general, composites exhibited significantly higher modulus than the polymer ($p<0.05$) (Table 3.1, Fig. 3.5). The initial dry modulus of C_{F70}, C_{F60} and C_{F50} was 21 - 27, 14 - 16 and 12 - 15 MPa respectively. After 1 day in water, the modulus of all composite samples decreased dramatically and was between 6 and 11 MPa. By 70 days, the composite modulus was further reduced to 4 - 9 MPa.

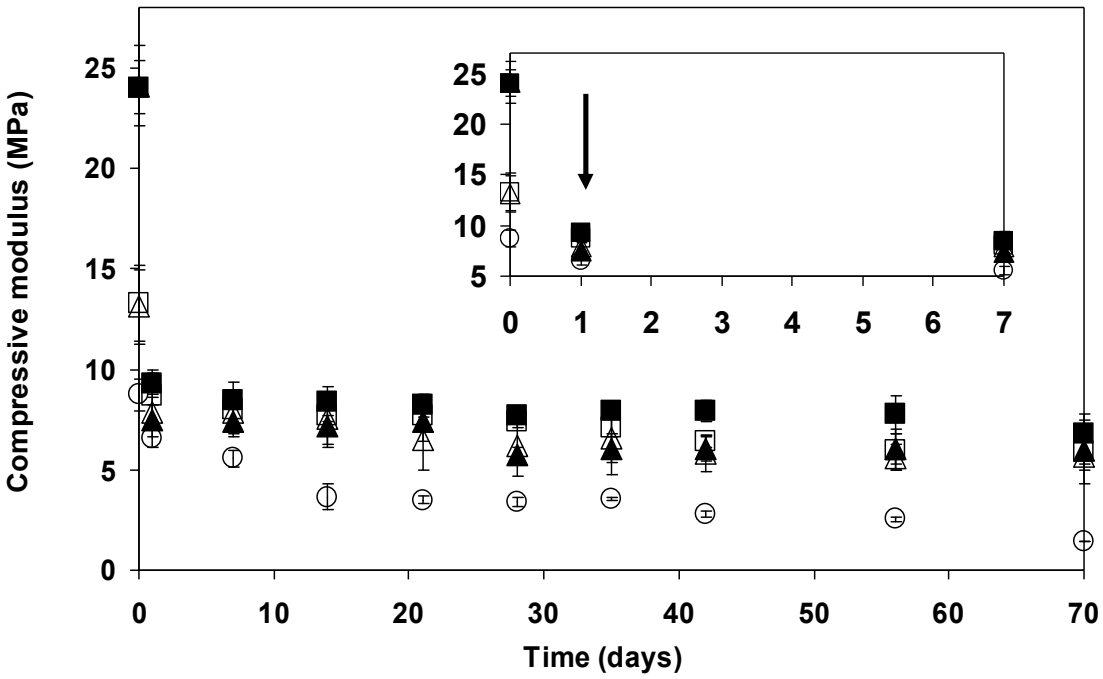

Fig. 3.5. Fig. 3.5. Compressive modulus of polymer and composites with time after immersion in water. ○polymer, □ F% = 50%, T/M =4, Δ F%=50%, T/M =1, ■ F% = 70%, T/M =4, ▲F% = 70%, T/M =1. Note the reduction in modulus (arrows) after 1 day of water immersion.

Table 3.3. Summary of filler components before (0 h) and after 24-h and 12-week water immersion.

Composites			0h		24 h			12 weeks		
F% (%)	T/M	M_d (μm)	β-TCP	MCPM	β-TCP	brushite	monetite	β-TCP	brushite	monetite
70	4	90	S	W	S	W	W	S	-	W
70	4	30	S	W	S	W	W	S	-	W
70	1	90	S	S	S	S	S	S	W	S
70	1	30	S	S	S	S	S	S	W	S
60	2	60	S	W	S	W	W	S	-	W
50	4	90	S	W	S	W	W	S	-	W
50	4	30	S	W	S	W	W	S	-	W
50	1	90	S	S	S	S	S	S	W	S
50	1	30	S	S	S	S	S	S	W	S

F% (filler content), T/M (molar ratio of β-TCP to MCPM) and M_d (MCPM particle size) are three variables involved in the composite filler factorial design. S/W means respectively strong and weak peak intensity of a calcium phosphate component in XRD spectra; '-'= not detectable.

Factorial analysis showed that the initial dry compressive modulus was dependant primarily on F%, with higher F% leading to greater modulus (Table 3.2). Additionally, reduction in modulus after immersion in water for 24 h was affected mostly by F% but additionally by T/M (Table 3.2). Increase in F% and decrease in T/M (i.e., higher MCPM content in fillers) resulted in greater reduction in modulus after water immersion.

3.3.4. Hydrolytic degradation

Polymer exhibited small and comparable mass (3%) and volume (3%) increase during the initial 24 h of water immersion (Fig. 3.6). All composite discs increased rapidly in mass during the initial 24 h of water submersion, but more so in volume (compare Fig. 3.6.A and B). Composites with F% = 50% and T/M = 4 (■) exhibited least mass (approximately 6%) and volume (approximately 13%) change whereas those with F% = 70% and T/M =1 (▲) showed greatest mass (approximately 18%) and volume (approximately 35%) increase (Fig. 3.6).

Regarding the initial water content (see Eq. 3.6), factorial analysis showed that this property was affected strongly by F% and T/M (Table 3.2). Increase in F% and decrease in T/M (i.e. increase in hydrophilic MCPM content in the specimens) encouraged greater water sorption. Composites with F% = 70%, T/M=1 (formulations 3 and 4) exhibited maximum initial water content, ~ 16%, followed by F% = 50%, T/M=1 (formulations 8 and 9), F% = 60%, T/M=2 (formulation 5) and F% = 70%, T/M=4 (formulations 1 and 2), ~ 10%, and last came F% = 50%, T/M=4 (formulations 6 and 7), ~ 6% (Table 3.1). All

composites exhibited significantly higher initial water content compared to polymer ($p<0.05$).

Between 24 h and 10 weeks, a slight decrease in polymer and composite mass and a lesser reduction in volume (compared to mass decrease) were generally observed (Fig. 3.7, compare A and B), indicative of combined bulk and surface erosion during hydrolytic degradation.

Regarding the final material loss (see Eq. 3.7), factorial analysis established that this property was affected mostly by T/M but additionally by F% (Table 3.2). Decrease in T/M and increase in F% (i.e., higher MCPM content in fillers) resulted in greater final material loss. Composites with T/M=1 ($C_{T/M1}$, i.e., formulations 3, 4, 8 and 9) exhibited maximum final mass loss, ~ 12%, followed by $C_{T/M2}$ (formulation 5), ~ 6%, and $C_{T/M4}$ (formulations 1, 2, 6 and 7), ~ 4% (Table 3.1). $C_{T/M1}$ or $C_{T/M2}$ exhibited significantly higher final material loss than that of polymer ($p<0.05$).

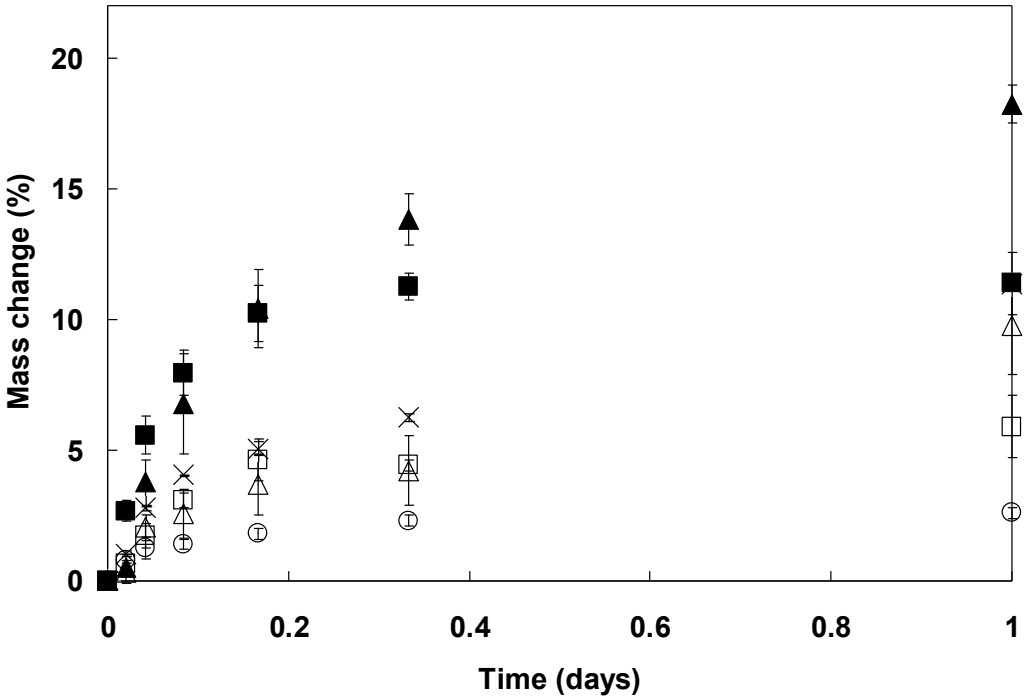

A

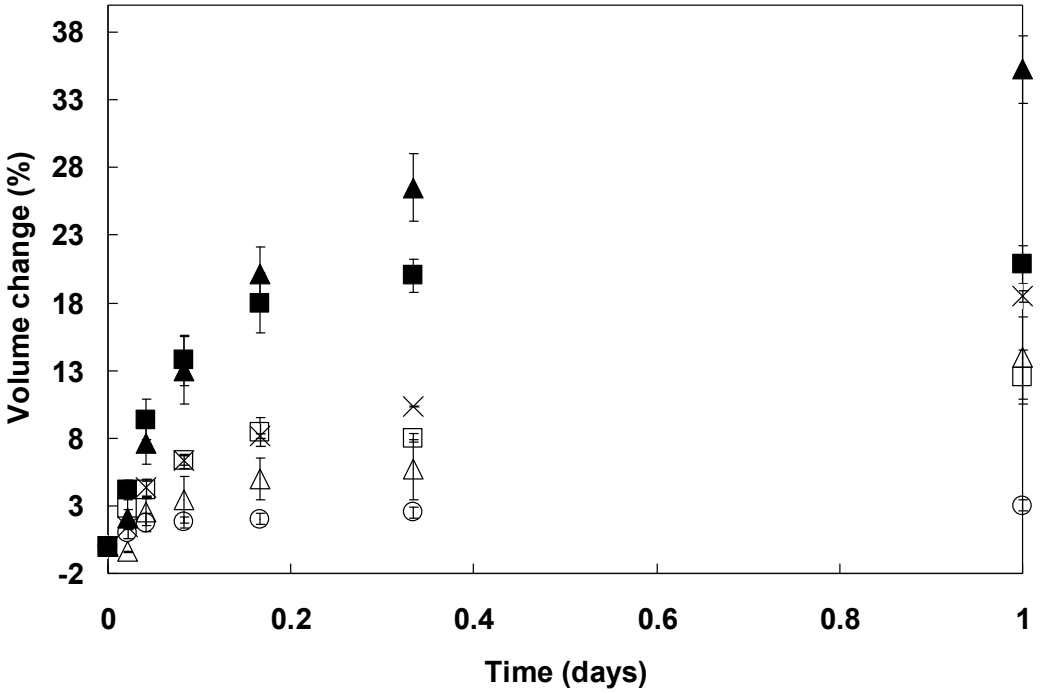

B

Fig. 3.6. Initial mass (A) and volume (B) change with time of polymer and composites after immersion in water. ○ polymer, □ F% = 50%, T/M =4, Δ F%=50%, T/M =1, X F% = 60%, T/M =2, ■ F% = 70%, T/M =4, ▲F% = 70%, T/M =1.

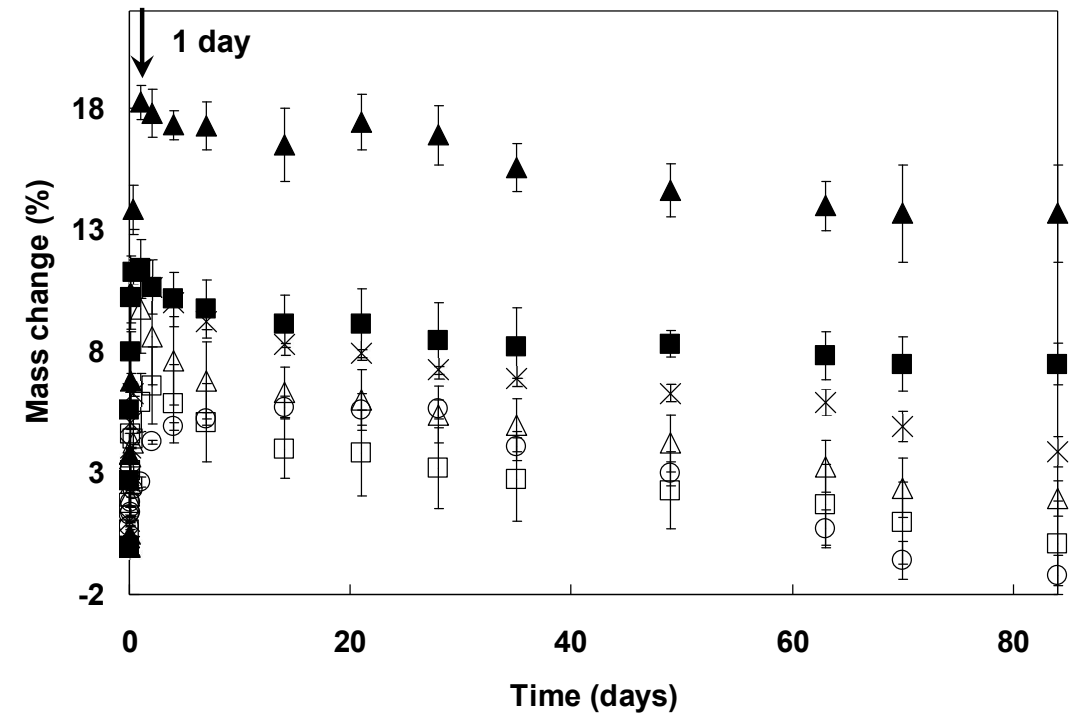

A

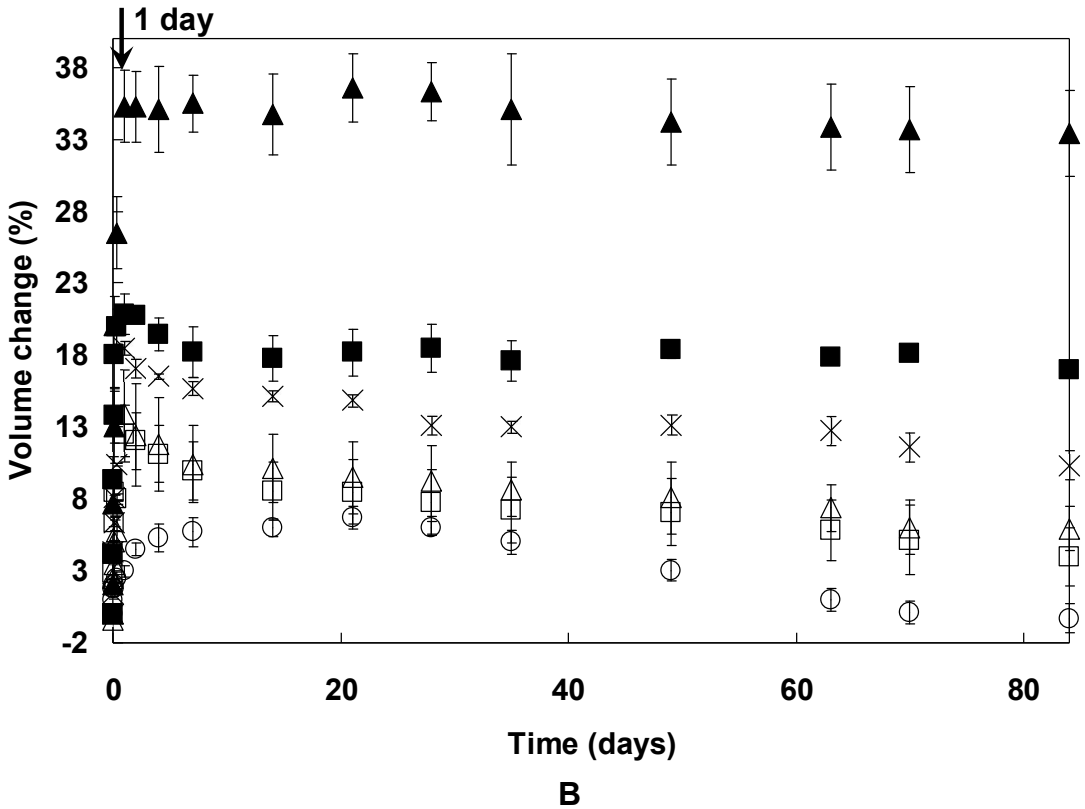

B

Fig. 3.7. Mass (A) and volume (B) change with time of polymer and composites after immersion in water. ○ polymer, □ F% = 50%, T/M =4, Δ F%=50%, T/M =1, X F% = 60%, T/M =2, ■ F% = 70%, T/M =4, ▲F% = 70%, T/M =1. Note the fast initial increase in mass and volume after one day (arrows) of water immersion and slow slight changes afterwards.

3.3.5. Ion and acid release

3.3.5.1. Phosphate and calcium ion release

The phosphate release profiles exhibited burst release in the first 24 h and then the release rate declined with time (Fig. 3.8.A). The phosphate release rate of different formulations increased in the order: F% = 50%, T/M =4 (□) < F% = 70%, T/M =4 (■) < F% = 60%, T/M = 2 (x) < F% = 50%, T/M =1 (Δ) < F% = 70%, T/M =1 (▲). At 24 h, the cumulative phosphate release was between 1 and 7% (Table 3.4). At 12 weeks, the cumulative phosphate release was between 7 and 23%. The phosphate release after 24 h was linear with square root (SQRT) of time ($R^2 > 0.95$, Fig. 3.8.B), indicating a diffusion-controlled release mechanism.

Factorial analysis has demonstrated that the initial 24-h phosphate release was affected mostly by F% and T/M, with M_d having much smaller effects (Table 3.2). Increase in F% and decrease in T/M, led to an increase in initial phosphate release. Moreover, with larger MCPM particle size more phosphate was found to be released. The long-term ion release (see release constant K in Table 3.4) was also enhanced upon increase in F% and decrease in T/M (i.e. upon raising the level of MCPM in the composite formulations) (Table 3.2).

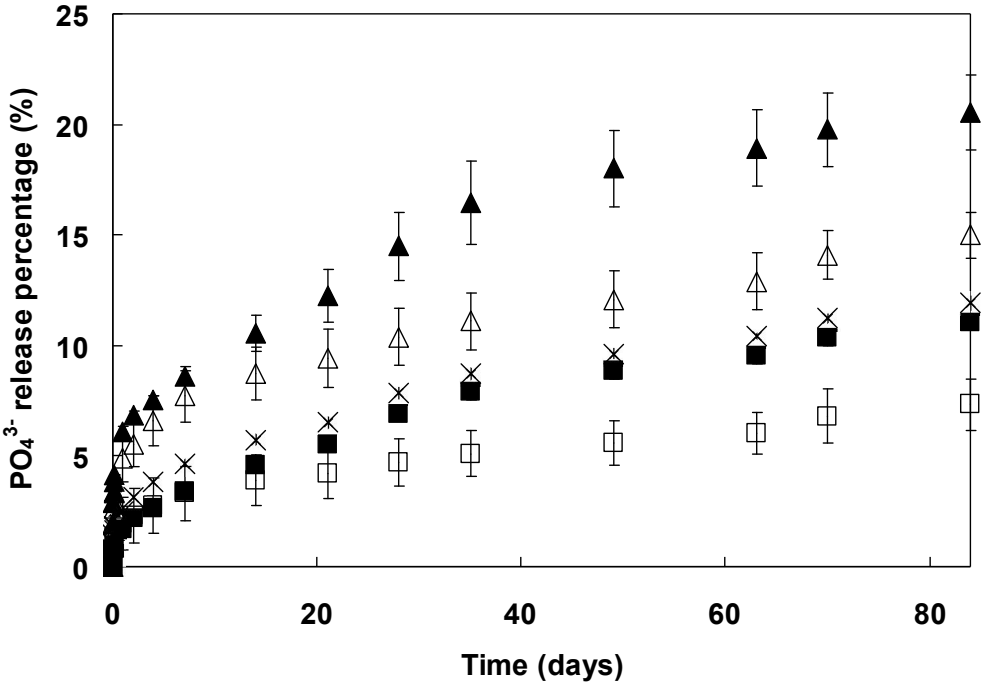

A

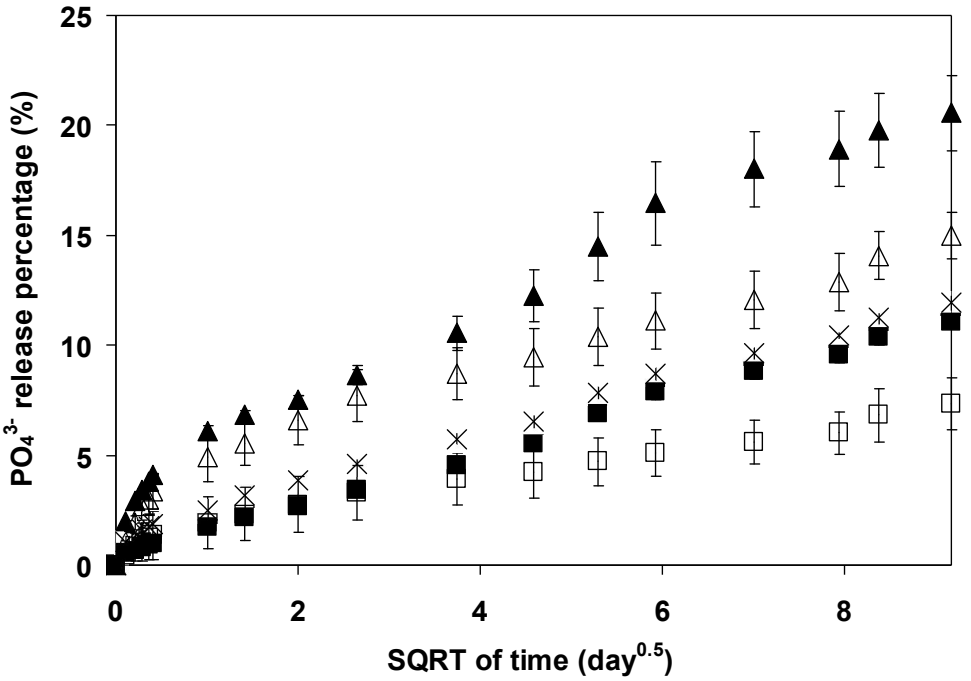

B

Fig. 3.8. Cumulative phosphate release from different composite formulations as a function of time (A) and square root (SQRT) of time (B). □ F% = 50%, T/M =4, ■ F% = 70%, T/M =4, X F% = 60%, T/M =2, Δ F%=50%, T/M =1, ▲F% = 70%, T/M =1. Note that the phosphate release after 1 day is more linear with SQRT of time than that with time.

Table 3.4. PO_4^{3-} and Ca^{2+} release; pH of storage solution; viability of cells proliferating on composite and polymer surfaces.

	Formulations			PO_4^{3-} release			Ca^{2+} release			Average pH		Relative cell viability
	F% (%)	T/M	M_d (μm)	24 h (%)	12 weeks (%)	K_{PO4} (%/day$^{0.5}$)	24 h (%)	12 weeks (%)	K_{Ca} (%/day$^{0.5}$)	2 – 24 h	24 h – 12 weeks	(%)
Composites	70	4	90	1.8 ± 0.1	10.5 ± 0.1	1.1 ± 0.1	0.9 ± 0.0	3.6 ± 0.8	0.3 ± 0.1	**4.3***	5.4*	**87±10***
	70	4	30	1.6 ± 0.1	10.3 ± 0.3	1.1 ± 0.1	0.8 ± 0.1	3.9 ± 0.4	0.4 ± 0.1	**4.2***	5.5*	**85±10***
	70	1	90	**5.9 ± 0.0**	**21.7 ± 0.7**	**1.9 ± 0.1**	**2.6 ± 0.0**	**7.8 ± 0.6**	**0.6 ± 0.2**	3.5*	**5.7***	44±4*
	70	1	30	**6.3 ± 0.2**	**19.4 ± 0.5**	**1.6 ±0. 3**	**2.4 ±0.2**	**7.3± 0.4**	**0.6 ± 0.1**	3.5*	**5.7***	46±7*
	60	2	60	2.5 ± 0.2	11.9 ± 0.3	1.1 ± 0.1	1.2 ± 0.0	5.8 ± 0.1	0.6 ± 0.1	4.0*	5.3*	50±7*
	50	4	90	1.1 ± 0.2	8.2 ± 0.8	0.9 ± 0.1	1.2 ± 0.1	3.7 ± 0.2	0.3 ± 0.1	**4.2***	4.6*	**69±3**
	50	4	30	1.1 ± 0.0	8.0 ± 0.5	0.8 ± 0.1	0.6 ± 0.0	3.6 ± 0.8	0.4 ± 0.1	**4.3***	4.6*	**70±4**
	50	1	90	**3.4 ± 0.2**	**16.5 ± 0.2**	**1.4 ± 0.1**	**3.2 ± 0.1**	**8.5 ± 0.6**	**0.6 ± 0.1**	3.7*	**5.4***	44±4*
	50	1	30	**2.5 ± 0.3**	**14.0 ± 0.0**	**1.4 ± 0.1**	**1.8 ± 0.1**	**6.4 ± 0.1**	**0.6 ± 0.1**	4.0*	**5.5***	42±4*
	Polymer			N/A	N/A	N/A	N/A	N/A	N/A	5.5	4.0	66±5

F% = filler content; T/M = molar ratio of β-TCP to MCPM; M_d = MCPM particle size. K_{PO4} and K_{Ca} are the gradient of the curve of 'cumulative percentage of phosphate or calcium release versus SQRT of time' between 24 h (1 day$^{0.5}$) and 12 weeks (9.2 day$^{0.5}$). Relative cell viability was determined as the ratio of the fluorescence intensity of the reduced alamarBlue™ caused by the cells proliferating on the material surfaces with that by the cells growing on Thermanox™ plastic coverslips. * significant differences ($p<0.05$) from control values (i.e., polymer). The best results are marked in bold.

The calcium release with time showed a similar profile to that of phosphate release (i.e. burst release in the initial 24 h and reduced release afterwards) and the release rate of different formulations increased with decrease in T/M (Fig. 3.9.A). Cumulative calcium release at 24 h and 12 weeks was respectively 0.6 ~ 3.3 and 3 ~ 9%, between one third and half of percentage phosphate release (Table 3.4). The calcium release after 24 h was linear with SQRT of time (R^2 > 0.95, Fig. 3.9.B), suggesting a diffusion-controlled release mechanism.

Factorial analysis has demonstrated that the initial 24-h calcium release was affected mostly by T/M, with F% and M_d having much smaller effects (Table 3.2). Decrease in T/M led to an increase in intial calcium ion release. Moreover, with higher filler content and larger MCPM particle size more calcium was found to be released. In addition, the long-term calcium release (see release constant K in Table 3.4) was enhanced upon increase in F% and decrease in T/M (i.e. upon raising the level of MCPM in the composite formulations) (Table 3.2).

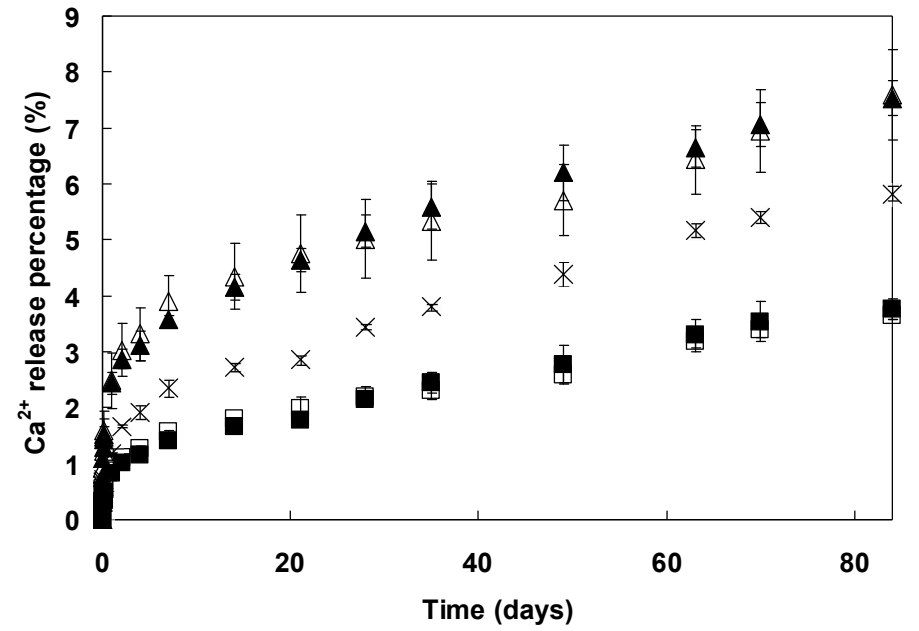

A

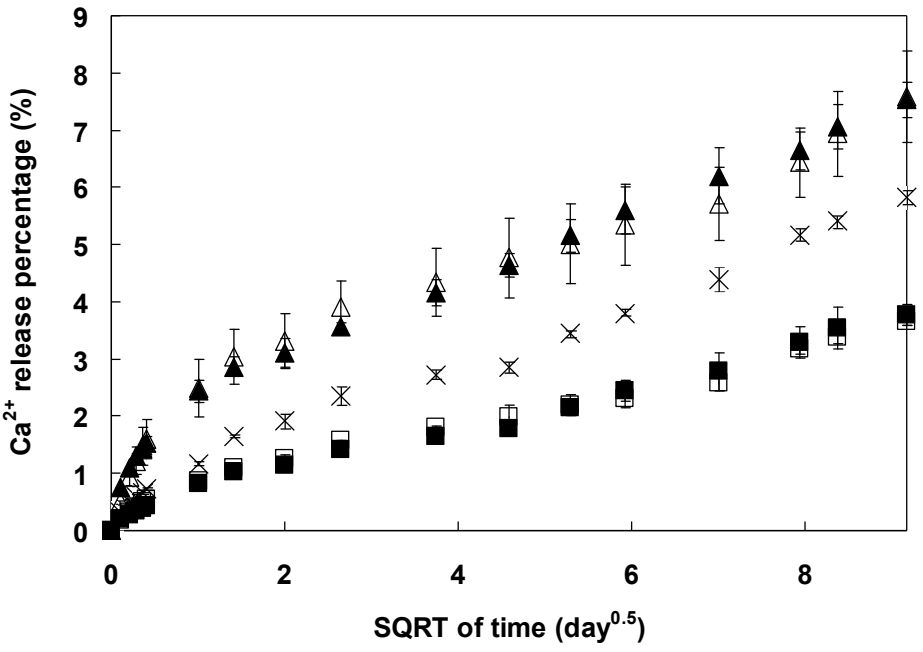

B

Fig. 3.9. Cumulative calcium release from different composite formulations as a function of time (A) and SQRT of time (B). □ F% = 50%, T/M =4, ■ F% = 70%, T/M =4, X F% = 60%, T/M =2, Δ F%=50%, T/M =1, ▲F% = 70%, T/M =1. Note that the calcium release after 1 day is more linear with SQRT of time than that with time.

3.3.5.2. Acid release

The pH of the polymer storage solution decreased to an average value of 5.5 in the first 2 - 24 h and then remained at approximately 4.0 for the following 12 weeks (Table 3.4). The polymer storage solution in the initial 2 – 24 h exhibited higher pH than that of all composites ($p<0.05$). However, for the following 12 weeks, the pH of the polymer storage solution was significantly lower than that of all composites ($p<0.05$).

The average pH of the first 2 - 24 h storage solutions for composites was lowest for formulations with the highest amount of MCPM (i.e. high F% and low T/M), being 3.5 with F% = 70% and T/M = 1 but between 3.7 and 4.3 for all other formulations (Table 3.4). Conversely, the average pH in the remaining 12-week period, was lowest for the formulations with least MCPM (i.e. low F% and high T/M) being 4.6 with F% =50% and T/M =4 but between 5.3 and 5.7 for all other formulations.

Factorial analysis demonstrated that initial storage solution pH was significantly affected by both F% and T/M. Decrease in F% and increase in T/M (i.e. reduction in MCPM amount of each specimen) resulted in higher early pH (Table 3.2). Conversely, the long-term storage solution pH was increased upon increase in F% and decrease in T/M (i.e. increase in MCPM amount of each specimen) (Table 3.2).

These above findings have suggested that, in the long term, less acid was released from the composites than polymer, although more acid was released from the composites in the initial 2 – 24 h. In addition, in the long term, formulations with higher levels of MCPM were more effective at buffering acid produced during polymer degradation, compared to the formulations with lower levels of MCPM.

3.3.6. Biocompatibility

3.3.6.1. *In vitro* biocompatibility

After 3 days of incubation, the MG-63 cells were found to be spread on the surfaces of the control Thermanox^{TM} plastic coverslips (flat surface) as well as all other material surfaces although those attached to the Thermanox^{TM} appeared to have the most pronounced cytoplasmic processes (Fig. 3.10.A-D). The polymer had a flat smooth surface appearance whereas that of the composites was granular. Moreover, needle-like crystal precipitation was observed on some areas of the surfaces of the composites with T/M =1. The MG-63 cells appeared able to spread over both these crystals and the underlying composite (Fig. 3.10.E). Elemental analysis has shown that the average atomic ratio of P/Ca of these precipitated crystals was 0.97:1, being close to 1.0. This suggests that the crystals were DCP (i.e., brushite and/or monetite).

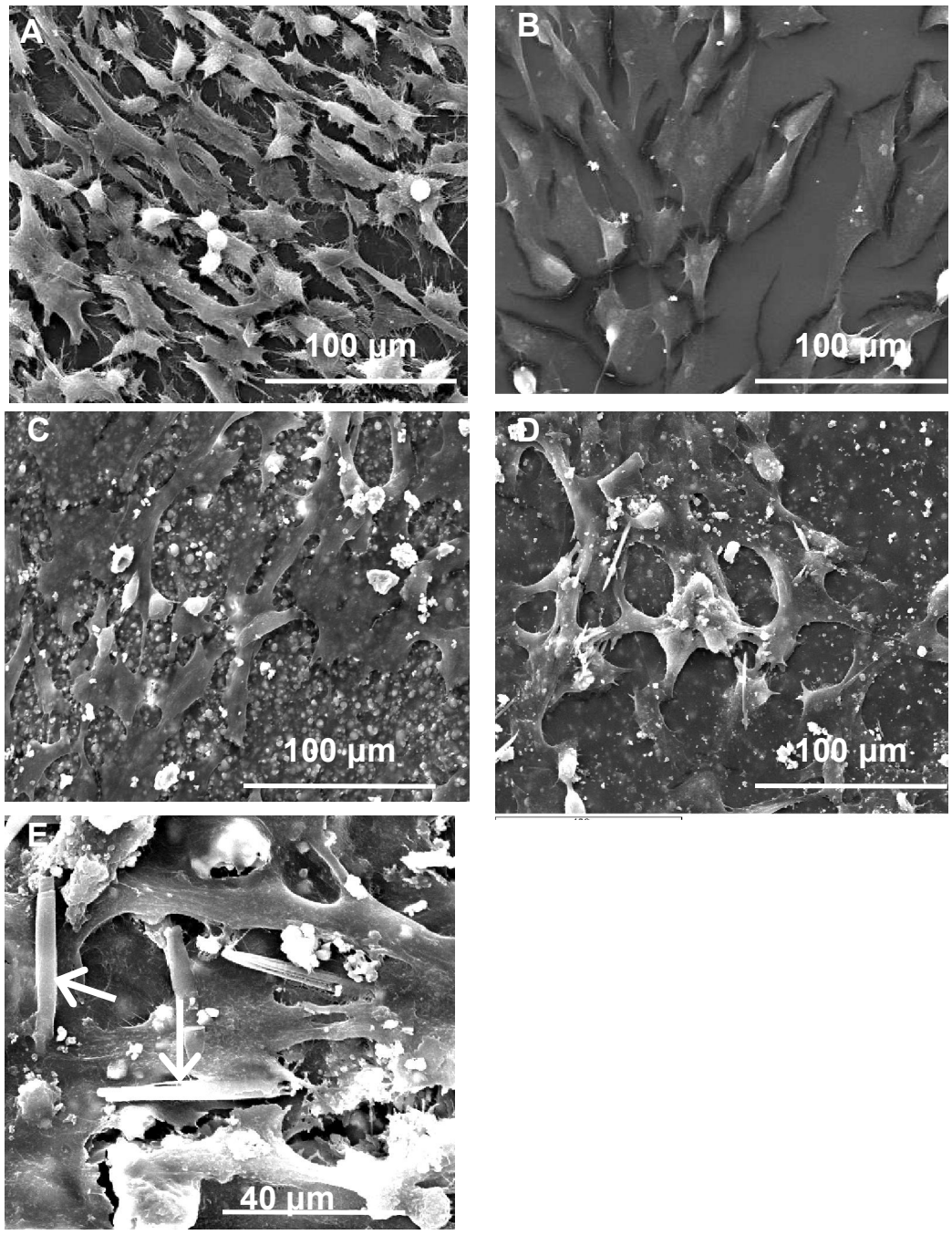

Fig. 3.10. SEM images of 3-day MG-63 cell proliferation on different material surfaces. A: a Thermanox™ plastic coverslip; B: a polymer; C: a composite with F% = 70%, T/M = 4 and M_d = 30 µm; D: a composite with F% = 70%, T/M = 1 and M_d = 30 µm; E: crystal precipitation (arrows) on the surface of a composite with F% = 70%, T/M = 1 and M_d = 30 µm.

The viability of cells after 3 days of incubation on the polymer and composite surfaces were found to be between approximately 40 and 90% of that on the control Thermanox^{TM} plastic coverslips (Table 3.4). Cell viability on the sample surfaces increased in the order: F% = 70% and T/M =1, F% = 50% and T/M =1, F% = 60% and T/M =2 < F% = 50% and T/M =4, polymer < F% = 70% and T/M = 4 (Table 3.4).

Factorial analysis showed that the cell viability was affected most by T/M but additionally by F% (Table 3.2). Increase in T/M and F% (i.e., higher β-TCP content of composites) resulted in greater number of cells proliferating on the composite surfaces.

3.3.6.2. *In vivo* biocompatibility

After 7 days of incubation, all chick femurs implanted with or without a composite film were found to be embedded in the CAM, with blood vessels surrounding the femur. The sample femurs with the implants appeared to have comparable cross-sectional diameter and anatomic structure with the control samples with no implant (compare Fig. 3.11.B and A). The bone marrow, trabecular bone, periosteal tissue and the implant could all be readily identified. The implants appeared to be in close proximity to the bone, with no indication of immunological reaction, e.g., no noticeable accumulation of leucocytes, as shown by higher magnification in Fig. 3.11.C. Bone adjacent to the implant site appeared histologically normal.

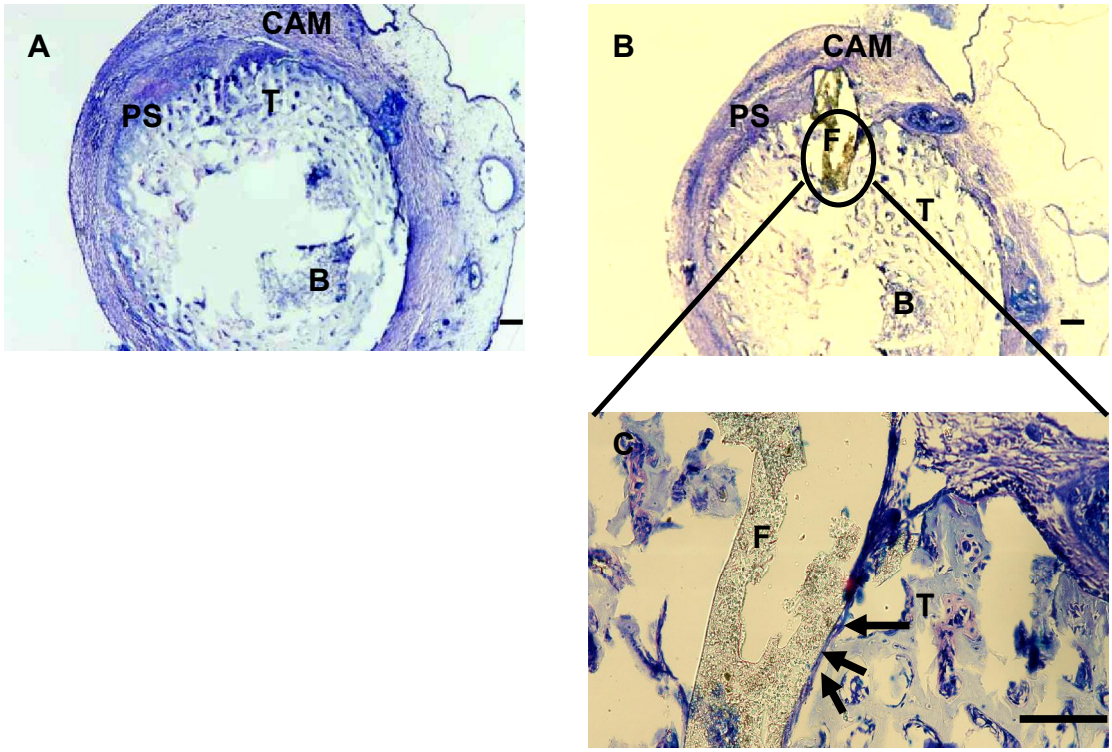

Fig. 3.11. Histology of toluidine blue stained cross-sections of chick embryo femurs without (A) and with (B) implantation with a composite film with F% = 50%, T/M = 1 and M_d = 30 µm. CAM: chorioallantoic membrane; B: bone marrow; T: trabecular bone; PS: periosteal tissue; F: implant. Note that the implant appeared to be in close proximity (arrows) to the bone (C). Scale bars: 100 µm.

In addition, the CAM response to the composite material, as shown in Fig. 3.12, has indicated that blood vessels appeared to be passing in close proximity to the implant, with no evidence of vessel haemorrhage in the region of the grafted material.

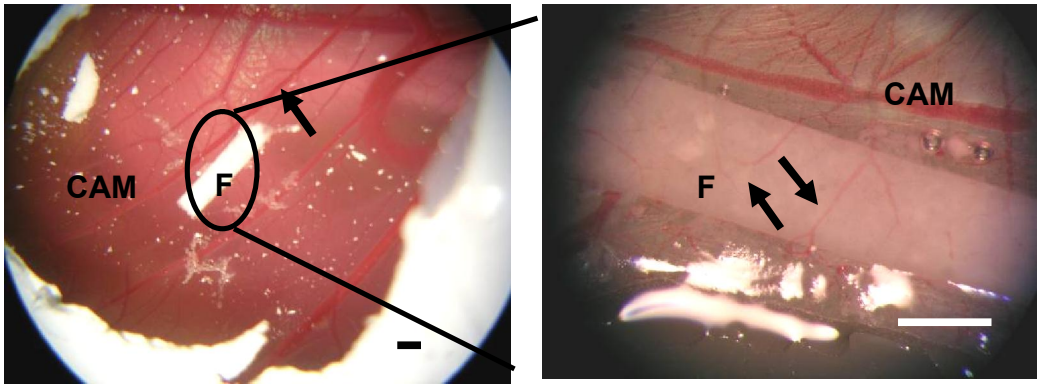

Fig. 3.12. CAM response to the implanted composite material. CAM: chorioallantoic membrane; F: composite implant. Note the absence of negative reaction (e.g., vessel haemorrhage) in the region of the grafted material and the presence of blood vessels (arrows) passing in close proximity to the implant. Scale bars: 1mm.

3.4. Discussion

In this study, the effect of calcium phosphate filler addition on material polymerisation, water-induced chemical changes, compressive modulus, hydrolytic degradation, ion release, acid release, and *in vitro* biocompatibility was quantified using factorial analysis. Additionally, *in vivo* biocompatibility, i.e., bone tissue response of a chick embryonic femur to a set composite implant was assessed.

3.4.1. Effect of filler addition on polymerisation

For all formulations, over 85% monomer conversion could be obtained with 120 s of blue light irradiation, although higher F% (i.e., 70%) led to slower polymerisation rate. This is likely due to the increased scattering of the initiating blue light by the high level of filler particles. Nevertheless, Raman confirmed that the adhesive monomer could be fully polymerised in the presence of calcium phosphate fillers. The level of monomer conversion is greater than normally observed in acrylates or methacrylates under comparable conditions (Sideridou *et al*. 2002), possibly because of the low glass transition temperature of the initial monomer, which would prevent the vitrification that limits final polymerisation (Bohner *et al.* 2005;Ho and Young 2006). Such rapid and complete photo-polymerisation is highly desirable as this may allow immediate material bonding to the surrounding tissues after injection and limit the release of reactive and potentially toxic double bond-containing components during degradation (Ho and Young 2006).

3.4.2. Effect of filler addition on water induced chemical changes

Raman with XRD proved that water sorption could catalyse conversion of β-TCP and MCPM to DCP, i.e., brushite and monetite within 24 h inside the crosslinked polymer. The primary chemical composition of the calcium phosphates after 24-h water immersion, DCP or β-TCP, was dependant on T/M. The ratio of produced DCP to β-TCP decreased in the order T/M = 1 > T/M = 2 > T/M = 4 as expected. In addition, the remaining β-TCP at T/M =1 after 24 h of water immersion has suggested that MCPM was partially reacted and partially dissolved into the surrounding storage solution prior to reaction, leading to the reduction of pH of the storage solution (see section 3.4.6 for details). In future study, to allow full reaction of β-TCP, higher molar ratio of MCPM to β-TCP (i.e., > 1) could be employed.

Additionally, the relative amount of DCP (particularly brushite) to polymer decreased whereas the amount of β-TCP to polymer kept almost constant during long-term water immersion. This was probably due to the higher solubility of DCP than β-TCP (solubility product constant (Ksp) at 25 ˚C of brushite, monetite and β-TCP = 2.59×10^{-7}, 1×10^{-7} and 2.07×10^{-33} respectively (Elliott 1994)). This result was consistent with the higher phosphate and calcium release from specimens with T/M =1 (high DCP formation) compared to specimens with T/M = 2 or 4 (low DCP formation). The formation of DCP may be beneficial since the resultant DCP fillers generated higher phosphate and calcium release associated

with higher pH compensation ability (see section 3.4.5 and 3.4.6 for more details).

3.4.3. Effect of filler addition on material modulus

The addition of calcium phosphate particles enhanced the dry compressive modulus of the polymer by up to three fold. The level of mechanical reinforcement depended mainly on the amount of added filler. During the first 24 h of water immersion, composite modulus decreased far more than that of polymer. This was consistent with higher initial MCPM amount and thus higher water content after 24 h water immersion of the composites. The water present in the composites could act as a plasticiser, leading to swelling of the material and reduction in the material modulus (Sideridou *et al.* 2003).

The modulus of the composites declined continuously but only very slightly over the remaining 10 weeks. The maintenance of modulus suggests the potential for long-term functional support. The dissolution of calcium phosphates within the polymer may contribute to the modulus maintenance via 'salt-bridge' or ionic bond formation within the composite during the course of degradation. When the polymer degrades, carboxylic acid groups are produced and the salt-bridges start to form between the carboxyl groups on polymer fragments and calcium cations from the calcium phosphate (this may explain the result of slower release of Ca^{2+} than PO_4^{3-}). This could produce 'an ionomer' whose ionic crosslinks combined

with partially degraded polymer networks, result in maintenance of compressive modulus (Chung *et al.* 2003;Peter *et al.* 1999;Xie *et al.* 2007).

The modulus of the composites obtained (10 ~ 30 MPa) was lower than that of human trabecular bone (20 ~ 500 MPa) (Agrawal and Athanasiou 1997;Bergsma *et al.* 1995). Such materials with low modulus could, however, be used as temporary bone adhesives for infiltration or stabilisation of, for example, osteoporotic bone that has become brittle due to the loss of collagen (Yaszemski *et al.* 1995). As new bone grows progressively against the receding surface of the degrading material, and eventually integrates and replaces the material, the temporarily formed 'bone-material' might be expected to have increased modulus compared with the implant material alone.

3.4.4. Effect of filler addition on hydrolytic degradation

It was found that adjustment of material degradation rate can be achieved by manipulating the composition of added calcium phosphates. Specimens with T/M =1 showed higher degradation rate compared to those with T/M = 4, probably due to the formation of more DCP whose solubility is higher than β-TCP (see section 3.4.2). In order to accelerate further the material degradation, higher molar ratio of MCPM to β-TCP (i.e., > 1) could be employed due to the higher solubility of MCPM and their reaction products (i.e., brushite and monetite). Moreover, dissolved MCPM is slightly acidic. This acidity might catalyse the polymer hydrolytic degradation (Walton and Cotton 2007).

In addition, generally, composites exhibited faster degradation rates than the polymer. This is considered to be an improvement over the polymer (only 3% material loss in 12 weeks) although the maximum degradation of composites (12% in 12 weeks) may not be fast enough for use as bone adhesives. However, the actual material degradation rate *in vivo* may be faster than *in vitro* because of possible additional enzymatic cleavage which may occur *in vivo* (Hou *et al*. 2004). Further studies of the *in vivo* degradation of these materials are required to determine whether the materials meet the previously suggested optimal *in vivo* degradation rate (complete degradation in 12 weeks) (Walton and Cotton 2007).

Degradation products of the composite materials are presumably, calcium and phosphate ions or particles (from the inorganic phase) and, polyethers, monomeric and oligomeric lactic acid, and oligo (methacylic acid) (from the organic phase). These degradation fragments are considereded to be of low toxicity and can be excreted directly or after entry and exit from various metabolic pathways (Sawhney *et al.* 1993).

3.4.5. Effect of filler addition on ion release

Composites with T/M =1 generated higher phosphate and calcium release than those with excess β-TCP. This may be because the formulations with T/M =1 had more resultant soluble DCP in the specimens whereas the formulations with T/M = 2 or 4 had more less soluble β-TCP in the specimens (see section 3.4.2 for details). The ability to release phosphate and calcium ions may be beneficial in

aiding bone re-mineralisation and regeneration, as these ions have shown to stimulate osteogenic differentiation (Ripamonti 1996). In addition, through a dissolution–precipitation process, a bone-like mineral layer could develop, leading to new bone formation initiated by the presence of osteogenic compounds in body fluids (e.g., bone morphogenetic proteins). Furthermore, the released ions could nucleate in the pores of bone collagen fibrils, resulting in increased mineralisation along the fibrils (Glimcher 1989).

The composites provided burst release of PO_4^{3-} and Ca^{2+} in the initial 24-h immersion in deionised water. This could be explained by largely dissolution of the fillers, particularly the MCPM, which has a higher solubility than β-TCP (K_{sp} at 25˚C of MCPM and β-TCP is 7.18×10^{-2} and 2.07×10^{-33} respectively (Elliott 1994).

The burst PO_4^{3-} and Ca^{2+} release was then followed by a substantial decline in the release rate for the remaining experimental period. The ratio of PO_4^{3-} to Ca^{2+} release (K_{PO4}/K_{Ca} = 2 ~ 3, see Table 3.4) suggested that the phosphate and calcium elements might be released in the form of $Ca(H_2PO_4)_2$ with possibly some phosphoric acid (H_3PO_4). In the presence of water, ion exchange with the produced brushite or monetite could neutralise the acidic polymeric fragments forming monocalcium phosphate via the following reaction:

$$2\ RCOOH + 2\ CaHPO_4(s) \rightarrow (RCOO^-)_2Ca^{2+}(aq) + Ca^{2+}(H_2PO_4^-)_2(aq) \qquad 3.10$$

The $CaHPO_4$ 'mops up' acidic protons (from degraded polymer) upon forming $Ca(H_2PO_4)_2$ and as a result, the solution would be buffered (Korrenhof and Timmer 1992). When there is excessive acid, $CaHPO_4$ will not be sufficient to 'mop up' the acidic protons and thus phosphoric acid will be formed. This neutralisation of polymer degradation products, i.e., control of pH, may be beneficial in reducing irritation to any tissues surrounding the implanted material. It could also reduce the possibility of sudden catastrophic core degradation of the material caused by acid build-up (Sabir *et al.* 2009).

3.4.6. Effect of filler addition on acid release

The initial pH drop with the composite specimens in the first 24 h might be attributed to the release of acidic MCPM. The initial burst acid release may not present a serious problem *in vivo*, because of the rapid and continuous circulation of body fluid as well as the high buffering capacity of serum (Mabilleau *et al.* 2004). The higher pH of the composite storage solution than polymer at later times indicated a buffering effect by the calcium phosphates (see Eq. 3.10 in section 3.4.5). This buffering effect was more pronounced for the formulations with T/M =1, compared to those with T/M = 2 or 4. This may be because the specimens with T/M =1 had higher amount of more soluble DCP and thus released more PO_4^{3-} to buffer the acidic polymer degradation products. However, the specimens with T/M = 2 or 4 had more β-TCP with lower solubility, and had released less PO_4^{3-} and thus provided less sufficient pH compensation.

The results of ion release as well as pH of the storage solution found above have suggested that the fillers (particularly when T/M = 1) could provide release of phosphate and calcium ions that may both aid bone regeneration and simultaneously, at least partly, buffer the released acidic polymer degradation products. Additionally, the overall final amount of released acids and organic degradation products would be reduced by raising the filler level, as the fraction of polymer is lower.

3.4.7. Effect of filler addition on *in vitro* biocompatibility

The *in vitro* biocompatibility test indicated that bone-like MG-63 cells could attach and spread on both the polymer and composite surfaces, with an apparently normal morphology despite the different surface nature of the polymer (smooth) and composites (granular). Composites with higher β-TCP content resulted in greater number of cells proliferating on their surfaces compared to those with higher MCPM content. This may be because the surfaces of the formulations with higher β-TCP content are more stable due to the less soluble β-TCP. Those with higher MCPM may be more dynamic.

In addition, precipitation of DCP crystals was observed on the surfaces of the formulations with T/M =1. MG-63 cells were found to be able to adhere to these crystals. Phosphate and calcium ion release from the material surface may cause over saturation in the culture medium, inducing the nucleation and growth of DCP crystals at the material-medium interface. This dissolution and reprecipitation of

calcium phosphate crystals might have superior properties for the stimulation of bone formation and bone bonding, by development of a bone-like mineral layer on the material surface (Barrere *et al.* 2006).

3.4.8. *In vivo* biocompatibility

The formulation of F% = 50%, T/M =1 and M_d = 30 μm was selected for the *in vivo* test due to its fluidity (spread when placed on a flat surface), high phosphate and calcium release and buffering capacity. When composite films of this formulation were implanted into the chick embryo femurs, they exhibited close contact with the adjacent bone, with no indication of adverse immunological reaction. In addition, the response of the CAM to the implant itself did not indicate any detectable vessel hemorrhage in the region of the grafted material, and apparently normal blood vessels could be seen passing under the implant and in close proximity to it. These observations have indicated that the implanted composite material was unlikely to have been toxic to normal bone *in vivo*, and suggested that such materials could have potential for clinical application as bone adhesives.

3.5. Conclusion

The injectable degradable composite materials investigated in this study are elastic, release phosphate and calcium ions, buffer acid production and appear to be biocompatible. Increase in the amount of calcium phosphate fillers (irrespective of β-TCP or MCPM) resulted in enhanced compressive modulus of

the dry materials although all composites exhibited a comparable modulus after water immersion. Composites with an equal molar ratio of β-TCP and MCPM (T/M =1) formed relatively more dicalcium phosphate, i.e., brushite and monetite after 24 h of water immersion, released higher levels of phosphate and calcium ions and were thus more capable of buffering acid production than those with excess β-TCP. All formulations tested were found to be biocompatible by the procedure used here.

Chapter 4

Drug Delivery

Abbreviations

In alphabetical order

CHX	chlorhexidine
CQ	camphorquinone
DCP	dicalcium phosphate
DMPT	*N,N*-dimethyl-*p*-toluidine
F%	filler content
FTIR	Fourier transform infrared
HEMA	hydroxyethyl methacrylate
MCPM	monocalcium phosphate monohydrate
M_d	MCPM particle size
MRSA-16	methicillin-resistant *Staphylococcus aureus* -16
PGLA-DMA	poly (propylene glycol -*co*- lactide) dimethacrylate
S. aureus	*Staphylococcus aureus*
SA 8325-4	*S. aureus* 8325-4
SD	standard deviation
SQRT	square root
TCP	tricalcium phosphate
T/M	molar ratio of β-TCP/MCPM

4.1. Introduction

In Chapter 3, reactive calcium phosphate particles of β-tricalcium phosphate (β-TCP) and monocalcium phosphate monohydrate (MCPM) (powder components of brushite – forming bone cements (Bohner 2007)) have been added to the synthetic poly (propylene glycol-*co*-lactide) dimethacrylate (PGLA-DMA) to produce composite bone adhesives (used to connect fractured bone) (Zhao *et al.* 2010). The filler of β-TCP and MCPM has been found to react and re-precipitate as dicalcium phosphate (DCP, brushite and monetite) upon water sorption. Modulus of the polymer was found to be enhaced upon addition of calcium phosphate fillers. Additionally, dissolution of the resultant DCP was found to generate phosphate and calcium ions that may aid bone re-mineralisation, with concomitant neutralisation of acidic degradation products. Importantly, these composite materials have been shown to be biocompatiblie with bone cells. Furthermore, after implantation into chick embryo femurs, the composite adhesives have been shown to be in close contact with the adjacent bone, with no indication of adverse immunological reaction.

The above findings have suggested that the composite materials developed in this project have potential clinical value as bone adhesives. Nevertheless, when such medical implants are used in bone fractures or as external fixation devices, bacterial infection caused by *Staphylococcus aureus* (*S. aureus)* are commonly associated (Mandal *et al.* 2002;Nair *et al.* 2000). As a result, the service life of

such medical implants would be reduced, which may prevent effective wound healing processes to take place (Mourino and Boccaccini 2009).

Thus controlled release of an antibacterial drug from these medical implants would be of substantial clinical value in limiting bacterial infection (Young and Ho 2008). As previously reported, *S. aureus* bacteria are generally highly susceptible to the antibacterial chlorhexidine (CHX, see molecular structure in Fig. 4.1) (Nascimento *et al.* 2008). This drug has been found to have very low incidence of resistance development (Harris *et al.* 2006) and minimal toxicity to host cells (Lee *et al.* 2005;Leung *et al.* 2005;Nerurkar *et al.* 1995;Riggs *et al.* 2000). Extensive testing has been performed with both topical application of CHX over prolonged periods and internal use of CHX (Dejong *et al.* 2001). For example, it has been incorporated into bone adhesives and has been shown to successfully prevent bacterial adhesion to the implants, without significant toxicity (Dejong *et al.* 2001;Harris *et al*. 2006). Moreover, CHX has Food and Drug Administration approval for human use when applied to internally placed medical devices, including intravenous catheters (Maki *et al*. 1997) and an implanted antimicrobial surgical mesh (Choe *et al*. 2000).

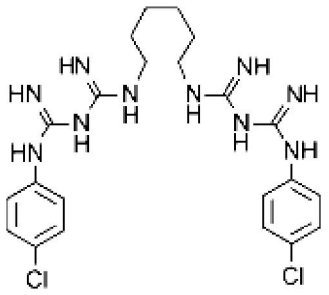

Fig. 4.1. Molecular structure of CHX.

In this study, adhesives were prepared consisting of fluid PGLA-DMA filled with calcium phosphate fillers (a reactive mixture of β-TCP and MCPM) and loaded with the antibacterial CHX. The effect of the addition of CHX and filler was measured on several material properties, including polymerisation rate and degree of monomer conversion, water sorption and material degradation, water accelerated chemistry changes, CHX release kinetics and antibacterial activity. Parts of this work have been submitted to *Journal of Materials Science: Materials in Medicine* in Nov. 2010.

4.2. Materials and methods

4.2.1. Sample fabrication

Fabrication of samples was described in Chapter 3, section 3.2.1. Briefly, the PGLA-DMA was mixed with camphorquinone (CQ), *N,N*-dimethyl-*p*-toluidine (DMPT) and hydroxyethyl methacrylate (HEMA). Varying levels of β-TCP and MCPM particles were then added in the monomer mixture. CHX (10 wt.% of the total mixture) was finally added to each formulation. Detailed composite formulations are listed in Table 4.1. Polymer and composite formulations without CHX were used as controls.

Polymerised discs of 5 mm (for agar diffusion tests) or 12 mm diameter (for all other studies) and 2 mm thickness were obtained by placing the polymer and composite pastes into steel rings with top and bottom surfaces covered by acetate sheets, and curing using blue light in a light box. Raman spectroscopy

was used to confirm full polymerisation and the density of the set samples was measured using an electronic balance with a density kit to confirm negligible air incorporation. Each test was performed in triplicate, and results were expressed as means ± standard deviation (SD). Results shown were samples with CHX unless otherwise stated.

4.2.2. Polymerisation kinetics

Determination of the polymerisation rate and degree of monomer conversion of the CHX loaded polymer and composite discs was determined using the same method as previously described for non-CHX loaded discs (detailed in Chapter 3, section 3.2.2.1).

Briefly, the unset materials were placed on a diamond top-plate within a Fourier transform infrared (FTIR) spectrometer, confined within a ring of 5 mm diameter and 2 mm depth and sealed with an acetate sheet. FTIR spectra were then generated continuously for 30 min after sample exposure to intensive blue light.

The difference in FTIR absorbance at 1716 and 1736 cm^{-1} was recorded and the change between time t=0 and t calculated. This was divided by the maximum change between the beginning and end of the experiment to calculate the extent of the reaction at time t. Multiplication by the final percentage reaction then gave monomer conversion percentage at time t. This was determined using the height

of the Raman 'C=C' peak at 1640 cm^{-1} of each sample after light cure divided by that of the uncured pastes.

Monomer conversion percentage (see Eq. 3.1 in Chapter 3) was then plotted versus light exposure time and the polymerisation rate (the gradient of the linear region of the plot between 20 and 60% conversion), was subsequently calculated and reported.

4.2.3. Mass and volume change upon water sorption

Determination of mass and volume change of specimens after immersion in water was described in Chapter 3, section 3.2.2.4.

Briefly, the specimen discs were placed upright in the conical end of a Sterilin tube, containing 10 ml of neutral deionised water. After 0, 15 min, 2, 8, 24 h, 2, 7 and 10 days and 3, 5, 6, 7, 8, 9 and 10 weeks at 37 °C, the specimen mass and density were measured prior to placement of samples in fresh storage solution.

Percentage wet mass and volume change were calculated using the difference in results at time t compared with initial values then divided by the initial values times 100 (see Eq. 3.2– 5 in Chapter 3).

At the end of the study period, specimens were dried under vacuum to constant mass. The final water content (ΔMw) and the material mass loss (ΔM) were calculated using:

$$\Delta Mw = \frac{W_f - M_f}{W_f} \times 100 \quad 4.1$$

where W_f and M_f are respectively the final wet and dry mass of the specimen.

$$\Delta M = \frac{M_0 - M_f - M_d}{(1-y)M_0} \times 100 \quad 4.2$$

where M_0 and M_d are respectively the intitial dry mass of the specimen and mass of the released drug from that specimen. y is the initial mass fraction of CHX (i.e.10 wt.%).

Specimens before and after 24 - h and 10 - week storage in water were used for Raman and XRD examination (detailed in section 4.2.5). The storage solution at each time point was used to determine the CHX concentration (detailed in section 4.2.6). The frequency of water change was selected to ensure the solubility limit of CHX (20 mg/ml) was not reached but that sufficient CHX was present for accurate determination by UV spectrometry (> 5 μg/ml) (Young and Ho 2008). To gain evidence for any anomalous effect arising due to MCPM/TCP reaction within the formulations, composite discs filled with 50, 60 and 70 wt.% brushite particles were used as additional controls in the CHX release studies.

4.2.4. Water sorption induced chemical changes

Samples stored as above for 0, 24 h and 10 weeks in water were analysed using Raman and XRD to assess any chemical changes in the filler upon water sorption. The specimens were air dried at room temperature for 24 h prior to Raman and XRD examination.

4.2.4.1. Raman

Each specimen was cut vertically with a razor blade prior to analysis. Surfaces produced were then examined using a LabRam spectrometer (Horiba Jobin Yvon, Stanmore, UK) equipped with a 633 nm wavelength laser, x 50 objective lens and 1800 grating. Mean sample spectra were generated by averaging 15 line Raman spectra. Each line spectrum was an average of 31 point spectra along a 150 μm line with step size of 5 μm. Exposure times for each single-point spectrum were 10 s and the accumulation number set at 6. The line spectrum was recorded every 100 μm from the top surface to the center of the specimen. Background subtraction was performed using Labspec software for each single point spectrum. The mean spectra were eventually normalised using the polymer 'CH' peak at 1447 cm^{-1}. The peak intensities due to other components then provide an indication of the level of that component relative to the polymer (Young *et al.* 2009; Mehdawi *et al*. 2009).

In the following only those spectra of formulations with CHX are provided. Corresponding spectra of formulations without the drug are reported earlier (see

Chapter 3, section 3.3.2.1). Standard Raman spectra of the polymer, β-TCP, MCPM, brushite, monetite and CHX were also recorded for comparison.

4.2.4.2. X-ray diffraction (XRD) spectroscopy

XRD was additionally used to identify the presence of different chemical components in each specimen. XRD spectra of the 0-h, 24-h and 10-week specimens (transverse sections of specimen core) of different formulations were recorded as previously described (see details in Chapter 3, section 3.2.2.2.B). Peak assignment of different chemical components was performed using the International Centre for Diffraction Data database volumes 1 and spectra of starting chemicals of β-TCP, MCPM and CHX.

4.2.5. *In vitro* chlorhexidine (CHX) release

4.2.5.1. Quantification of drug release rate

To quantify the rate of CHX release, UV absorbance spectra of the above sample storage solutions were measured between 200 and 350 nm at a scan speed of 120 nm/min with spectral bandwidth of 2 nm and data interval of 1 nm using a Unicam UV 500 Thermospectronic® Spectrometer (Thermo Spectronic, Cambridge, UK). These were compared with solution spectra of pure CHX at concentrations of 5 to 50 μg/ml to obtain the CHX concentration in each sample (see Eq. 4.3). The CHX concentration was then converted to cumulative mass of CHX released from each specimen (see Eq. 4.4). The percentage of the released

CHX at time t was finally calculated as the ratio of the amount of released CHX at that time to the total amount of CHX in the original specimen, defined as 100%.

$$m = \left(\frac{A}{k} \times u \right) \times m' \quad 4.3$$

$$M = \sum_{0}^{t} m_t \quad 4.4$$

where m is the amount of released CHX at a given time t, A is the absorbance due to CHX at the wavelength of 254 nm, k is the gradient calculated from the calibration curve of 'the CHX absorbance versus concentration', u is a dilution factor, m' is the mass of storage solution (i.e. 10 g), and M is the cumulative mass of the released CHX at anytime t.

One assumption of using these equations was that the absorbance at 254 nm due to impurities (e.g., degraded polymer) was negligible. This could be confirmed by the fact that the full UV spectrum matched that of the pure CHX (data not shown). The full UV spectrum could also provide some evidence for maintenance of the chemical structure of CHX after release.

4.2.5.2. Evaluation of drug release mechanism

To evaluate the CHX release mechanism, an empirical equation, proposed by Ritger and Peppas was used (see Eq. 4.5). This equation is popular for analysis of drug release from swelling/degradable tablets (Ritger *et al.* 1987a).

$$\frac{M_t}{M_\infty} = kt^n \quad 4.5$$

where M_t is the amount of drug released at time t, and M_∞ is the amount of drug released after infinite time; k is a constant incorporating structural and geometric characteristics of the discs, t is the release period and n is a diffusion exponent, indicative of the release mechanism. A 'n' value between 0.45 and 0.89 suggests anomalous transport (a coupling of diffusion and macromolecular relaxation mechanisms) in which there may be some influence of swelling and/or erosion (Ritger *et al.* 1987b).

The release data from these systems are also often analysed as a function of the square root (SQRT) of time if drug release is governed by pure diffusion. However, the use of this relationship in swelling/degradable systems is not completely justified (Colombo *et al.* 2000). To quantify the contribution of diffusion and swelling/degradation mechanism, drug release data was also fitted in a binomial equation (see Eq. 4. 6), proposed by Young *et al* (Young and Ho 2008):

$$\frac{M_t}{M_\infty} = k_{0.5}t^{0.5} + k_1 t \qquad 4.6$$

where M_t again is the amount of drug released at time t, and M_∞ is the amount of drug released after infinite time; $k_{0.5}$ is the diffusion constant and k_1 is the swelling/degradation constant respectively. A higher value of k_1 / $k_{0.5}$ indicates drug release versus time is more linear.

4.2.6. Antibacterial susceptibility assessment

The antibacterial activity of the polymer and composites containing CHX was assessed by an agar diffusion assay (British Society for Antimicrobial Chemotherapy standardised disc susceptibility testing method (Andrews 2008)), using bacterial strains of *S. aureus* 8325-4 (SA 8325-4) and methicillin-resistant *S. aureus* -16 (MRSA-16). Briefly, the test bacterium was spread onto the surface of blood agar plates (Oxoid, Basingstoke, UK). Sample discs (5 mm diameter, 2 mm thick) were then placed on top and the plates incubated at 37 ºC in a 5% CO_2 atmosphere for 24 h. Diameters of inhibition zones (including specimens) were measured in three different directions using calipers.

4.2.7. Statistical evaluation

The statistical significance of differences between the formulations with and without CHX on various material properties including polymerisation rate, initial mass and volume change, final water content and material loss, was evaluated using one-way ANOVA with the Bonferroni post hoc test. Data were evaluated using SPSS 14.0 for Windows (SPSS, Inc., Chicago, Ill., USA). The results were expressed as means ± SD, and p values <0.05 were considered statistically significant.

4.2.8. Factorial analysis

Factorial analysis was used in this study to assess the effect of three variables (F%, T/M and M_d) on different material properties of formulations containing CHX

(Ho and Young 2006;Mehdawi *et a*l. 2009;Young and Ho 2008;Zhao *et al.* 2010). These material properties included polymerisation rate, initial mass and volume change, final water content, final material mass, CHX release at 10 day and 10 weeks and antibacterial activity.

The effect of each variable on a material property was expressed using 'a values' (see Eqs. 3.8 - 9 in Chapter 3). If error bars on 'a' values (means ± SD) do not cross zero, the variable has on average a significant effect on the property. A positive 'a value' means that the property increases with increasing variable and vice versa for a negative 'a'. Higher values of 'a' indicate greater effects of the variable on a property.

4.3. Results

4.3.1. Effect of CHX and filler addition on polymerisation rate and degree of monomer conversion

Polymerisation on the FTIR diamond began immediately upon turning on the high intensity curing light irrespective of formulation. For formulations with the same level of filler (see example in Fig. 4.2, circle or square), the curves of monomer conversion percentage versus light exposure time of formulations with CHX (filled symbols) overlapped with those without CHX (non-filled symbols). There was no significant difference in the polymerisation rate between the samples with and without CHX (Table 4.1).

Additionally, increasing the filler content from 50 wt.% to 70 wt.% resulted in slower polymerisation (see example in Fig. 4.2, compare circle and square) although adding filler to the polymer at a level of 50 or 60 wt.% had no measurable effect (Table 4.1). The average polymerisation rate was found to be 1.7 %/s for polymer, 1.6 %/s for composites with F% = 50 % (i.e. composite formulations 6-9 in Table 4.1), 1.5 %/s for composites with F% = 60 % (i.e. composite formulation 5 in Table 4.1), and 0.9 %/s for composites with F% = 70% (i.e. composite formulations 1-4 in Table 4.1) (Table 4.1). According to factorial analysis, the only variable which significantly affected the polymerisation rate was the filler content, F%, and the polymerisation rate was reduced with increase in F% (Table 4.2).

For all samples, over 85% of the monomer was polymerised following 120 s of blue light exposure and 100% monomer conversion was observed by 200 s (see example in Fig. 4.2). This result established that the final degree of monomer conversion was not affected by CHX and filler addition.

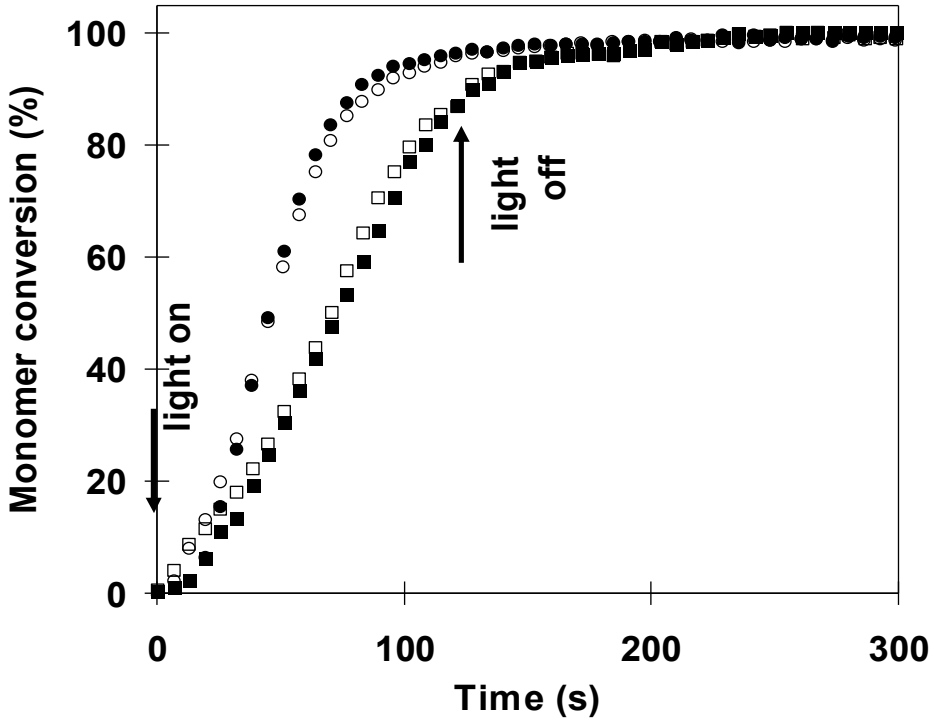

Fig. 4.2. Percentage monomer conversion with time of representative composite formulations. The results demonstrate the lack of effect of CHX but decline in rate (gradient of the linear region of the plot between 20 and 60% conversion) with higher filler content. ● and ○ F% = 50%, T/M =4, M_d = 30 μm with and without CHX respectively; ■ and □ F% = 70%, T/M =4, M_d = 30 μm with and without CHX respectively.

Table 4.1. Polymerisation rate, initial mass and volume change, final water content and material loss of composites and polymer.

		F% (%)	T/M	M_d (μm)	Polymerisation rate (%/s)		Initial mass change at 24 h (%)		Initial volume change at 24 h (%)		Final water content at 10 weeks (%)		Final material loss at 10 weeks (%)	
					- CHX	+ CHX	- CHX	+ CHX	- CHX	+ CHX	- CHX	+ CHX	- CHX	+ CHX
Composites	1	70	4	90	0.9±0.2	0.9±0.2	12±1	13±1*	20±1	24±1*	11±1	20±1*	4±1	4±1
	2	70	4	30	1.0±0.2	0.9±0.2	11±1	12±1*	20±1	22±1*	11±1	19±1*	4±1	4±1
	3	70	1	90	0.9±0.2	1.0±0.2	19±1	20±1*	35±1	39±1*	20±1	40±2*	**10±1**	**10±1**
	4	70	1	30	0.9±0.2	0.9±0.2	18±1	21±1*	34±1	37±1*	21±1	33±2*	**10±1**	**9±1**
	5	60	2	60	1.5±0.3	1.5±0.3	10±1	12±1*	18±1	21±1*	13±1	19±2*	6±1	6±1
	6	50	4	90	**1.7±0.3**	**1.6±0.3**	6±1	8±1*	8±1	14±1*	8±1	15±1*	4±1	4±1
	7	50	4	30	**1.6±0.3**	**1.5±0.3**	6±1	7±1*	10±1	12±1*	9±1	12±1*	4±1	4±1
	8	50	1	90	**1.6±0.3**	**1.6±0.3**	8±1	12±1*	15±2	18±1*	14±1	23±1*	**8±1**	**10±1**
	9	50	1	30	**1.7±0.3**	**1.6±0.3**	10±1	10±1	13±1	14±1	15±1	20±2*	**9±1**	**10±1**
	Polymer				1.6±0.3	1.6±0.3	2±1	5±1*	3±1	5±1*	3±1	8±1*	3±1	4+1

F% (filler content), T/M (molar ratio of β-TCP to MCPM) and M_d (MCPM particle size) are three variables involved in the composite filler factorial design. With three variables (F%, T/M and M_d), each at two levels, high (e.g. F%=70%) and low (e.g. F%=50%), plus one intermediate level (e.g. F%=60%), there are nine formulations. Formulation 5 is defined as intermediate formulation in this study. '-' and '+' stand for formulations without and with CHX respectively. Results = means ± SD (n=3). * significant differences ($p<0.05$) from control values (formulations without CHX). The best results are marked in bold.

Table 4.2. 'a terms' demonstrating the effect of filler variables on properties of CHX – containing materials

	Polymerisation rate	Initial mass change	Initial volume change	Final water content	Final material loss	CHX release at 10 days	CHX release at 10 weeks	Inhibition zone sizes SA 8325-4	Inhibition zone sizes MRSA-16
$a_{F\%}$	-0.3±0.02	0.3±0.1	0.4±0.1	0.2±0.1	-	0.3±0.01	0.2±0.01	0.1±0.04	0.1±0.1
$a_{T/M}$	-	-0.2±0.01	-0.2±0.01	-0.3±0.1	-0.4±0.1	-	-	-	-
a_{Md}	-	0.1±0.01	0.1±0.02	0.1±0.04	-	-	-	-	-

F% (filler content), T/M (molar ratio of β-TCP to MCPM) and M_d (MCPM particle size) are three variables involved in the filler design. The results shown are 'a values' calculated using Eq 3.8 – 9 (see Chapter 3, section 3.2.4). Results = means ± SD (n=3). The magnitude of the 'a' value and its sign indicate the size and direction of the effect of each variable on a material property. A positive 'a value' means that the property increases with increasing variable and vice versa for a negative 'a'. Higher values of 'a' indicate greater effects of the variable on a property. '-' means the effect of a variable on a property is negligible.

4.3.2. Effect of CHX and filler addition on water induced mass and volume change

Polymer and composites with CHX showed higher initial mass and volume change compared to the control formulations without CHX ($p<0.05$, see Table 4.1). This result demonstrated that addition of CHX significantly raised the initial mass and volume change of polymer and composites. The drug addition also significantly raised the final water content ($p<0.05$, see Table 4.1), but had no measurable effect on the final material loss of either the polymer or the composites (Table 4.1).

Polymer exhibited small and comparable mass (5±1%) and volume (5±1%) increase during the initial 24 h of water immersion (Table 4.1). All composite discs increased rapidly in mass (see example in Fig. 4.3.A) during the initial 24 h of water submersion, but more so in volume (see example in Fig. 4.3.B). Formulations with F% = 50% and T/M = 4 (i.e. composite formulations 6 and 7 in Table 4.1) exhibited minimum mass (approximately 7%) and volume (approximately 13%) change whereas those with F% = 70% and T/M =1 (i.e. composite formulations 3 and 4 in Table 4.1) showed maximum mass (approximately 20%) and volume (approximately 38%) increase (Table 4.1). Factorial analysis showed that the initial mass and volume change was affected strongly by F% and T/M, but less so by M_d (Table 4.2). Increase in F% and decrease in T/M (i.e. increase in MCPM content in the specimens), as well as increase in M_d, encouraged greater water sorption and thus mass and volume increase.

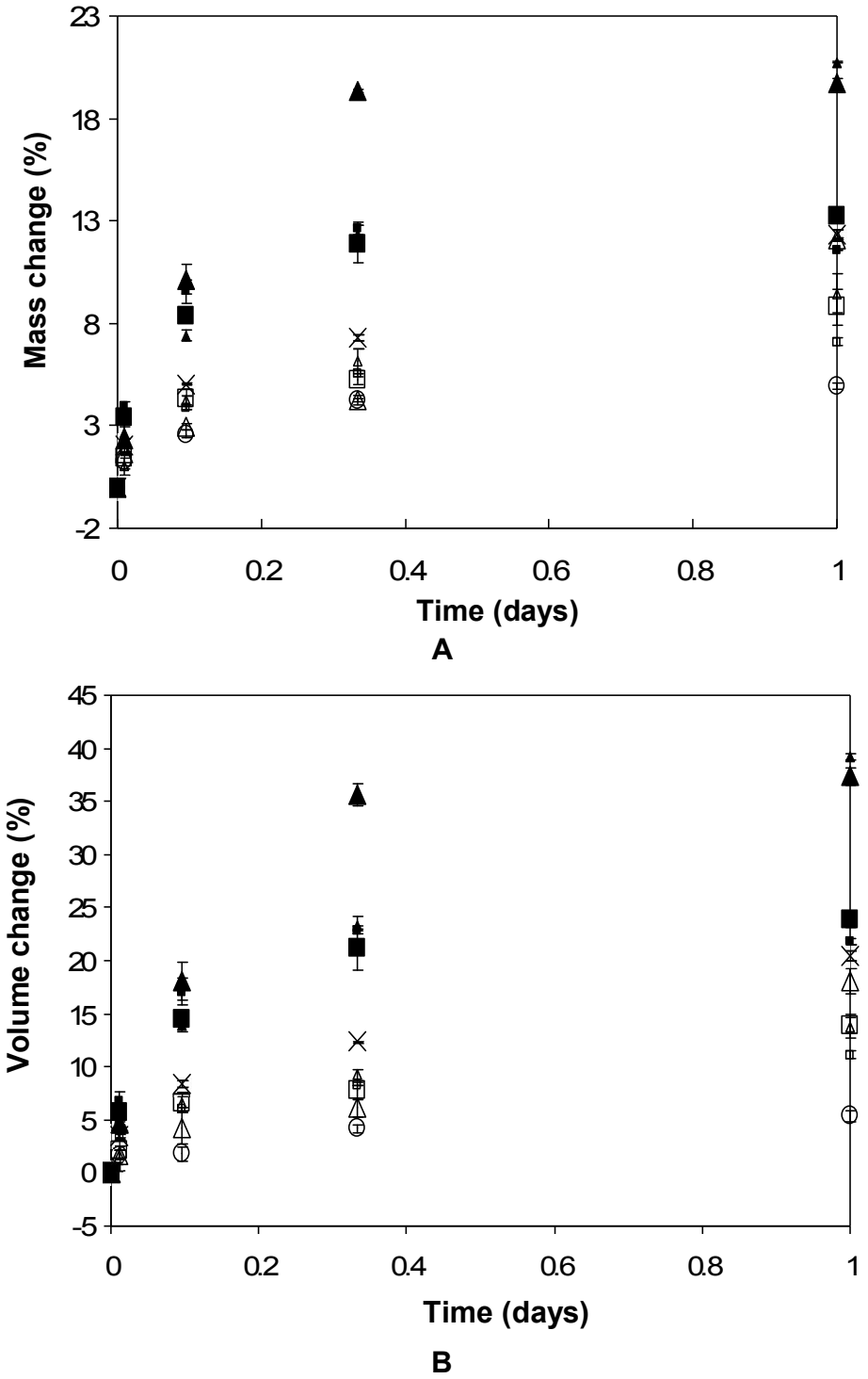

Fig. 4.3. Initial mass (A) and volume (B) change with time of polymer and composites with CHX after immersion in water. ○ polymer; □ and ▫ F% = 50%, T/M = 4, M_d = 90 and 30 μm respectively; Δ and △ F% = 50%, T/M =1, M_d = 90 and 30 μm; x F% = 60%, T/M = 2, M_d = 60 μm; ■ and ▪ F% = 70%, T/M =4, M_d = 90 and 30 μm; ▲and ▲ F% = 70%, T/M =1, M_d = 90 and 30 μm.

Between 24 h and 10 weeks, a slight decrease in polymer and composite mass and less reduction in volume (compared to mass decrease) were generally observed (Fig. 4.4, compare A and B), indicative of combined bulk and surface erosion during the hydrolytic degradation.

Factorial analysis has shown that the final water content was affected strongly by F% and T/M, but less so by M_d (Table 4.2). Increase in F%, decrease in T/M and increase in M_d, resulted in higher final water content.

Regarding the final material loss, factorial analysis established that varying the F% or the M_d had no substantial effect on this property (Table 4.2). However, a decrease in T/M significantly enhanced final material loss. Composites with T/M=1 (i.e. composite formulations 3, 4, 8 and 9 in Table 4.1) exhibited maximum final mass loss ~ 10%, followed by composites with T/M=2 (composite formulation 5 in Table 4.1, ~ 6%) and composites with T/M=4 (composite formulations 1, 2, 6 and 7, ~ 4%). Composites with T/M=4 exhibited comparable mass loss to the polymer (Table 4.1).

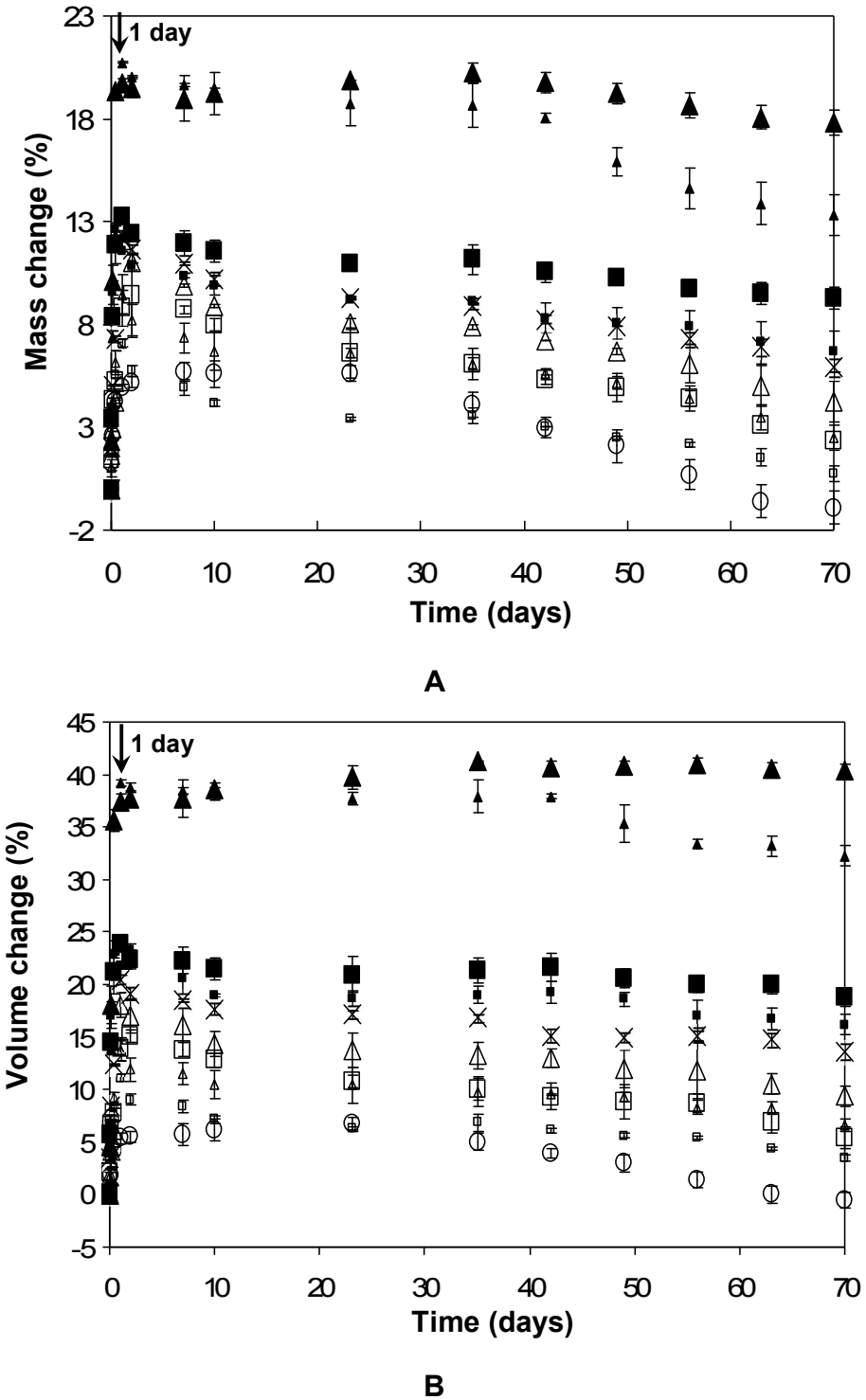

Fig. 4.4. Mass (A) and volume (B) change with time of polymer and composites with CHX after immersion in water. ○ polymer; □ and ▫ F% = 50%, T/M =4, M_d = 90 and 30 μm respectively; Δ and △ F% = 50%, T/M =1, M_d = 90 and 30 μm; x F% = 60%, T/M = 2, M_d = 60 μm; ■ and ▪ F% = 70%, T/M =4, M_d = 90 and 30 μm; ▲and ▲ F% = 70%, T/M =1, M_d = 90 and 30 μm. Note the fast initial increase (arrows) in mass and volume after one day of water immersion and slow slight changes afterwards.

4.3.3. Effect of CHX and filler addition on water accelerated chemical changes

4.3.3.1. Raman

In general, no characteristic 'C=C' peak at 1640 cm^{-1} was observed in any of the polymer and composite Raman spectra (see example in Fig. 4.5), consistent with full monomer conversion during light exposure. By comparison with the standard CHX spectrum, no shift of characteristic CHX peaks were observed before and after photo-polymerisation and upon 24 - h or 10 - week storage in water (data not shown), indicative of maintenance of CHX chemical structure after light exposure and water storage respectively.

The major factor affecting changes in the average Raman spectra with time was CHX and T/M.

With T/M=1 (see for example Fig. 4.5.A), β-TCP (main peaks at 945, 970 and 1045 cm^{-1}), MCPM (main peaks at 903, 915 and 1108 cm^{-1}) and CHX (main peaks at 1093, 1298 and 1600 cm^{-1}) were readily detectable (see Raman spectra of standards of single element in Fig. 4.5.C). Following 24-h water immersion, the MCPM peaks vanished. The peaks of β-TCP and CHX were substantially reduced, and a peak at 980 cm^{-1}, assigned to DCP (mixture of brushite and monetite) appeared. The brushite peak was more intense for those formulations containing CHX. In the absence of CHX, spectra were consistent with greater monetite formation (see Chapter 3, section 3.3.2.1). In the 10-week specimens,

little change occurred in the level of β-TCP whereas DCP and CHX peak intensity were both markedly reduced.

Conversely, with excess β-TCP (particularly T/M=4, see for example Fig, 4.4.B), peaks due to β-TCP dominated the average Raman spectra at all times. The MCPM peaks vanished after 24-h water immersion. A small shoulder at 980 cm^{-1} attributed to DCP could be observed in both 24-h and 10-week spectra. CHX peaks were easily detectable in the 0 and 24-h specimens but less obvious in the 10-week specimen. In summary, excluding any peaks associated with CHX, Raman spectra with and without drug were comparable when β-TCP was in excess.

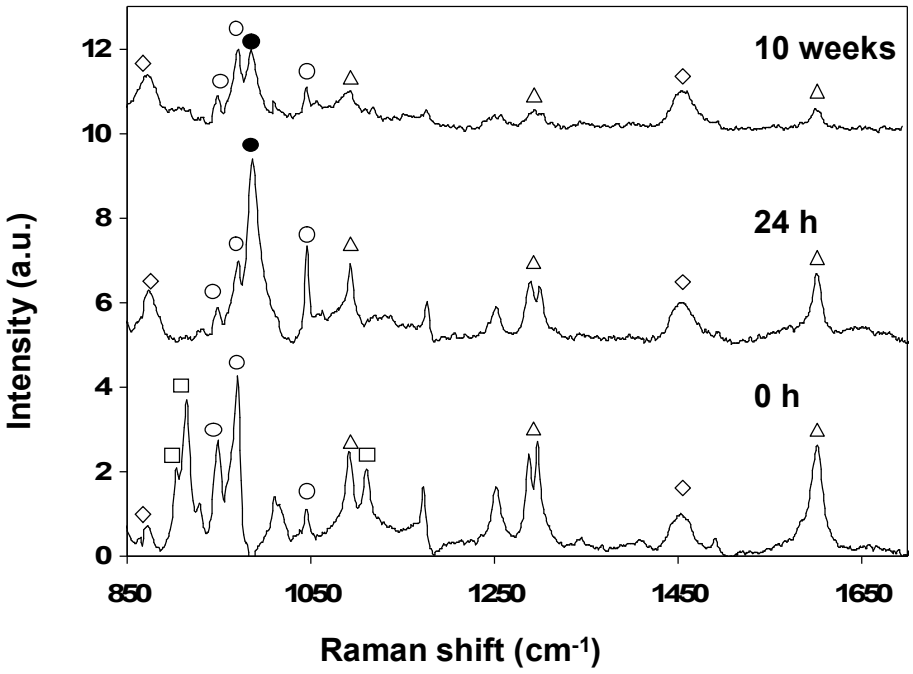
10 weeks
24 h
0 h
Intensity (a.u.)
Raman shift (cm-1)
0
2
4
6
8
10
12
850
1050
1250
1450
1650

A

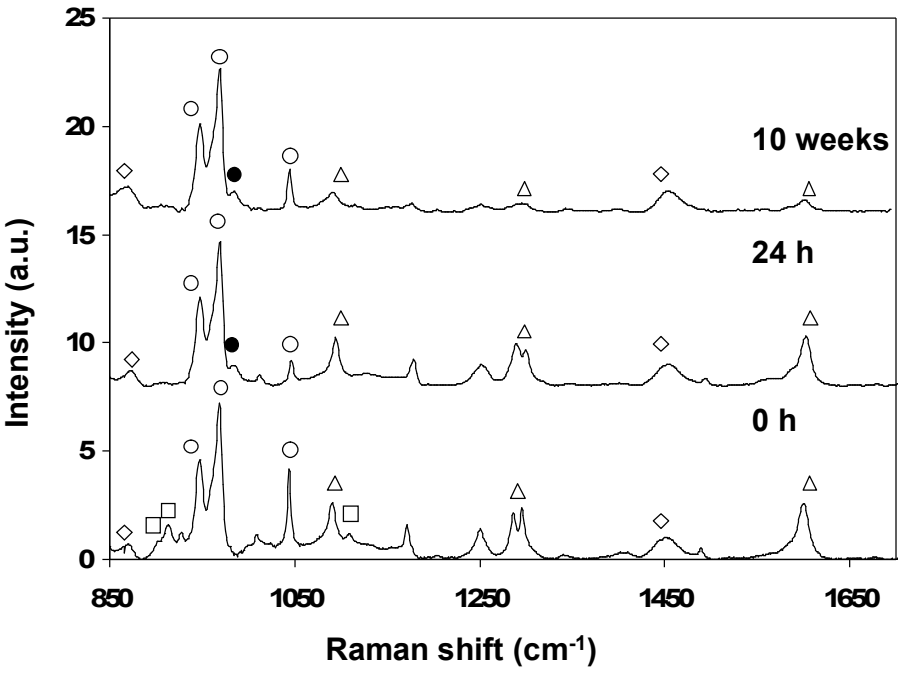
10 weeks
24 h
0 h
Intensity (a.u.)
Raman shift (cm-1)
0
5
10
15
20
25
850
1050
1250
1450
1650

B

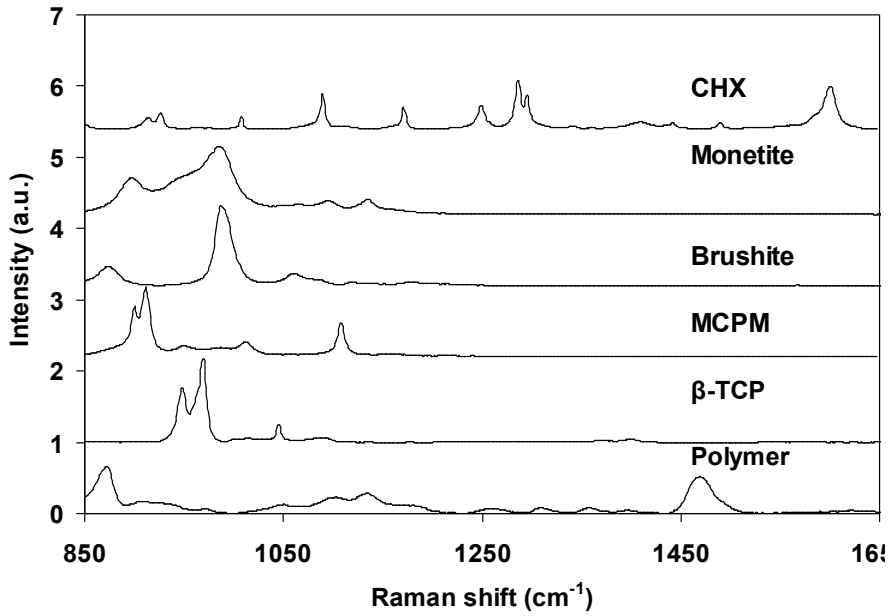

C

Fig. 4.5. A and B: Raman spectra of an example composite with F% = 70 %, T/M = 1 and M_d = 30 µm and an example composite with F% = 70 %, T/M = 4 and M_d = 30 µm before (0 h) and after 24-h and 10-week immersion in water. ◊ polymer, ○ β-TCP, □ MCPM, Δ CHX, ● dicalcium phosphate (mixture of brushite and monetite). C: Raman spectra of standards including the set polymer, β-TCP, MCPM, brushite, monetite and CHX. Note the absence of MCPM and presence of dicalcium phosphate after composite immersion in water for 24 h.

4.3.3.2. XRD

In all specimen XRD spectra, CHX was not detectable at the concentration of 10 wt.%. Before water immersion, β-TCP (peaks at 27.9, 31.2 and 34.5 º2θ) and MCPM (peaks at 23 and 24.3 º2θ) were clearly observed with formulations with T/M = 1 or 2 (see for example Fig.4.5.A) but less pronounced with T/M = 4 (see for example Fig.4.5.B). XRD spectra of standards are shown in Fig. 4.6.C.

After 24-h water immersion, the β-TCP peak intensity was reduced with T/M =1 or 2 (see for example Fig.4.5.A) but remained intense when β-TCP was in excess (particularly T/M =4) (see for example Fig. 4.6.B). MCPM was not detectable in any 24-h XRD spectra. Intense peaks at 12, 21 and 29.4 º2θ indicating brushite and peaks at 26.7 and 30.3 º2θ, identified as monetite, were apparent if T/M =1 or 2 but just detectable with T/M = 4. With T/M =1 or 2, the brushite peak was more intense for the formulations containing CHX. In the absence of CHX, spectra were instead consistent with greater monetite formation (see Chapter 3, section 3.3.2.2). With T/M = 4, brushite peak intensity was not significantly affected by CHX addition.

After 10-week water immersion, β-TCP was readily detectable in all specimen XRD spectra, particularly with T/M = 4. Brushite vanished in any specimen XRD spectra. Monetite was readily visible with T/M=1 or 2 (see for example Fig. 4.6.A) but less clear with T/M = 4 (see for example Fig. 4.6.B).

The above Raman and XRD analysis are consistent with the formation of brushite and monetite in 24 h as a result of the reaction of β-TCP and MCPM. It was also found that the CHX addition raised the formation of brushite over monetite particularly when composites had T/M =1 or 2. In the formulations with T/M = 4, the effect of CHX addition was not measurable. During long-term water immersion, any produced brushite has largely dissolved into the storage solution.

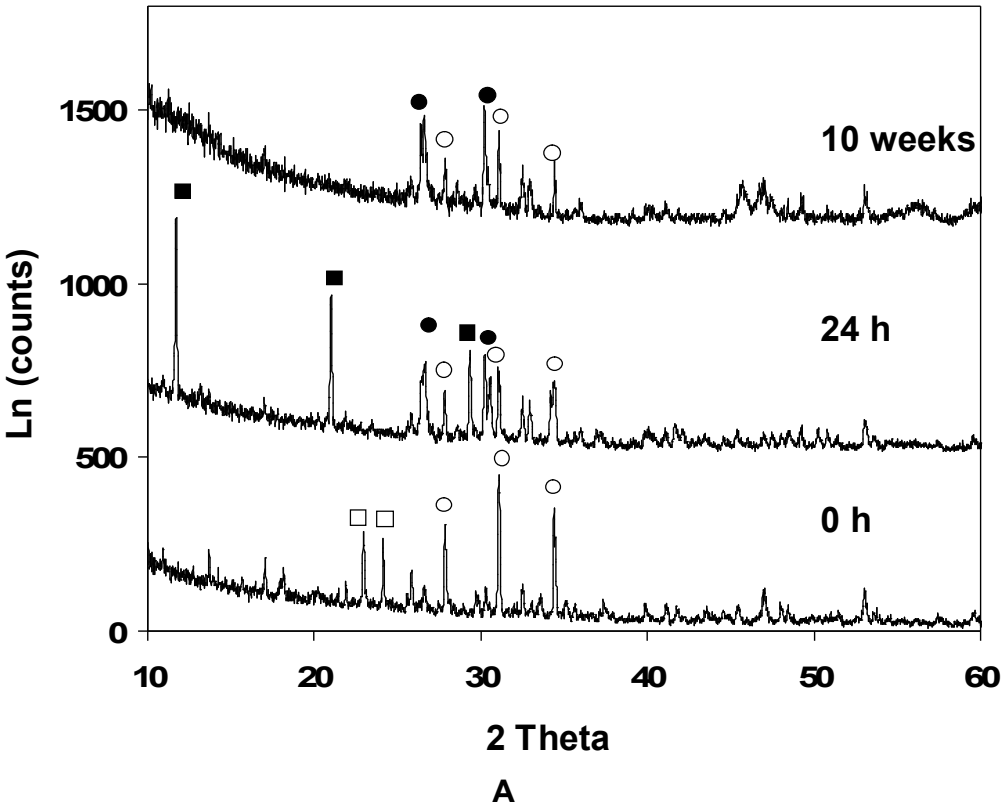
1500
1000
500
0
Ln (counts)
10 weeks
24 h
0 h
10
20
30
40
50
60
2 Theta

A

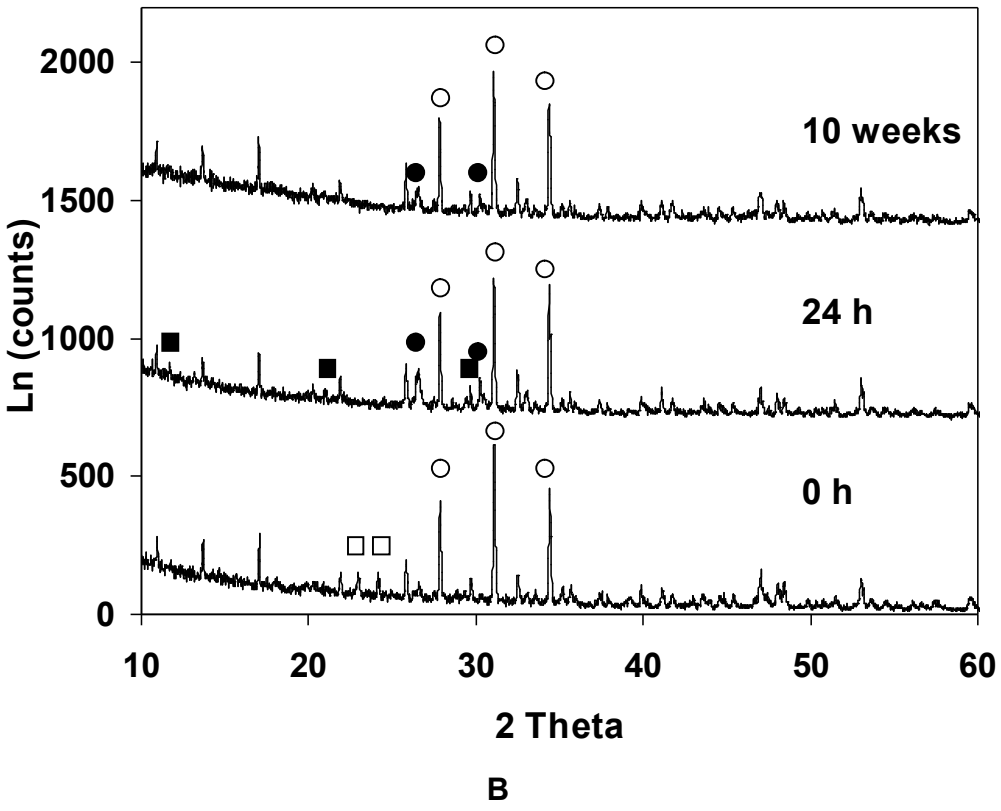
2000
1500
1000
500
0
Ln (counts)
10 weeks
24 h
0 h
10
20
30
40
50
60
2 Theta

B

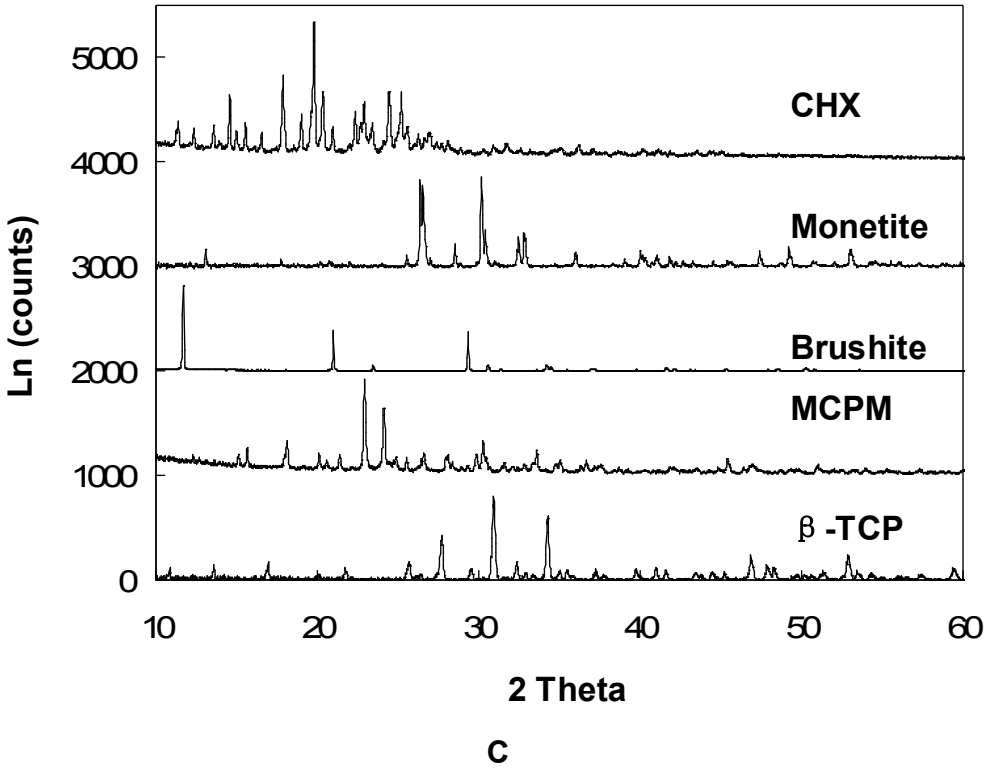

C

Fig. 4.6. A and B: XRD spectra of an example composite with F% = 70%, T/M = 1 and M_d = 30 μm and an example composite with F% = 70%, T/M = 4 and M_d = 30 μm before (0 h) and after 24-h and 10-week immersion in water. ○ β-TCP, □ MCPM, ■ brushite, ● monetite. CHX could not be detected in all specimen XRD spectra. C: XRD spectra of standards including β-TCP, MCPM, brushite, monetite and CHX. Note the absence of MCPM and presence of brushite and monetite after composite immersion in water for 24 h.

4.3.4. Effect of filler addition on CHX release

UV spectra of sample storage solutions exhibited identical profiles to those of pure CHX solutions, indicating that the CHX was released without any obvious change in chemical structure (data not shown). CHX was released faster in the initial 10 days and then the release rate declined with time (Fig. 4.7). CHX release rate increased in the order: polymer < composites with F% = 50% (C_{F50}) < C_{F60} < C_{F70} (Fig. 4.7). At 10 days, the average cumulative CHX release was 14, 26, 42, and 52% of the original CHX when the filler content increased from 0, 50, 60 to 70 wt.%, respectively. At 10 weeks, the average cumulative CHX release from polymer, C_{F50}, C_{F60}, and C_{F70} was 43, 57, 66 and 77%, respectively (Table 4.3). Factorial analysis demonstrated that F% was the only factor having a significant effect on CHX release rate (at 10 days or 10 weeks, Table 4.2), with CHX release enhanced by raising F%.

For control formulations with brushite fillers, the released CHX at 10 days and 10 weeks, respectively, was 23 and 51% for C_{F50}, 26 and 59% for C_{F60}, and 35 and 66% for C_{F70} (Table 4.3). Like composites with β-TCP and MCPM fillers, CHX release rate from control formulations with brushite fillers increased in the order: polymer < C_{F50} < C_{F60} < C_{F70} (Fig. 4.7). In addition, in general, composites filled with β-TCP and MCPM exhibited significantly higher CHX release than the composites filled with brushite ($p<0.05$) at corresponding F% (Fig. 4.7).

The above results have demonstrated that CHX release was enhanced with raised F% (regardless of filler composition of β-TCP and MCPM or brushite) and with reactive filler of β-TCP and MCPM (compared to brushite filler).

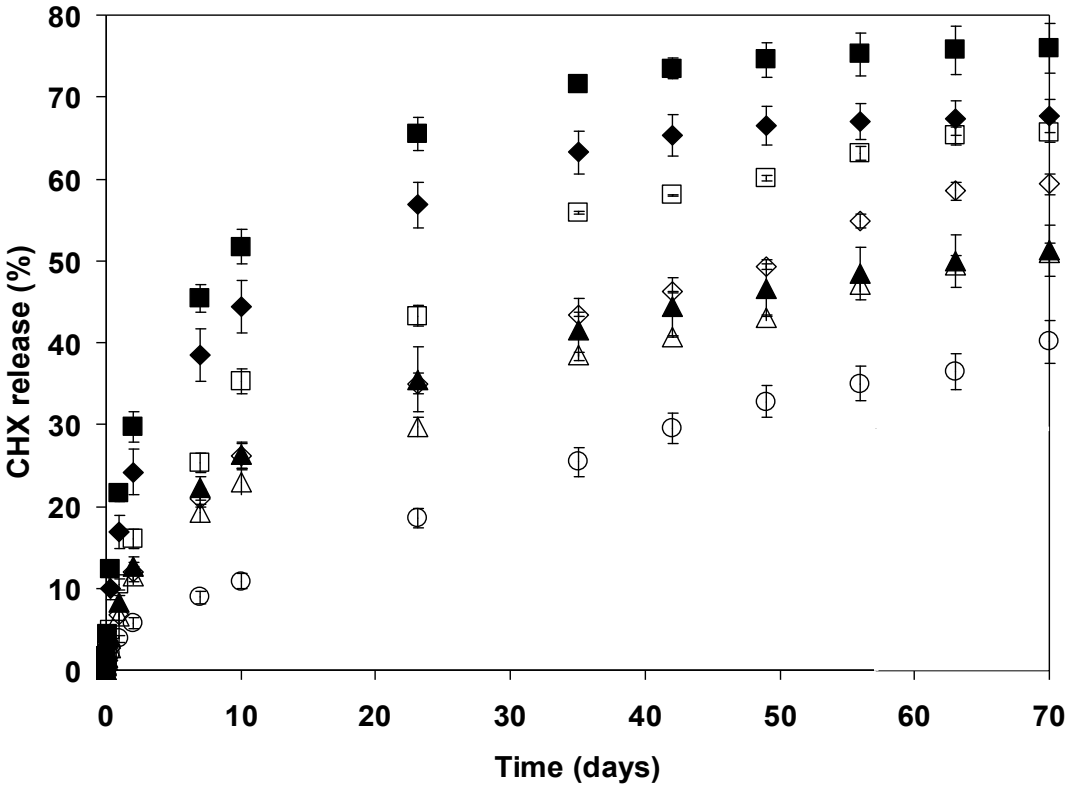

Fig. 4.7. CHX release versus time from polymer (o), composites filled with brushite at 50 (Δ), 60 (◊) and 70 wt.% (□) and composites filled with reactive β-TCP and MCPM at 50 (▲), 60 (♦) and 70 wt.% (■). This figure demonstrates the enhancement of CHX release with raised filler content and with reactive filler of β-TCP and MCPM.

Table 4.3. CHX release at 10 days and 10 weeks; results of fitting the CHX release data to Eq s 4.5 and 6; inhibition zone sizes against SA 8325-4 and MRSA-16.

	Formulations			10 day CHX release (%)	10 week CHX release (%)	k	n	$k_{0.5}$ (%/day$^{0.5}$)	k_1 (%/day)	k_1/ $k_{0.5}$ (day$^{-0.5}$)	Inhibition zone diameter (mm)	
	F% (%)	T/M	M_d (μm)								SA 8325-4	MRSA-16
Reactive β-TCP and Brushite	70	4	90	**54 ± 1**	**75 ± 1**	**16**	0.52	**23**	-1.8	-0.08	**14±1**	**13±1**
	70	4	30	**50 ± 5**	**81 ± 5**	**16**	0.51	**23**	-2.0	-0.09	**14±1**	**13±1**
	70	1	90	**53 ± 2**	**74 ± 1**	**18**	0.49	**23**	-1.9	-0.08	**13±1**	**11±1**
	70	1	30	**50 ± 5**	**77± 5**	**17**	0.46	**21**	-1.6	-0.08	**15±1**	**13±1**
	60	2	60	42 ± 1	66 ±3	13	0.51	16	-1.0	-0.06	12±1	11±1
	50	4	90	27 ± 1	59 ± 2	7	0.53	10	-0.39	-0.04	12±1	11±1
	50	4	30	24 ± 1	58 ± 1	6	0.54	8	-0.28	-0.03	12±1	11±1
	50	1	90	28 ± 1	58 ± 1	8	0.50	10	-0.44	-0.04	12±1	11±1
	50	1	30	26 ± 3	54 ± 1	7	0.51	9	-0.34	-0.04	12±1	10±1
	70	N/A	N/A	35 ± 2	66 ± 2	9	0.49	11	-0.37	-0.03	N/A	N/A
	60	N/A	N/A	26 ± 2	59 ± 2	7	0.53	8	-0.09	-0.01	N/A	N/A
	50	N/A	N/A	23 ± 2	51 ± 2	6	0.52	7	-0.14	-0.02	N/A	N/A
	Polymer			14 ± 2	43 ± 2	4	0.53	3	0.26	0.87	11±1	10±1

F% (filler content), T/M (molar ratio of β-TCP to MCPM) and M_d (MCPM particle size) are three variables involved in the factorial design. k is a drug release rate constant incorporating structural and geometric characteristics of the specimen and n is a diffusion exponent; k and n were obtained by fitting the CHX release data to Eq. 4.5 (fitting range corresponded to release% < 60%); n value between 0.45 and 0.89 suggests a release mechanism by diffusion and macromolecular relaxation. $k_{0.5}$ is a diffusion constant and k_1 is a swelling/degradation constant, both of which were determined by fitting the CHX release data to Eq. 4.6 (fitting range corresponded to release% < 60%); A higher value of k_1 / $k_{0.5}$ indicates more linear drug release. Inhibition zone diameter was measured including the specimen (5 mm diameter). Results = means ± SD (n=3). The best results are marked in bold

To evaluate the CHX release mechanism, the CHX release data was plotted versus SQRT of time. The plot of CHX release versus SQRT of time was more linear than that versus time (compare Fig. 4.8 and 4.7), as expected for a diffusion-controlled process. For all formulations, the gradients of the curves (CHX release percentage versus SQRT of time) were almost constant at any time points when the release percentage was less than 60% but these gradients decreased when the release percentage was larger than 60%.

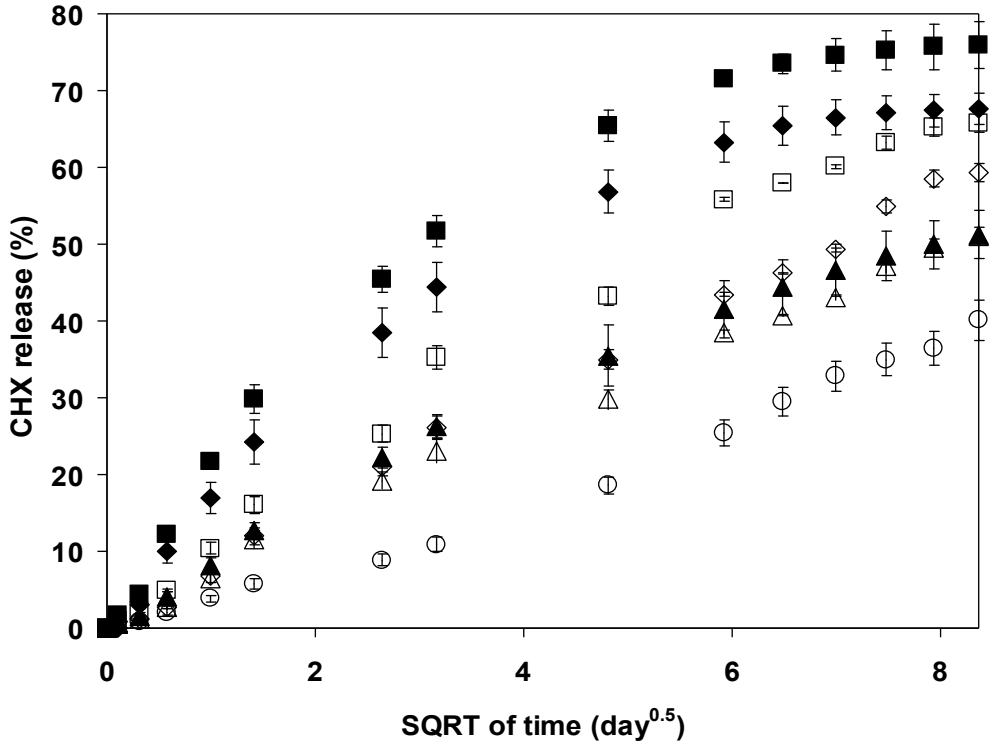

Fig. 4.8. CHX release versus square root (SQRT) of time from polymer (o), composites filled with brushite at 50 (Δ), 60 (◊) and 70 wt.% (□) and composites filled with reactive β-TCP and MCPM at 50 (▲), 60 (♦) and 70 wt.% (■). Note that the CHX release percentage is more linear with SQRT of time than that with time (compare Fig. 4.7).

The release data were then fitted in Eqs. 4.5 and 6 to further investigate the release mechanism. Eq. 4.5 could fit drug release data up to 60% with all R^2 values greater than 0.99. Composites with reactive β-TCP and MCPM or brushite fillers, with higher F% generated faster CHX release (higher k value, Table 4.3). The diffusion exponent n ranged between 0.46 – 0.54 for all formulations, indicative of a coupling of diffusion and swelling/erosion mechanism according to Peppas (Ritger *et al*.1987b).

Eq. 4.6 could also fit drug release data up to 60% with all R^2 values greater than 0.99. The result that $k_{0.5}$ is greater than k_1 has indicated that the release mainly followed a diffusion mechanism although swelling/erosion had some effect on CHX release. $k_{0.5}$ increased in the order: polymer < composites with F% = 50% (C_{F50}) < C_{F60} < C_{F70} (Table 4.3). Composites with reactive filler had larger $k_{0.5}$ than those with brushite filler at the same F%.

4.3.5. Effect of CHX and filler addition on adhesive antibacterial activity

Although a small thin halo of growth inhibition around some of the control formulations with no CHX was occasionally observed, all the CHX – containing formulations (both polymer and composites) had very much larger and clearer inhibition zones (see example in Fig. 4.9). Inhibition zone sizes increased when the F% was increased, with average diameters for the SA 8325-4 strain of 11, 12, 12 and 14 mm for 0, 50, 60 and 70 wt.% filler, respectively. With the MRSA-16 strain, the zone diameters were on average 10, 11, 11 and 13 mm for 0, 50, 60

and 70 wt.% filler, respectively (Table 4.3). Factorial analysis showed that F% was the only factor having a significant effect on the sizes of the inhibition zone, with zone diameters enlarged by raising the F% (Table 4.2).

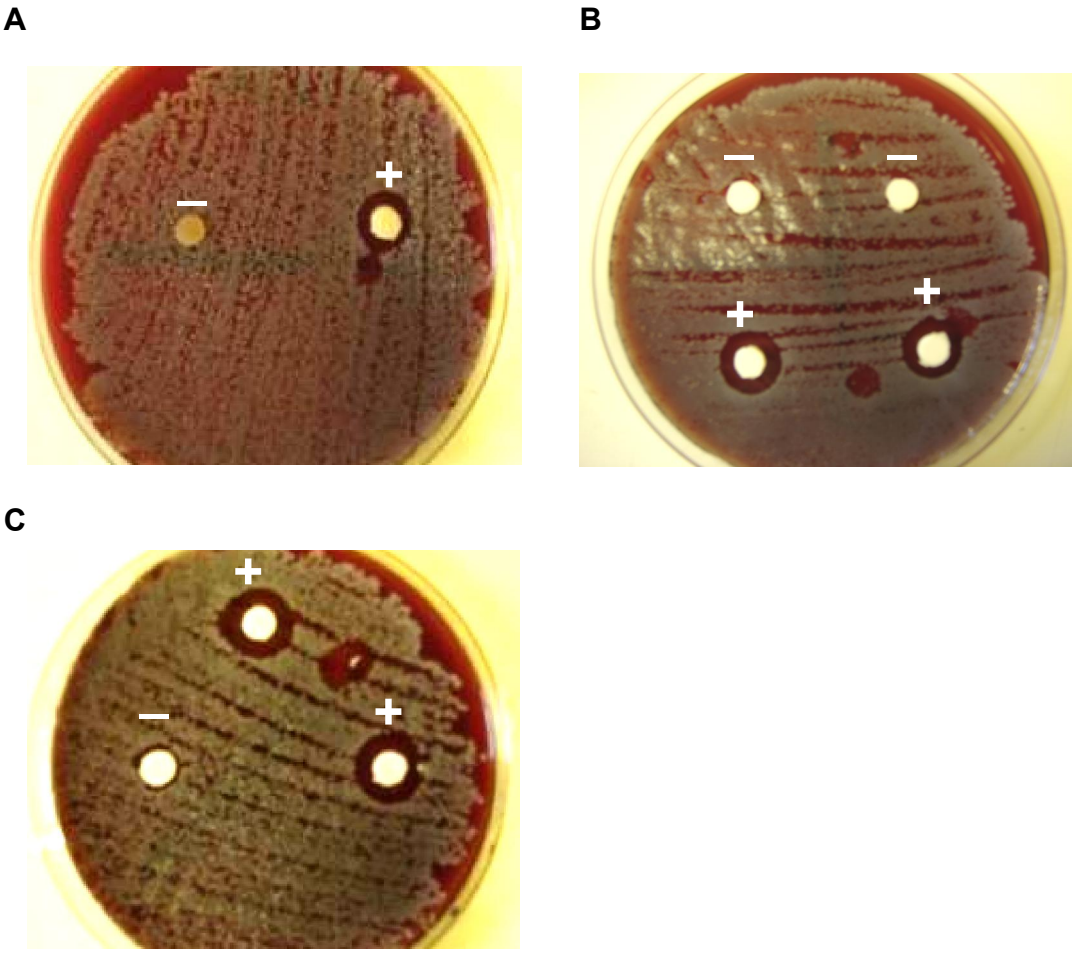

Fig. 4.9. Inhibition zones against bacteria strain SA 8325-4. A: Polymer specimen with (+) and without (-) CHX; B: An example composite specimen (F% =50%, T/M =1, M_d = 30 μm) with (+) and without (-) CHX; C: An example composite specimen (F% =70%, T/M =1, M_d = 30 μm) with (+) and without (-) CHX. Note the increase in inhibition zone size with addition of CHX and with increase in specimen F%.

4.4. Discussion

In this chapter, the effect of CHX addition on polymerisation rate and degree of monomer conversion, water sorption and material degradation in addition to water accelerated chemical changes of the composite materials discussed in Chapter 3 were reported. Effect of filler variables on CHX release kinetics and adhesive antibacterial activity were then investigated.

4.4.1. Effect of CHX and filler addition on polymerisation rate and degree of monomer conversion

The lack of effect of CHX addition on the monomer polymerisation rate found here is similar to a previous study of photo-polymerisation kinetics of non-degradable methacrylate composites, although CHX was found to increase subsequent dark cure in that study (Mehdawi *et al.* 2009). This enhanced dark cure effect was not detected in the present study possibly because the monomer conversion percentage was already more than 85% when the light was turned off. However, a high level of filler addition (i.e. 70 wt.%) was found to lower the polymerisation rate, which may have been due to the increased scattering of the initiating blue light because of the high level of filler particles.

All formulations were found to set rapidly and completely on light exposure, with full monomer conversion being achieved regardless of CHX and filler addition. Such fast and full cure as shown here could allow rapid material bonding to surrounding tissues after injection and would, additionally, limit the release of

reactive and potentially toxic double bond-containing monomers (PGLA-DMA) during placement (Ho and Young 2006).

4.4.2. Effect of CHX and filler addition on water sorption and hydrolytic degradation

The initial increase in mass and volume could be ascribed to water sorption which exceeded material degradation and drug release. The addition of CHX raised the early water sorption of both the polymer and the composites. This may be attributed to the water soluble nature of CHX: the dissolved CHX increasing the adhesive internal osmotic pressure, attracting water sorption (Young and Ho 2008). The increase in the amount of MCPM present per specimen was also found to substantially enhance early water sorption. With molar ratios of β–TCP (Ca_3 $(PO_4)_2$)/MCPM (Ca $(H_2PO4)_2{\cdot}H_2O$) of 4, 2 or 1, the MCPM amount was found to determine the water needed for brushite ($CaHPO_4{\cdot}2H_2O$) formation, according to the following equation, with 0.5 g of water being required to convert 1 g of MCPM into brushite (Bohner 2007):

$$Ca_3\ (PO_4)_2 + Ca\ (H_2PO4)_2{\cdot}H_2O + 7H_2O \rightarrow 4CaHPO_4{\cdot}2H_2O \qquad 4.7$$

The water sorption levels found in this study (data not shown) was just sufficient for this reaction to occur. This may explain the formation of monetite (Ca $(H_2PO4)_2$) in addition to brushite, as shown by the Raman and XRD analysis (see details in section 4.4.3).

In addition, larger MCPM particles were also found to enhance early water sorption. MCPM with large particle sizes would be expected to dissolve and react more slowly, thereby increasing the time over which MCPM was present in the formulations and thus enhancing the early water sorption.

The incorporation of CHX into the material was also found to raise the final water content, possibly due to the replacement of the released CHX with water. In addition, CHX addition did not affect the material degradation. Based on factorial analysis, final material loss was only enhanced by reducing T/M which could have resulted in the formation of higher levels of more soluble brushite and monetite (relative to β-TCP).

As mass reduction was greater than that of volume between 24 - h and 10 - week hydrolytic degradation of these bone adhesives was likely to be a combination of bulk and surface erosion. With bulk filler loss decrease in mass and maintenance in volume is expected (Abou Neel *et al.* 2010). This is because higher density filler is replaced by lower density water. Bulk loss of lower density drug and polymer and their replacement by water would have less effect on overall mass. Additionally, during water immersion, chemical reactions causing changes in component solubility may alter the osmotic pressure within the material matrix. This may result in extra water sorption and material expansion and thus mass and volume increase. With surface erosion alone (i.e. materials are eroded from the surface of the matrix), decrease in mass and volume at a comparable rate

would have been seen (Abou Neel *et al*. 2010). The results found in this study (the mass reduction was greater than the volume reduction) thus indicated the co-occurrence of the two types of degradation but the proportion of either degradation type is uncertain.

4.4.3. Effect of CHX and filler addition on water accelerated chemical changes

Raman and XRD results were consistent with the reaction of β-TCP and MCPM to form brushite and monetite upon water sorption in 24 h in absence or presence of CHX. Higher ratios of brushite/monetite in formulations containing CHX was observed in 24-h Raman and XRD spectra, particularly with T/M =1 (Zhao *et al*. 2010). This might be due to the basic nature of CHX which may help stabilise brushite and prevent its conversion to monetite in presence of water (Grover *et al.* 2005*)*. Additionally, as shown in this study, CHX addition raised the initial water sorption which may promote more brushite (hydrous DCP) formation.

The major factor affecting the composite chemical composition after immersion in water was T/M. With T/M =1, brushite and monetite were the major calcium phosphates after placement in water whereas with T/M = 2 and 4, β-TCP was the major calcium phosphate. Composites with T/M = 1 would thus degrade faster than composites with T/M = 2 and 4 as brushite and monetite have higher solubility than β-TCP (Elliott 1994; Zhao *et al.* 2010). This may explain the observation that the final material loss was enhanced by reducing T/M. The faster

degradation rate may be clinically beneficial in that faster degradation would result in higher calcium and phosphate ion release, possibly providing greater potential for bone regeneration (Ripamonti *et al.* 1996;Zhao *et al.* 2010). In addition, too slow or insufficient degradation of an implant may influence body fluid invasion and cell migration, possibly preventing proper healing of bone defects and impeding tissue remodelling, as suggested by other studies *(*Rizzi *et al*. 2006).

4.4.4. Effect of filler addition on CHX release

The CHX release was governed mainly by diffusion although swelling/erosion of the composite matrix had also some effect. With diffusion – controlled processes gradient of drug release versus time decreases with time due to increasing distance that the drug must diffuse through the matrix.

It was expected that faster CHX release might couple with higher MCPM amount as the resultant increase in water content of the vehicle may plasticise the polymer phase. Enhanced mobility of polymeric chains could then favour transport of entrapped drug and raise drug release rate (Carr *et al.* 1997). Surprisingly, as shown by factorial analysis, faster CHX release was only associated with increased amount of fillers but not water sorption. This may be because the absorbed water was ‘bound in’ brushite crystals (particularly when T/M =1) and not ‘free’ to facilitate drug release. Raising F% did, however, substantially increase drug diffusion. Higher filler addition may create more

interface between the calcium phosphate particles and the polymer, which could provide “channels” for small molecules to diffuse through (Lin *et al.* 2007). In addition, increase in the amount of the released drug with progressively increasing filler content may be due to the reduced amount of polymer in the corresponding formulations. The presence of degradable polymer may generate insoluble acidic polymer degradation fragments to bind basic CHX and thus limit the drug release (Young and Ho 2008).

In addition, composites with reactive filler (β-TCP and MCPM) yielded faster CHX release than those filled with brushite. This may be due to the more soluble MCPM in the reactive system allowing faster water sorption to facilitate drug release compared to the less soluble brushite. Moreover, both the brushite and the reactive system showed the same trend: drug release was raised with increased F%. These findings further support the “channel” hypothesis as mentioned above: higher filler addition may create more interface between the filler particles and the polymer as the “channel” for small molecules to diffuse out (Lin *et al*. 2007). These results have suggested a simple approach to control polymeric drug delivery systems via incorporation of different levels of inorganic soluble or insoluble filler particles.

The CHX release slowed down at later time points possibly due to the interaction between the basic CHX (due to the amine groups in the CHX molecular structure) and the acidic polymer degradation fragments. High F% may have

allowed more complete CHX release at later times since less polymer was present to interact with CHX as explained below. The acid / base equilibrium can be described by the following Bronsted-Lowery expression (Atkins 1994) :

$C_{22}H_{29}Cl_2N_9NH\ (aq) + H_3O^+\ (aq) <---> C_{22}H_{29}Cl_2N_9NH_2^+\ (aq) + H_2O\ (l)$ 4.8

$C_{22}H_{29}Cl_2N_9NH_2^+\ (aq) + RCOO^-\ (s) <---> C_{22}H_{29}Cl_2N_9NH_2\,OOCR\ (s)$ 4.9

The acidic degradation products could possibly drive the equilibrium to the right. During the polymer degradation, the $RCOO^-$ groups could 'mop' up the dissolved CHX molecules and hence inhibit further release of CHX into the storage solution. The drug trapped within the polymer structure may not be released until the polymer fully degrades.

4.4.5. Effect of CHX and filler addition on adhesive antibacterial activity

Addition of CHX to the bone adhesives was found to endow them with antibacterial activity. The bacterial assays confirmed that the CHX released from the polymer and the composites in the first few hours could effectively inhibit the growth of *S. aureus (*methicillin-resistant or not*)*. Higher filler content was found to generate larger bacterial inhibition zones on agar plates, indicative of higher antibacterial activity. The ability to inhibit bacterial growth is often regarded as a critical step in infection prevention, thereby improving the service life of medical implants (Mourino and Boccaccini 2009).

4.5. Conclusion

The PGLA-DMA based bone adhesives containing CHX have been found to be rapid setting, degradable and with controllable drug release properties, making them potentially suitable as antibacterial bone adhesives. The addition of CHX had no effect on either the material polymerisation or subsequent degradation kinetics, although it enhanced initial water sorption and the ratio of resultant brushite to monetite. Increasing the total filler percentage above 60 wt.% decreased the adhesive polymerisation rate. Early water sorption of the set adhesive discs increased with total MCPM level, while decreasing T/M from 4 to 1 substantially enhanced total mass loss at 10 weeks. Drug release was found to occur by diffusion and was enhanced by raising the total filler percentage and reducing polymer content. Growth inhibition of *S. aureus* (methicillin susceptible or resistant) was found to increase at higher total filler content.

Chapter 5

DNA delivery

Abbreviations

In alphabetical order

CQ	camphorquinone
DMPT	*N,N*-dimethyl-*p*-toluidine
FBS	fetal bovine serum
FCM	flow cytometry
FSC	forward scatter
GFP	green fluorescent protein
hMSC	human mesenchymal stem cell
HEMA	hydroxyethyl methacrylate
LD	lipid-DNA complex
LD_{PBS}	LD generated in phosphate buffered saline
LD_{W}	LD produced in deionised Water
MEM	modified Eagle's medium
PBS	phosphate buffered saline
PGLA-DMA	poly (propylene glycol -*co*- lactide) dimethacrylate
PLD	PGLA-DMA film containing LD
SD	standard deviation
SEM	scanning electron microscopy
SSC	side scatter

5.1. Introduction

The continuing and prolonged presence of growth factors such as bone morphogenic proteins at wound sites has previously been demonstrated to be of biomedical value (Woo *et al.* 2003). DNA plasmids that encode growth factors have therefore been incorporated into bone-repair materials in order to improve or increase bone regeneration efficacy (Huang *et al*. 2005). The advantages of delivering DNA plasmids rather than proteins lies in the greater DNA stability and the ability of DNA, after being taken up by cells, to provide protein production (Nussenbaum and Krebsbach 2006) over a prolonged period of time (Bonadio 2000).

Ideally, DNA loaded bone - repair materials should provide not only structural support for the diseased or damaged bone to be replaced, but also a controllable long-term supply of a therapeutic gene to the surrounding bone tissue. The purpose of localised and long-term gene delivery is ultimately to expose cells to DNA for a prolonged period of time in order to increase the possibility of DNA uptake and expression in the target cells and to achieve successful tissue regeneration (Betz *et al*. 2008).

A number of different DNA - releasing materials are currently under investigation, e.g., poly (lactide-*co*-glycolide) scaffolds (Huang *et al.* 2005), photo-polymerisable di-methacrylated lactide - poly (ethylene glycol) - lactide hydrogels (Quick and Anseth 2004), surface-eroding polyanhydrides *(*Quick *et al*. 2004) and calcium phosphate cements (Itaka *et al.* 2007). These particular materials, however, have several fundamental problems. For example, they

are either not injectable or have limited mechanical strength (Huang *et al*. 2005;Quick and Anseth 2004). Moreover, the released DNA is often ineffectual or the delivery period is short (Itaka *et al.* 2007;Quick *et al.* 2004). Injectable materials that could provide structural support and simultaneously release effective therapeutic DNA for a long term would therefore constitute a significant advance.

The fluid poly (propylene glycol -*co*- lactide) dimethacrylate (PGLA-DMA) studied in this project has previously been shown to be capable of solidification within seconds of intense blue light exposure (Ho and Young 2006), and the set PGLA-DMA found to have readily controllable mechanical and degradation properties (Ho and Young 2006). Moreover, the set polymer was highly compatible with bone cells (Zhao *et al*. 2010). Furthermore, an antibacterial drug, chlorhexidine was found to be released from the set polymer in a controllable manner (Young and Ho 2008). Consequently, it would be advantageous if the adhesive could also release a therapeutic gene to facilitate bone healing. However, release of DNA from this polymeric adhesive has not previously been investigated.

In this study, DNA plasmids containing a gene encoding green fluorescent protein (GFP) was first condensed with a nonviral gene delivery vector, Metafectene^{TM} Pro, to produce a lipid-DNA complex (LD). The GFP gene was used as a marker for gene transfection (gene transfer and expression) as the target cells (i.e., human mesenchymal stem cells (hMSC)) have little background green fluorescence and the cells become highly green

fluorescent after successful transfection (Soboleski *et al*. 2005). This enables accurate measurement of transfection efficiency (the proportion of the cells which take up and express the gene relative to the total cell population being transfected). Metafectene^{TM} Pro, formulated with cationic lipids with colipids in water, is a transfection reagent that facilitates gene transfection at a high efficiency with low cytotoxicity (Iczhowski *et al.* 2004). hMSC were selected because such cells occur in the periosteum and bone marrow and are capable of proliferation and differentiation into bone cells *in vitro* (Heyde *et al.* 2007).

In order to obtain maximum transfection efficiency in hMSC with minimal cytotoxicity, the ratio of Metafectene^{TM} Pro: GFP plasmid was first optimised. The optimal LD was then dispersed in the PGLA-DMA monomer and light cured to fabricate polymer films containing LD (PLD). Thin films rather than the thicker discs used in earlier chapters were produced as these would require less GFP plasmids and Metafectene^{TM} Pro, which are expensive. Additionally, the greater surface area to volume ratio of the thin films should increase the LD release rates.

Relative cell number and gene transfection efficiency was quantified after hMSC were incubated in direct contact with PLD or after the cells were incubated with components released from PLD (termed 'PLD extracts'). Relative cell number (%) was determined as the number of cells present in 'test' samples relative to that in 'control' samples (PLD with no LD). Gene transfection efficiency was defined as the number of cells which express

GFP relative to the total number of cells present in 'test' samples, also expressed as a percentage. The aim of the approach 'hMSC in direct contact with PLD' was to investigate whether DNA could effectively be transferred directly from the surfaces of the films into the cells (Woo *et al.* 2003). The rationale of this approach is that if the cells could take up the LD directly from the PLD then delivery might be better controlled, localised and protected in any subsequent *in vivo* application (Bonadio *et al.* 1999). The method utilising 'PLD extracts' was performed in order to examine whether the PLD enables non-localised gene expression, i.e., whether GFP expression can be observed in hMSC incubated in culture media containing DNA released from the PLD as a model of long-term DNA transfection in adjacent and surrounding cells during tissue regeneration (Woo *et al*. 2003).

5.2. Materials and methods

5.2.1. Optimisation of lipid-DNA complexes (LD)

An optimisation procedure recommended by the Metafectene^{TM} Pro manufacturer (Biontex Laboratories GmbH, Martinsried, Germany) was used to determine the optimal ratio of Metafectene^{TM} Pro solution to DNA for highest relative cell number and transfection efficiency. Briefly, a DNA solution containing 1 µg of GFP plasmids in 50 µl of phosphate buffered saline (PBS) was added to 50 µl of PBS containing 0 (used as control), 2, 4, 6, 8 or 10 µl of Metafectene^{TM} Pro. The mixture was incubated at room temperature for 15 min before dropwise addition to a hMSC suspension (containing 1 x 10^5 cells) in 500 µl of α-modified Eagle's medium (α-MEM) supplemented with 15% fetal bovine serum (FBS) (termed 'full culture medium') in a 24 well plate

(Krystal™, Flowgen Bioscience Ltd, Nottingham, UK). The wells had black walls and clear bottoms to enable direct imaging using a fluorescence microscope. After 24 h of incubation at 37 ºC in 5% CO_2 in air, the culture medium was removed and replaced with 1 ml of fresh full medium supplemented with 50 IU/ml of penicillin and 50 µg/ml of streptomycin. Each Metafectene™ Pro:DNA ratio had 4 replicates.

After 48 h, relative cell number was measured to determine the effect of increasing ratios of Metafectene™ Pro: DNA on it. Relative cell number was defined as the number of cells present in each 'test' well relative to that in the 'control' wells, i.e., cells present in a well containing only GFP plasmids but no Metafectene™ Pro. The number of cells in each well was counted in four random fields of view under a light microscope (20x objective, Olympus BH-2, Tokyo, Japan).

To investigate the effect of increasing ratios of Metafectene™ Pro: DNA on gene transfection efficiency, GFP plasmid transfection of hMSC (i.e. presence of green fluorescent cells) was examined using a Leica DM IRB fluorescence microscope (Leica Microsystems Ltd., Milton Keynes, UK). Images were produced using Leica FW4000 software. Flow cytometry (FCM, see Appendix B for more details) was then used to quantify gene transfection efficiency as follows. The cells were detached using trypsin-EDTA (0.25% (w/v) trypsin, 1 mmol/l EDTA) for 5 min at room temperature, washed with PBS, centrifuged at 1000 rpm for 5 min, and suspended and fixed in 500 µl/well of 4% formalin for 30 min. FCM was carried out using a FACScan (Becton Dickinson, Oxford,

UK) and data analysis performed using CellQuest software upon collection of 10, 000 cells. Instrument settings were adjusted using normal hMSC (incubated with neither DNA nor Metafectene™ Pro) to optimise the parameters of forward scatter (FSC, indicative of cell size) and side scatter (SSC, indicative of cell granularity). Dot plots of SSC versus FSC were obtained to identify the cell population. This was then plotted versus fluorescence intensity (FL1, green channel) as a histogram to identify and quantify the GFP-positive cells in the cell population (see details in section 5.3.1). Transfection efficiency was calculated as the percentage of GFP positive cells (cells with increased fluorescence intensity) relative to the total number of cells in each examined sample.

5.2.2. Preparation of polymer films containing LD (PLD)

5.2.2.1. Preparation of freeze-dried LD

0.5 mg of GFP plasmid in 50 ml aqueous solution and 1 ml of Metafectene™ Pro in 50 ml aqueous solution was combined to produce LD. Two types of solution was used, PBS and deionised water. PBS use is recommended by the Metafectene™ Pro manufacturer. Precipitation of salts after lyophilisation of the PBS solution (NaCl, KCl, Na_2HPO_4 and KH_2PO_4), however, might affect the PLD structure and thus DNA release. Deionised water was therefore used as an alternative to avoid the potential problem.

After incubation as above (see section 5.2.1), the solution mixtures were frozen using liquid nitrogen and lyophilised to solid powders in a Heto Drywinner freeze drier (Heto-Holten, Allerod, Denmark), operating at 0.5 Pa

with a condenser temperature of −90 °C for 48 h. LD_{PBS} and LD_W indicate dried LD produced using PBS and deionised water, respectively.

5.2.2.2. Fabrication of PLD

The resultant freeze-dried LD powders (0.5 g of LD_{PBS} or 2 mg of LD_W) were mixed with 0.2 g of PGLA-DMA monomer mixture (PGLA-DMA (90 wt.%), hydroxyethyl methacrylate (HEMA, 8 wt.%), camphorquinone (CQ, 1 wt.%) and *N,N*-dimethyl-*p*-toluidine (DMPT, 1 wt.%)) and each powder-monomer mixture placed onto 4 Thermanox™ plastic coverslips (13 mm diameter, NUNC™, Thermo Fisher Scientific, Loughborough, UK), giving 4 samples of PLD_{PBS} and 4 samples of PLD_w. Thermanox™ plastic coverslips were used to limit the diameter of the resultant PLD to 13 mm so that they would fit into a 24 well plate. The coverslips were removed after the polymer films were photo-polymerised (see below). Details of components and their mass in each film are summarised in Table 5.1.

Table 5.1. Components and their theoretical mass in each PLD film.

Components / PLD formulations	PGLA-DMA (mg)	Metafectene™ Pro (mg)	GFP plasmid (mg)	NaCl (mg)	KCl (mg)	Na_2HPO_4 (mg)	KH_2PO_4 (mg)
PLD_{PBS}	50	0.5	0.125	100	2.5	1.8	3
PLD_W	50	0.5	0.125	-	-	-	-

'-'= not applicable.

After covering with an acetate sheet the resultant monomer films were cured in a light box (Triad® 2000™ visible light cure system, Dentsply Trubyte, Palo Alto, USA) for 2 min. Full monomer conversion (i.e., no presence of the peak at 1640 cm^{-1} due to 'C=C' in PGLA-DMA) was confirmed using a Raman spectrometer (LabRAM HR, Horiba Jobin Yvon Ltd., Stanmore, UK, see

details in Chapter 3. section 3.2.1). The set films were subsequently sterilised by immersion in 50 ml of 70% ethanol for 5 min and air-dried at room temperature for 24 h prior to use in the transfection experiments.

5.2.3. Relative cell number and gene transfection efficiency using PLD

Each film of both PLD formulations (PLD_{PBS} and PLD_{W}) was placed in the bottom of a 24 well plate. Each PLD formulation had 4 replicate films. 1 ml of hMSC suspension (1 x 10^4 cells/ml) in full culture medium (defined in section 5.2.1) was added and then incubated at 37 °C for 3 days.

To investigate the effect of 'direct contact with PLD' on cell morphology, after 3 days of incubation, the cells on 4 of the 8 films (2 from each PLD formulation) were washed with PBS and fixed using 3% (v/v) gluteraldehyde in 0.1 mol/l sodium cacodylate buffer for 24 h. The specimens were finally dehydrated in a graded series of ethanol (50, 70, 95 and 3 x 100%) for 10 min each, immersed in hexamethyldisilazane for 2-3 min, air-dried for 3 h, mounted and coated with gold/palladium (Polaron E5000 sputter coater, Quorum Technologies, Sussex, UK). Cell morphology was then examined by scanning electron microscope (SEM, JEOL JSM-5410LV, Tokyo, Japan) at an accelerating voltage of 15 kV.

Relative cell number (%) was calculated as the number of cells on each SEM image of 'test' PLD divided by that on the SEM image of control PGLA-DMA films without LD. Two films of each PLD formulation were used and four SEM images were produced for each film. There were two controls in this test.

PGLA-DMA films without LD were used as a control to determine the effect of the LD on relative cell number; Thermanox^{TM} plastic coverslips were also used as a control to determine the effect of PGLA-DMA films alone, without LD, on relative cell number.

In a parallel study, the remaining 4 films were used to determine the effect of 'direct contact with PLD' on gene transfection efficiency of hMSC. In this case, cells after 3 days of incubation on the remaining 2 replicate films of PLD_{PBS}, PLD_W and control PGLA-DMA films without LD, were washed with PBS and fixed using 4% formalin for 10 min. The fixed cells were then washed with PBS, permeabilised with 0.1% Triton X-100 for 10 min and washed again with PBS. Nuclei were then stained using 0.1 µg/ml Hoechst 33258 dye (a fluorescent stain for labelling DNA) for 3 min and after further washing by PBS, viewed under the Leica DM IRB fluorescence microscope (20 x objective). Transfection efficiency (%) was calculated as the percentage of GFP positive cells (green fluorescent cells) relative to the total number of cells in an examined area (i.e., the number of blue nuclei present).

5.2.4. Relative cell number and gene transfection efficiency using 'PLD extracts'

hMSC suspension (1 ml, 1 x 10^4 cells/ml) in full culture medium (defined in section 5.2.1) was seeded into a 24 well plate and incubated for 4 h to allow cell attachment. Each of the PGLA-DMA films with no LD (control), PLD_{PBS} and PLD_w were then suspended in the culture medium above the cell monolayer. After incubation for 1 day, each film was removed from the first

well and suspended above a fresh second cell monolayer in a new well for a further 5 days of incubation. At the end of each time point (1 and 5 days), the film was removed and the culture medium renewed.

After 48 h of film removal and culture medium renewal, the cells were washed with PBS and fixed using 4% formalin for 10 min, washed with PBS, permeabilised with 0.1% Triton X-100 for 10 min and washed again with PBS. Nuclei were then stained using 0.1 μg/ml Hoechst 33258 dye for 3 min and, after further washing with PBS, visualised under the Leica DM IRB fluorescence microscope (20 x objective).

Relative cell number was then determined as the percentage of the number of cells (i.e., blue nuclei) present in the well incubated with PLD relative to that of cells incubated in parallel with control PGLA-DMA films with no LD, defined as 100%. Transfection efficiency was calculated as the percentage of GFP positive cells (green fluorescent cells) relative to the total number of cells (i.e., the number of blue nuclei present) in each examined area. Each experiment had 4 replicates.

5.2.5. Statistical evaluation

The statistical significance of differences in relative cell number and gene transfection efficiency under different circumstances was evaluated using one-way ANOVA. If the values of a property were uniformly distributed, the Bonferroni post hoc test was used. Data were evaluated using SPSS 14.0 for Windows (SPSS, Inc., Chicago, Ill., USA). The results are expressed as mean

± Standard Deviation (SD), and p values <0.05 were considered statistically significant.

5.3. Results

5.3.1. Optimal Metafectene™ Pro:DNA ratio for relative cell number and gene transfection efficiency

As the ratio of Metafectene™ Pro:DNA was increased from 2 to 10 (µl/µg), there was a linear decrease in relative cell number (R^2=0.95; Fig. 5.1), from approximately 80 to down 40% (Table 5.2). However, although the difference in relative cell number between the ratios of Metafectene™ Pro:DNA at 2, 4 and 6 µl/µg was not statistically significant, at the ratio of Metafectene™ Pro:DNA of 8 and 10 µl/µg, the relative cell number was substantially lower than that at 2 µl/µg ($p<0.05$). This finding has suggested that high concentrations of Metafectene™ Pro to DNA or cells may result in cell death.

Table 5.2. Effect of Metafectene™ Pro:DNA ratios on relative cell number and gene transfection efficiency of human mesenchymal stem cells (hMSC).

	Metafectene™ Pro: DNA (µl/µg)				
	2	4	6	8	10
Relative cell number (%)	83±8	80±9	67±7	57±5*	39±4*
Transfection efficiency (%)	53±9	56±8	49±8	47±7	37±7*

Relative cell number (%) was determined as the ratio of the number of cells present in each well after transfection at Metafectene™ Pro:DNA ratios between 2 and 10 µl/µg relative to that of 'control' cells incubated with DNA alone but no Metafectene™ Pro. Transfection efficiency (%) was quantified using FCM as the proportion of the cells with increased fluorescence intensity (> background fluorescence intensity compared with the control cells incubated with DNA alone but no Metafectene™ Pro) relative to the total cell population being examined after transfection (see below). Results are expressed as means ± SD, n= 4. * indicates significant differences ($p<0.05$) from values of Metafectene™ Pro:DNA ratio at 2 µl/µg.

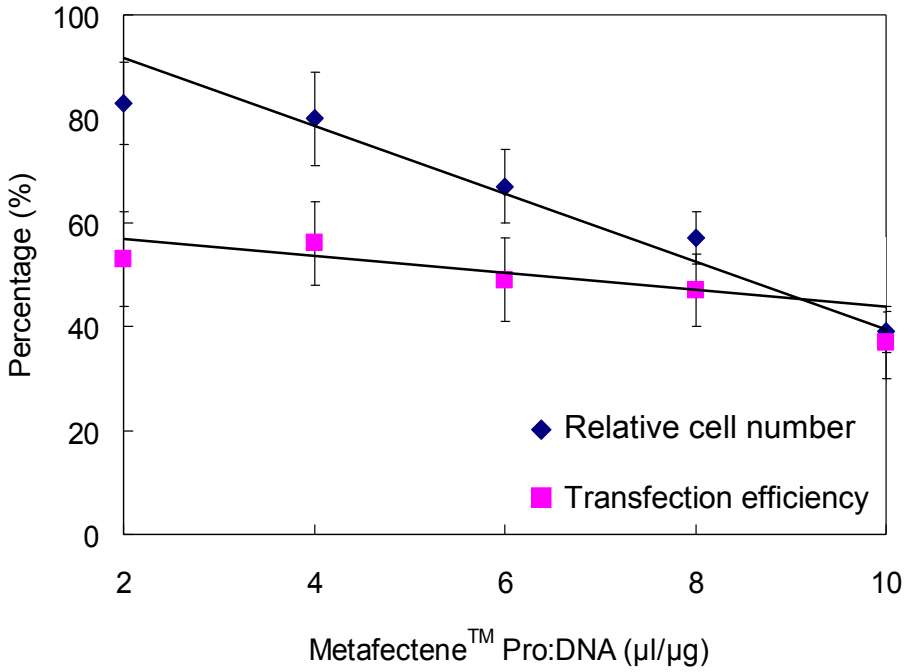

Fig. 5.1. Effect of Metafectene™ Pro : DNA ratios on relative cell number and transfection efficiency of hMSC.

Normal hMSC without any transfection had undetectable background green fluorescence using fluorescence microscope (data not shown). Control hMSC after incubation with GFP plasmids alone also showed little green fluorescence (see example in Fig. 5.2.A). In contrast, cells incubated with both DNA and Metafectene™ Pro, i.e., LD, became highly fluorescent, indicating successful transfection (see example in Fig. 5.2.B).

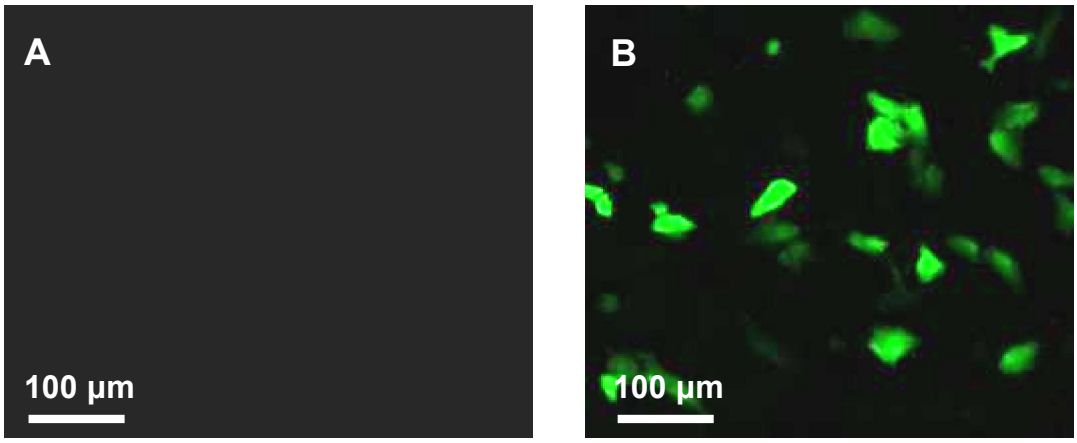

Fig. 5.2. Representative fluorescence images of hMSC after incubation with 1 µg DNA alone (A) and 1 µg DNA and 2 µl Metafectene™ Pro (LD) (B). In these images, the green fluorescent hMSC are successfully transfected whereas the hMSC not transfected remain non-fluorescent (background).

FCM was additionally used to quantify the transfection efficiency. First, FCM was used to compare the changes of the cell population due to different Metafectene™ Pro:DNA ratios by measuring changes in cell size (FSC) and granularity (SSC). Dot plots showing SSC versus FSC exhibited an oval-shaped region (see example in Fig. 5.3.A). A comparison of the normal hMSC and the control hMSC incubated with DNA alone showed very similar FSC and SSC data distribution (data not shown). A comparison of the control hMSC incubated with DNA alone and the hMSC incubated with DNA and Metafectene™ Pro (i.e., LD), however, showed a slight reduction in cell size distribution, as indicated by the left-shifted FSC data and no apparent change in cell granularity as indicated by the similar SSC data (see example in Fig. 5.3.A, compare i and ii). However, at high Metafectene™ Pro:DNA ratio (i.e. Metafectene™ Pro:DNA = 10 µl/µg), an additional population of particles near the lower left corner (indicative of cell debris or fragments) appeared (data not shown). These results suggested that the transfection procedures did not induce apparent cell death when the Metafectene™ Pro:DNA ratio was less than 10 µl/µg.

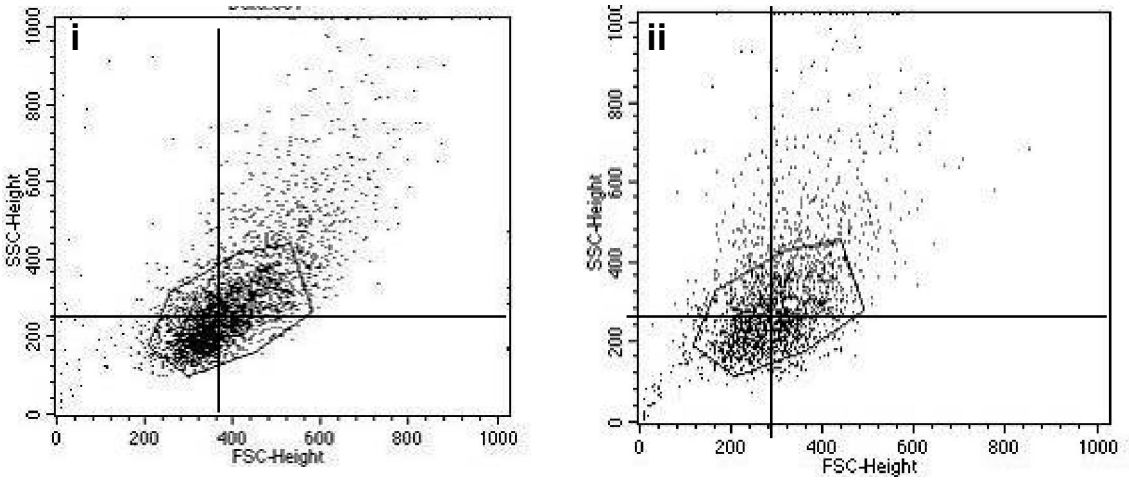

Fig. 5.3.A. Representative dot plots of side scatter (SSC) versus forward scatter (FSC) of the control hMSC after incubation with 1 µg DNA alone (i) and the test hMSC after incubation with 1 µg DNA and 2 µl Metafectene™ Pro (LD) (ii). Each dot represents a single cell. 1000 cells are displayed in each graph. A region has been drawn around the cells and the subsequent data analysis is based on the gated cell population.

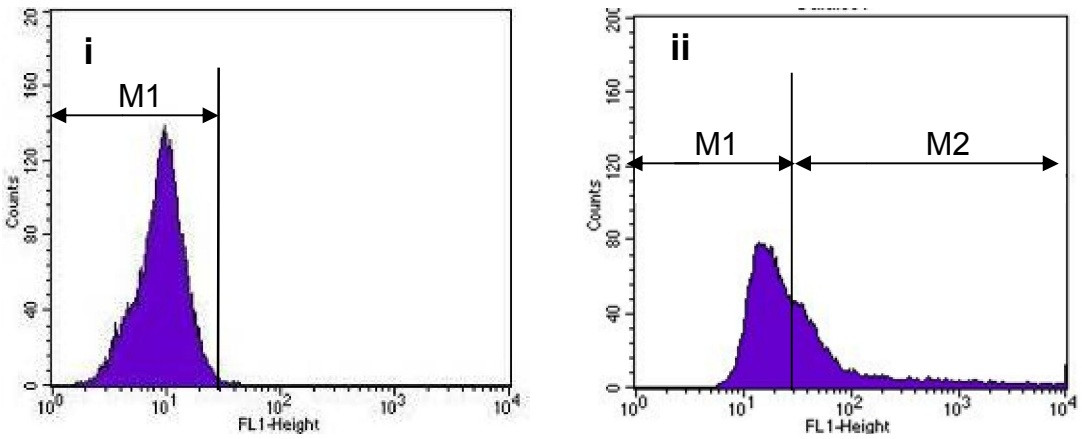

Fig. 5.3.B. Distribution histogram of the corresponding fluorescence data of the gated population of the control hMSc after incubation with 1 µg DNA alone (i) and the hMSC after incubation with 1 µg DNA and 2 µl Metafectene™ Pro (LD) (ii). The markers M_1 and M_2 represent the cells with low (< or = 30, background fluorescence) and high (>30) fluorescence intensity, respectively.

In order to quantify the percentage of cells with successful transfection in the examined cell population, a region has also been drawn around the hMSC cell cluster to include the population with the highest cell density for subsequent fluorescence data analysis. This selected region was found to contain more than 70% of the total cell population.

The histogram of fluorescence data of control hMSC incubated with DNA alone showed a distribution with a slight negative skew, with the fluorescence intensity ranging from 1 to 30, peak intensity approximately around 9 (see example in Fig. 5.3.B.i). In contrast, histograms of the tranfected hMSC using LD showed a distribution with a significant positive skew, with the fluorescence intensity ranging from 5 to 10^4 (see example in Fig. 5.3.B.ii), indicating that the population contained many cells which had been transfected, i.e. expressing GFP. The distribution had two peaks, the first located at a fluorescence intensity of 15 and the second 35. Markers M_1 and M_2 were arbitrarily set to represent the cells with low fluorescence intensity (< or = 30, background fluorescence intensity) and high fluorescence intensity (> 30). The transfection efficiency was then calculated as the percentage of cells in M_2 relative to the total number of cells (i.e., total cells in M_1 + M_2).

The calculated transfection efficiency at different Metafectene^{TM} Pro:DNA ratios was between 40% (Metafectene^{TM} Pro:DNA = 10 µl/µg) and 55% (Metafectene^{TM} Pro:DNA = 2 µl/µg) (Table 5.2). There was no significant difference in transfection efficiency between the Metafectene^{TM} Pro:DNA ratios at 2, 4, 6 and 8 µl/µg. At the Metafectene^{TM} Pro: DNA ratio of 10 µl/µg,

the transfection efficiency was significantly lower than that at 2 µl/µg ($p<0.05$). From the results of relative cell number and transfection efficiency experiments reported above, the ratio of Metafectene^{TM} Pro:DNA of 2 µl/µg was chosen as optimum and used for further studies.

5.3.2. Relative cell number and gene transfection efficiency using PLD

After 3 days of incubation, the hMSC were found to be spread on the surfaces of control Thermanox^{TM} plastic coverslips (smooth surface), control PGLA-DMA films (which were observed to have smooth surface) and PLD_{PBS} (which had a granular surface) (Fig. 5.4.A-C). The size and morphology of the cells cultured on control PGLA-DMA films and on PLD_{PBS} (see example in Fig. 5.4.B and C) appeared comparable with that of the cells on control Thermanox^{TM} plastic coverslips (see example in Fig. 5.4.A). However, no hMSC could be observed on the surface of PLD_w (see example in Fig. 5.4.D).

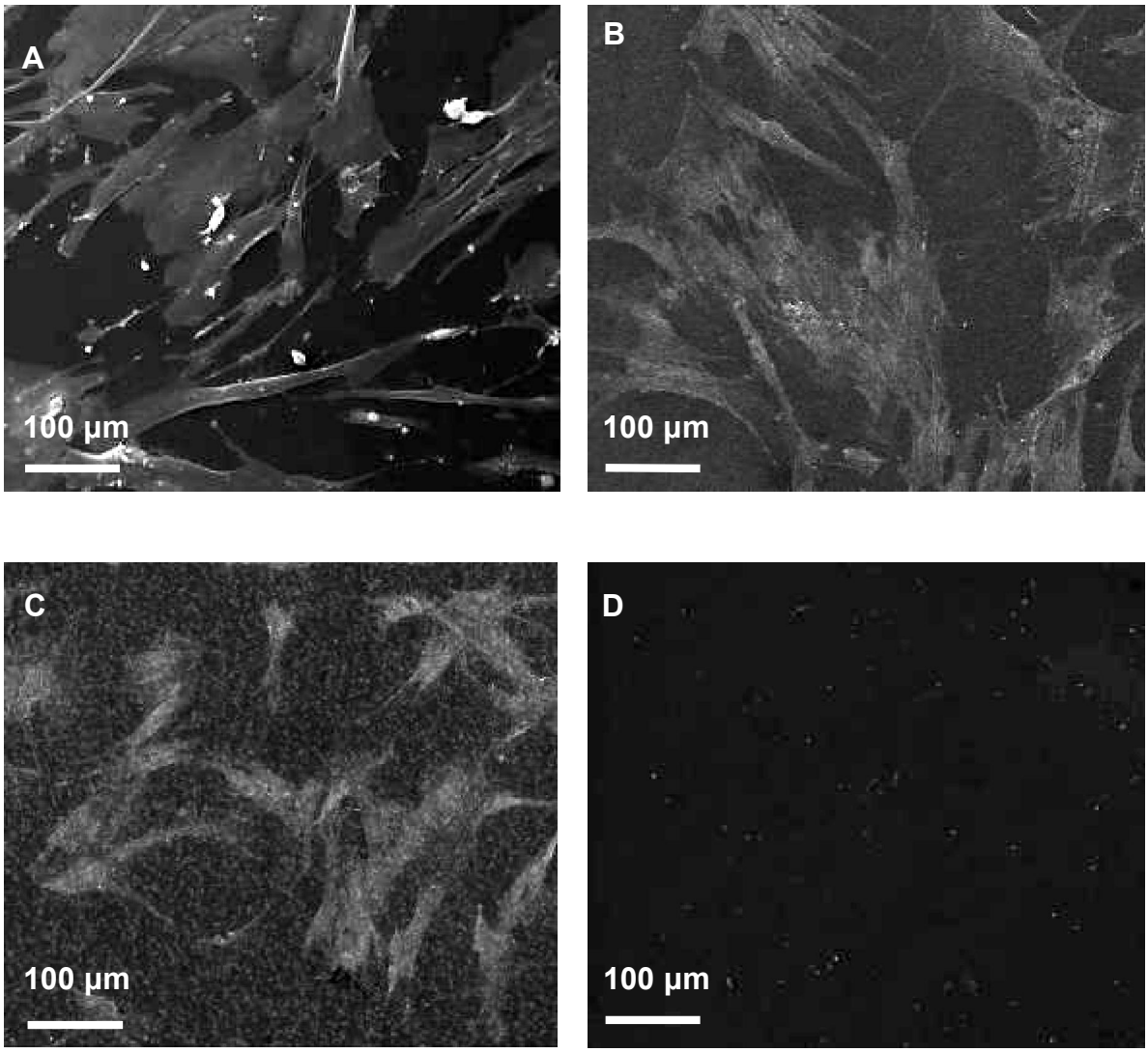

Fig. 5.4. Representative SEM images of hMSC incubated for 3 days on a Thermanox™ plastic coverslip (A), a PGLA-DMA film with no LD (B), a PLD_{PBS} (C) and a PLD_W (D). Note the granular surface of PLD_{PBS}.

There was no significant difference between the number of cells in each examined area on Thermanox™ plastic coverslips (30±10 cells/0.36 mm^2) and that of cells on PGLA-DMA films containing no LD (30±10 cells/0.36 mm^2). The number of cells on PLD_{PBS} (25±5 cells/0.36 mm^2) and PLD_W (0 cells/0.36 mm^2) was 66±17% and 0% of that of cells on plain PGLA-DMA films, respectively.

Moreover, no GFP expression in hMSC (green fluorescent cells) on any of these material surfaces could be observed using a fluorescence microscope (data not shown).

5.3.3. Relative cell number and gene transfection efficiency using 'PLD extracts'

The percentage number of hMSC incubated with components released from PLD_{PBS} compared with that of hMSC incubated with control PGLA-DMA films with no LD after the first day and after a subsequent period of 5 days were found to be 72±8 and 95±8%, respectively. In contrast, the percentage of cells after incubation with components released from PLD_W was only 33±4% for the initial 1 day ($p<0.05$), although this was increased to 90±9% for the subsequent 5 days. These results suggested that components released from PLD_{PBS} and PLD_W (particularly PLD_W) on the first day had a detrimental effect on the cells. Thereafter, however, the hMSC appeared to grow well in the presence of the components released from PLD_{PBS} and PLD_W at least for the subsequent 5 days.

GFP expression (the presence of green fluorescent cells) was not detected in hMSC transfected by the initial 1-day (see example in Fig. 5.5.A.ii) and subsequent 5-day (see example in Fig. 5.5.B.ii) components released from PLD_{PBS}. However, GFP expression was clearly observed in hMSC transfected by the initial 1-day components released from PLD_W (see example in Fig. 5.5.A.iii). This system exhibited transfection efficiency of 80±15%. GFP expression was also observed in the hMSC transfected by components released from PLD_W after 5 days (see example in Fig. 5.5.B.iii), although the

percentage of transfected cells was found to be less than 5%. These results suggested that only the components released from PLD_W on the first day were able to effectively transfect hMSC, whereas the components released thereafter (5 days) had only limited transfection activity.

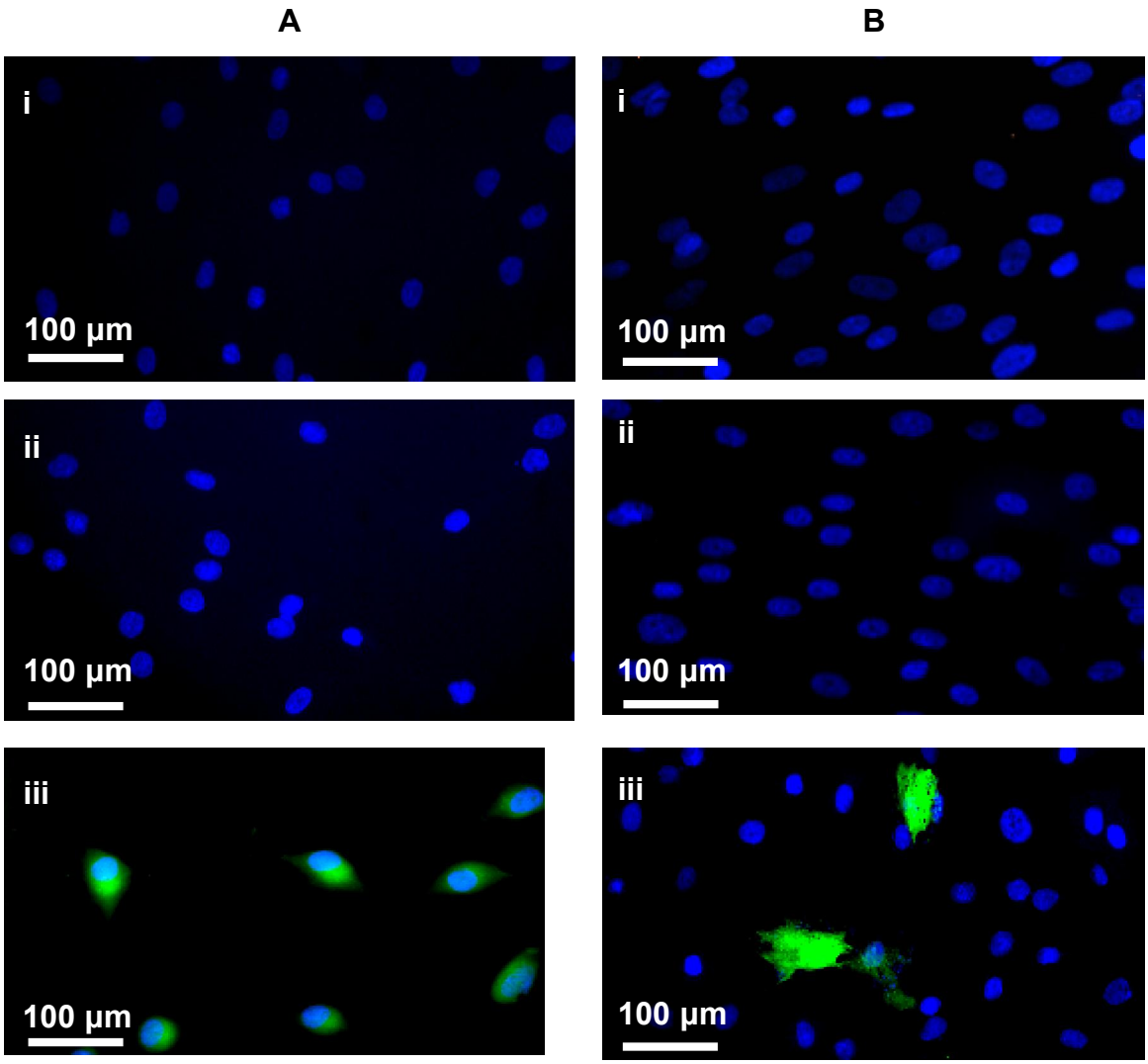

Fig. 5.5. Representative fluorescence images of hMSC incubated with 1-day (A) and subsequent 5-day (B) components released from the control PGLA-DMA films with no LD (i), PLD_{PBS} (ii) and PLD_W (iii). Cell nuclei are stained blue and cells successfully transfected are green fluorescent.

5.4. Discussion

5.4.1. Effect of Metafectene™ Pro:DNA ratio on relative cell number and gene transfection efficiency

Relative cell number decreased with progressively increasing Metafectene™ Pro:DNA ratios between 2 and 10 µl/µg, while the transfection efficiency varied little at Metafectene™ Pro:DNA ratios between 2 and 8 µl/µg but was significantly reduced when the ratio was increased to 10 µl/µg. In view of low cytotoxicity (i.e. high relative cell number) and high transfection efficiency, the ratio of Metafectene™ Pro:DNA of 2 µl/µg was chosen as optimum.

The reduced relative cell number and transfection efficiency of hMSC at high Metafectene™ Pro:DNA ratios may be due to the toxicity of cationic lipids in Metafectene™ Pro solution. As reported previously, cytotoxicity is normally closely associated with the charge ratio between the cationic lipid species and the nucleic acids (e.g. the ratio of Metafectene™ Pro:DNA in the present study), as well as the concentration of LD used for a certain number of cells (e.g. the amount of Metafectene™ Pro per cell in the present study) (Lv *et al.* 2006). Higher charge ratios have been found to cause higher cell death to a variety of cell types although they sometimes produce higher transfection efficiency (Lv *et al.* 2006). In addition, the toxic effect of cationic lipids can include cell shrinking and reduced number of mitoses, possibly resulting from the large size of the LD, and the high positive zeta potential required for their uptake (Lv *et al.* 2006).

5.4.2. Relative cell number and gene transfection efficiency using PLD

5.4.2.1. PLD_{PBS}

hMSC were found to be able to adhere to and spread on PLD_{PBS} although the number of cells on the PLD_{PBS} was lower compared with that on the control PGLA-DMA films after 3 days of culture. This may be due to the presence of salts (NaCl, KCl, Na_2HPO_4, KH_2PO_4, see Table 5.1) precipitated from PBS after lyophilisation for production of LD powders. The presence of these salts might have changed the film surface structure for cell attachment and also altered the salt concentration of the culture medium in the direct vicinity of the attached cells.

Regarding gene transfection using PLD_{PBS}, no GFP expression of hMSC was observed on the PLD_{PBS}. This may be due to the dissolution of the highly soluble salts (NaCl, KCl, Na_2HPO_4, KH_2PO_4) with LD from the PLD_{PBS} in the sterilising solution prior to hMSC seeding on these films. It is also possible that the physical structure (e.g., particle size) of LD may have been destroyed during the freeze-drying process in the presence of PBS, resulting in loss of tansfection activity (Yadava *et al*. 2008), as this process can sometimes cause fracture of the liposomal bilayers leading to liposomal fusion and phase separation (Crowe and Crowe 1988). However, this is uncertain until further study to investigate the effect of lyophilisation on LD structure in presence of PBS.

5.4.2.2. PLD_W

hMSC were found not be able to adhere to or spread on PLD_W, possibly due to the high concentration of cationic lipids on the surface of the PLD_W. As indicated in section 5.4.1, this high concentration of cationic lipids (i.e. high cationic lipids/DNA and high cationic lipids/cell) may cause cell death, thereby reducing the number of attached cells as shown in this study. As no hMSC were attached to the PLD_W, no GPF transfection of hMSC was observed on these films.

5.4.3. Relative cell number and gene transfection efficiency using 'PLD extracts'

5.4.3.1. PLD_{PBS} extracts

The number of hMSC incubated in the 'PLD_{PBS} extracts' for the initial 1 day and for the subsequent 5 day was higher than 70% and 90%, respectively, of that in the 'extracts' of the control PGLA-DMA films. Although hMSC were found to proliferate relatively well in these systems, no hMSC transfection by the 'PLD_{PBS} extracts' at any time was detected. This may be due to the dissolution of the highly soluble salts (precipitated from PBS with LD) from the PLD_{PBS} in the sterilising solution prior to film incubation with hMSC in culture medium. In addition, the LD shape, size and structure may be partially destroyed during lyophilisation in PBS.

5.4.3.2. PLD_W extracts

The number of hMSC incubated in the 'PLD_W extracts' for the initial 1 day was less than 40% of that in the 'extracts' of the control PGLA-DMA films whereas

the percentage of hMSC was as high as 90% when the cells were incubated in the 'PLD_w extracts' for the subsequent 5 days. The initial lower cell number of day-1 'PLD_W extracts' may be due to the large amount of LD_W released from the surface of the PLD_W. As indicated in section 5.4.1, this high concentration of LD may cause cell death, thereby reducing the number of cells in the 'PLD_W extracts'.

GFP expression could be clearly observed in hMSC exposed to the day-1 'PLD_W extracts' but not in the subsequent 5-day extracts. The initial short-term transfection activity of 'PLD_W extracts' might be due to the LD_W released from the surface of the PLD_W. However, the LD_W within the bulk of the PLD_W would not have been readily released (prior to polymer degradation), reducing the gene expression at later time points.

In order to allow long term DNA release for sustained transfection, it would be beneficial to increase the polymer degradation rate. This is because it was found that release of particles with large size (e.g. LD) from the poly (ether-*co*-ester) networks usually depends on the rate of hydrolysis of the polymer crosslinks (Quick and Anseth 2004). Nevertheless, more sustained transfection *in vivo* than found here *in vitro* may occur as polymer degradation might be accelerated by the presence of enzymes (Hou *et al*. 2004) and cells (Mabilleau *et al*. 2004).

5.5. Conclusion

The present work is an initial study of DNA delivery using PGLA-DMA. Relative cell number of hMSC using PLD_{PBS} alone or 'PLD_{PBS} extracts' was both found to be relatively high, but no GFP transfection could be observed using these systems. Additionally, no hMSC could be observed on the $PLD_{W,}$ with no GFP transfection. However, GFP transfection of hMSC by the 'PLD_w extracts' could be clearly observed, despite of reduced cell number. The effective transfection period *in vitro*, nevertheless, lasted for 1 day only although it is possible that this period could be longer *in vivo* as a result of potentially higher polymer degradation rates.

Chapter 6
Summary and Future Work

Abbreviations

In alphabetical order

CHX	chlorhexidine
hMSC	human mesenchymal stem cells
LA	lactide
LD	lipid-DNA complexes
MCPM	monocalcium phosphate monohydrate
PGLA-DMA	poly(propylene glycol -*co*- lactide) dimethacrylate
PPG	poly (propylene glycol)
TCP	tricalcium phosphate

6.1. Summary

The new materials investigated in this project consisted of fluid poly(propylene glycol-*co*-lactide) dimethacrylate (PGLA-DMA) filled with varying levels of β-tricalcium phosphate (β-TCP) and monocalcium phosphate monohydrate (MCPM) powders. These composite materials were found to be injectable, rapid-setting, elastic, degradable, and capable of releasing ions active in bone re-mineralisation and therapeutic agents in a controllable manner. Such materials could therefore be considered to have potential clinical value as bone adhesives and drug delivery devices.

Synthesis of PGLA-DMA with expected chemical structure, high methacrylation efficiency as well as high purity was achieved via adjusting the reaction conditions. The resultant PGLA-DMA was fluid and colourless.

Incorporation of β-TCP and MCPM into PGLA-DMA did not appear to elicit any detrimental effect on material polymerisation, with composites fully polymerised within 200 s upon blue light exposure. Advantages of the incorporation of β-TCP and MCPM into PGLA-DMA were found to include elevated modulus with increased total filler content, closer to that of bone, particularly trabecular bone. In addition, the composite materials had accelerated degradation rate with increased MCPM content, resulting in faster phosphate and calcium release and higher buffering capacity of the acidic

polymer degradation products. The increase in release of phosphate and calcium ions could be of value in enhancing bone regeneration *(*Ripamonti *et al.* 1996), while the pH compensation ability of the fillers could potentially reduce the likelihood of pH-catalysed polymer bulk degradation and neutralise localised acid production (Sabir *et al*. 2009). Moreover, both polymers and composites appeared to exhibit a suitable level of biocompatibility as indicated by the spreading and increase in cell number on the material surfaces *in vitro* and close apposition of the implanted materials to the chick embryo femurs *in vivo*. Therefore, the formulation with highest filler and MCPM content were considerd to be the optimal for application as bone adhesives due to its high modulus, high phosphate and calcium release and buffering capacity.

The set polymers and composites were found to be capable of releasing, locally and in a controllable manner, the antibacterial chlorhexidine (CHX; used as a model of small molecule drugs). Addition of 10 wt.% CHX did not affect the composite polymerisation and hydrolytic degradation. The release of CHX was found to be via diffusion, which increased with the total filler content and was associated with higher antibacterial activity.

Large molecules such as freeze-dried powders of lipid-DNA complexes (LD) were incorporated into the unset PGLA-DMA, and preliminary studies demonstrated that the ‘extracts’ of the set polymer films containing LD (i.e.

components released from the polymer films) enabled non-localised gene expression over a short period, i.e., gene expression could be observed in human mesenchymal stem cells (hMSC) incubated in culture media containing DNA released from the set polymer films.

6.2. Future work

In order to improve the potential value of the composite materials as candidates for bone adhesives and drug delivery devices, certain material properties could be improved by further investigation.

6.2.1. Mechanical properties

The elastic modulus of the composites obtained (10 ~ 30 MPa) was lower than that of human trabecular bone (20 ~ 500 MPa) (Agrawal and Athanasiou 1997;Bergsma *et al.* 1995) and might not be able to provide sufficient functional support during bone regeneration. As no more filler can be added (since materials containing 70% filler have been found to be paste-like and would thereby reduce injectability), PGLA-DMA with shorter unit length of poly(propylene glycol) (PPG) could be produced as alternatives. This is because, as previously reported, PGLA-DMA consisting of shorter PPG unit length (e.g., PPG with molecular weight of 425 g/mol and unit length = 7) had a higher modulus after set than that with longer PPG unit length (e.g., in

present study, PPG with molecular weight of 1,000 g/mol and unit length = 17) due to its higher crosslinking density (Ho and Young 2006).

In addition to the material elastic modulus, strength (e.g., tensile and compressive) of the materials should also be tested in future as this is an important parameter of engineering materials used in structures and mechanical devices (Yaszemski *et al.* 1996).

6.2.2. Degradability

Although *in vitro* degradation of the polymers and composites was investigated in this study, the *in vivo* degradation of these materials should be tested in future as this may differ due to the presence of enzymes in the body (Hou *et al.* 2004). If the *in vivo* degradation rate of these materials does not match the suggested optimal degradation rate (complete degradation in 12 weeks (Ekholm *et al*. 1995), it would be possible to optimise the composite materials by adjusting the number of lactides (LA) per PGLA-DMA molecule (Ho and Young 2006) or by incorporation of β-TCP and MCPM at different levels (e.g. molar ratio of β-TCP to MCPM <1).

6.2.3. Biocompatibility

The present work examined bone cell proliferation on the material surfaces and bone tissue responses to the implanted materials using chick embryo

femurs. However, osteocompatibility and osteointegration of implanted materials in bone using other experimental models, e.g., sheep, need to be investigated to obtain information about the long-term *in vivo* biocompatibility. In addition, bonding strength between the implanted materials and the bone tissue after implantation could also be examined.

6.2.4. Drug delivery

In current study, it was found that the CHX release rate was reduced at later times, possibly due to the interaction between the basic CHX and the acidic polymer degradation products. Further study can include acidic drugs (e.g., ketoprofen, used for the treatment of arthritis) and neutral drugs (e.g., prednisolon, used in the treatment of rheumatic disease) to determine the effect of drug acid-base property on the drug release rate from the material (Young and Ho 2008).

In addition, only one drug concentration and one sample dimension were used in this study. Further work would be required to assess how drug release would vary with drug concentration and sample dimension as these are important factors affecting the drug diffusion rate (Young and Ho 2008).

6.2.5. DNA delivery

It was found that gene expression could be observed only in hMSC incubated in culture media containing LD initially released from the set polymer films.

These LD were assumed to be released from the surface of the polymer films and the LD within the bulk of the polymer films would not be readily released prior to polymer degradation due to its large size. As previously reported, release rate of large particles from poly (ether-*co*-ester) networks usually depends on the rate of hydrolysis of the polymer crosslinks (Quick and Anseth 2004). It would therefore be possible to increase the DNA release rates by increasing the polymer degradation rate, allowing more sustained gene transfection. Thus, a future work could examine a PGLA-DMA with higher LA content per molecule (this PGLA-DMA would be expected to degrade faster) (Ho and Young 2006). Thereafter, it would be of great benefit to use genes encoding osteogenic signaling molecules, such as bone morphogenetic proteins, in further study.

Chapter 7

Appendices

Appendix A. Raw materials and suppliers

In alphabeic order

Materials	Suppliers	Description
α-modified Eagle's medium	Invitrogen, Paisley, UK	
β-TCP	Fluka, Gillingham, UK	95%
acetone	Sigma-Aldrich, Gillingham, UK	99.9%
alamarBlue™ assay	AbD serotec, Düsseldorf, Germany	
brushite	Sigma-Aldrich, Gillingham, UK	98%
camphorquinone	Sigma-Aldrich, Gillingham, UK	97%
deionised water	Eppendorf, Hamburg, Germany	molecular biology grade
D,L- lactide	Purac, Gorinchem, the Netherlands	molecular weight ~ 144 g/mol
dichloromethane	Sigma-Aldrich, Gillingham, UK	99.8%
Dulbecco's modified Eagle's medium	Invitrogen, Paisley, UK	
fetal bovine serum	Invitrogen, Paisley, UK	
gWiz™ GFP plasmids	Aldevron, Fargo, USA	
hMSC	Lonza, Basel, Switzerland	passage 2-5 was used for experiment
Hoechst 33258 dye	Invitrogen, Paisley, UK	
hydroxyethyl methacrylate	Invitrogen, Paisley, UK;	99%
Metafectene™ Pro	Biontex, Martinsried, Germany	
methacryloyl chloride	Fluka, Gillingham, UK	97%
MG-63 cells	European Collection of Cell Cultures at the Health Protection Agency, Salisbury, UK	human osteosarcoma cell line
monetite	Sigma-Aldrich, Gillingham, UK	98%
monocalcium phosphate monohydrate	Sigma-Aldrich, Gillingham, UK	95%
N,N-dimethyl-*p*-toluidine	Sigma-Aldrich, Gillingham, UK	99%
penicillin	Invitrogen, Paisley, UK	
phosphate buffered saline	Invitrogen, Paisley, UK	Ca^{2+}/Mg^{2+} free
poly (propylene glycol -*co*-lactide) dimethacrylate		synthesised by author (see Chapter 2, section 2.2.1 for details).
propylene glycol	Sigma-Aldrich, Gillingham, UK	average molecular weight ~ 1000 g/mol

toluidine blue	Fluka, Gillingham, UK.	
triethylamine	Fluka, Gillingham, UK	98%
trypsin-EDTA	Invitrogen, Paisley, UK	
stannous octoate	Sigma-Aldrich, Gillingham, UK	95%
streptomycin	Invitrogen, Paisley, UK	

All reagents were used as received unless otherwise specified. β-TCP were sieved (Laboratory test sieve, Endecotts Ltd, London, UK) to obtain particles of diameter less than 20 μm. MCPM were ground using a ball mill (Retsch Mixer Mill MM 301, Haan, Germany) at 30 Hz shaking frequency for 4 min and sieved (Laboratory test sieves of 20, 38, 75 and 106 μm, Endecotts Ltd, London, UK) in a vibratory shaker (Fritsch Analysette 3 Spartan, Obertein, Germany) for 30 min to obtain particles of diameters: 20~38 (denoted as 30), 38~75 (60) and 75~106 (90) μm.

Appendix B. General techniques

7.B.1. Raman spectroscopy

Raman spectroscopy is based on inelastic scattering, or Raman Scattering, of a laser light. The laser light interacts with a sample, resulting in molecular vibrations or other excitation of the sample molecules and scattered laster light of a different wavelength. The difference in the wavelength between the scattered and the incedent light is a characteristic of the nature of the molecules present in the sample and can therefore be used to identify different functional groups (Ferraro *et al*. 2002a; Ferraro *et al*. 2002b).

7.B.2. Dynamic mechanical analysis

A typical dynamic mechanical analyser (DMA) has a force motor, a drive shaft, a linear variable displacement transformer positional sensor (LVDT) and two parallel plates. DMA can used to determine compressive modulus of a material. During the test, a compressive force (stress) is applied from the motor and transmitted through the drive shaft onto the sample. The deformation of the sample is measured by the LVDT and the strain is calculated. Compressive modulus is then determined from the slope of the stress-strain curve created by the DMA (Menard 2008a; Menard 2008b).

7.B.3. Ion chromatography

Ion chromatography is a form of liquid chromatography, separating and measuring ion concentrations of various species based on their affinity (ion interactions) with a resin of a chromatographic column (Fritz and Gjerde 2009). An ion chromatograph is a plot of intensity versus ion retention time. In the graph, each peak represents a separated ion and the ion concentration can be calculated using the area under the peak.

7.B.4. AlamarBlue™ assay

AlamarBlue™ reagent is a buffered solution containing highly purified resazurin. Resazurin is dark blue in colour and has little intrinsic fluorescence. It can be reduced to pink and highly fluorescent resorufin when taken up by viable cells. The amount of resorufin produced is proportional to the number of viable cells. Cell viability can therefore be quantified by measuring resorufin fluorescence level (O'Brien *et al*. 2000; Oriowo *et al*. 2003).

7.B.5. Chick embryo chorioallantoic membrane (CAM) assay

The chick embryo chorioallantoic membrane (CAM) assay employs fertilised egg during the period of chick embryo development (Vargas *et al*. 2007). CAM itself is a transparent and highly vascularised extra-embryonic membrane. During the test, an implant or an implanted tissue is placed on the top of a CAM and incubated with the CAM for several days. This model allows investigation of CAM/tissue response to the implant. The CAM model generally exhibits similar tissue response with other mammalian models. Due to the advantages such as low cost and simplicity, this model is particularly attractive for rapid *in vivo* screening of biomaterials (Valdes *et al*. 2002).

7.B.6. Flow cytometry (FCM)

Flow cytometry (FCM) is base on light scattering which occurs when a particle (e.g., cell) deflects incident laser light. It can provide information regarding the size of the cells, their internal compleity and fluorescence level (if the cells examined have fluorophores inside or on their surface). Thus, FCM can be used to differentiate different cell types in a heterogeneous cell population and to quantify the number of cells with a specific property (e.g., with fluorescence at a specific wavelength) (Ormerod 2000;Carter and Ormerod 2000).

Appendix C. Factorial analysis

Factorial experimental design (three variables, two level) was used in this project to investigate the effects of three variable on the measured outcome whilst minimising the number of samples for the experiments. The following section explains the layout of a factorial experiment and its mathematical interpretation.

7.C.1. Factorial design

A typical three-variable, two level factorial design of sample formulations is shown in Table 7.C.1.

Table 7.C.1. Factorial design of sample formulations involving three variables (V) with two levels, high (H, indicated by +1) and low (L, indicated by -1).

Sample number	Sample formulations	V_1	V_2	V_3
1	S_{HHH}	+1	+1	+1
2	S_{HHL}	+1	+1	-1
3	S_{HLH}	+1	-1	+1
4	S_{HLL}	+1	-1	-1
5	S_{LHH}	-1	+1	+1
6	S_{LHL}	-1	+1	-1
7	S_{LLH}	-1	-1	+1
8	S_{LLL}	-1	-1	-1

Regarding sample formulations, for example, S_{HHH} stands for the formulation with V_1, V_2 and V_3 at their high levels and S_{HHL} for the formulation with V_1, V_2 and V_3 at their high, high and low levels respectively.

7.C.2. Mathematical interpretation

Kinetic and equilibrium properties, P, are often related to variables by a power law. When there are three variables (V), the kinetic equation and its logarithmic form are:

$$P = kV_1^{b1}V_2^{b2}V_3^{b3} \qquad 7.C.1$$

where k is a constant, b_i is the power of its corresponding variable.

$$\ln P = \ln k + b_1 \ln V_1 + b_2 \ln V_2 + b_3 \ln V_3 \qquad 7.C.2$$

$$\ln P_{HHH} = \ln k + b_1 \ln V_{1H} + b_2 \ln V_{2H} + b_3 \ln V_{3H} \quad A$$
$$\ln P_{HHL} = \ln k + b_1 \ln V_{1H} + b_2 \ln V_{2H} + b_3 \ln V_{3L} \quad B$$
$$\ln P_{HLH} = \ln k + b_1 \ln V_{1H} + b_2 \ln V_{2L} + b_3 \ln V_{3H} \quad C$$
$$\ln P_{HLL} = \ln k + b_1 \ln V_{1H} + b_2 \ln V_{2L} + b_3 \ln V_{3L} \quad D$$
$$\ln P_{LHH} = \ln k + b_1 \ln V_{1L} + b_2 \ln V_{2H} + b_3 \ln V_{3H} \quad E$$
$$\ln P_{LHL} = \ln k + b_1 \ln V_{1L} + b_2 \ln V_{2H} + b_3 \ln V_{3L} \quad F$$
$$\ln P_{LLH} = \ln k + b_1 \ln V_{1L} + b_2 \ln V_{2L} + b_3 \ln V_{3H} \quad G$$
$$\ln P_{LLL} = \ln k + b_1 \ln V_{1L} + b_2 \ln V_{2L} + b_3 \ln V_{3L} \quad H$$

where H and L represent the variable (V) at its high (H) and low (L) value respectively.

A suitable factorial expression in this case could therefore be:

$$\ln P = \langle \ln P \rangle + F_1 a_1 + F_2 a_2 + F_3 a_3 + F_1F_2 a_{1,2} + F_1F_3 a_{1,3} + F_2F_3 a_{2,3} + F_1F_2F_3 a_{1,2,3} \qquad 7.C.3$$

where <lnP> is the average value of ln P for all 8 possible formulation combinations (see Table 7.C.1), F_i = +/- 1 and $F_{i,j} = F_iF_j$ (see Table 7.C.2 for the values of F_i and $F_{i,j}$), a_i indicates the level of an effect that a factor has on a material property (P).

Table 7.C.2. Property combinations for a factorial experimental design involving three factors (F) with two levels, high (F=+1) and low (F=-1).

Property of different sample formulation	F_1	F_2	F_3	$F_{1,2}$	$F_{1,3}$	$F_{2,3}$	$F_{1,2,3}$
P_{HHH}	1	1	1	1	1	1	1
P_{HHL}	1	1	-1	1	-1	-1	-1
P_{HLH}	1	-1	1	-1	1	-1	-1
P_{HLL}	1	-1	-1	-1	-1	1	1
P_{LHH}	-1	1	1	-1	-1	1	-1
P_{LHL}	-1	1	-1	-1	1	-1	1
P_{LLH}	-1	-1	1	1	-1	-1	1
P_{LLL}	-1	-1	-1	1	1	1	-1

F_i standards for each individual factor whereas $F_{i,j}$ for interaction factors ($F_{i,j} = F_iF_j$).

Thus, Eq. 7.C.3. can also be expressed:

$$\ln P = <\ln P> \pm a_1 \pm a_2 \pm a_3 \pm a_{1,2} \pm a_{1,3} \pm a_{2,3} \pm a_{1,2,3} \qquad 7.C.4$$

$$\ln P_{HHH} = <\ln P> + a_1 + a_2 + a_3 + a_{12} + a_{13} + a_{23} + a_{123} \qquad A'$$
$$\ln P_{HHL} = <\ln P> + a_1 + a_2 - a_3 + a_{12} - a_{13} - a_{23} - a_{123} \qquad B'$$
$$\ln P_{HLH} = <\ln P> + a_1 - a_2 + a_3 - a_{12} + a_{13} - a_{23} - a_{123} \qquad C'$$
$$\ln P_{HLL} = <\ln P> + a_1 - a_2 - a_3 - a_{12} - a_{13} + a_{23} + a_{123} \qquad D'$$
$$\ln P_{LHH} = <\ln P> - a_1 + a_2 + a_3 - a_{12} - a_{13} + a_{23} - a_{123} \qquad E'$$
$$\ln P_{LHL} = <\ln P> - a_1 + a_2 - a_3 - a_{12} + a_{13} - a_{23} + a_{123} \qquad F'$$
$$\ln P_{LLH} = <\ln P> - a_1 - a_2 + a_3 + a_{12} - a_{13} - a_{23} + a_{123} \qquad G'$$
$$\ln P_{LLL} = <\ln P> - a_1 - a_2 - a_3 + a_{12} + a_{13} + a_{23} - a_{123} \qquad H'$$

From the definition of an arimetic mean

$$<\ln P> = (\ln P_{HHH} + \ln P_{HHL} + \ln P_{HLH} + \ln P_{HLL} + \ln P_{LHH} + \ln P_{LHL} + \ln P_{LLH} + \ln P_{LLL})/8$$
$$= \ln \sqrt[8]{(P_{HHH}P_{HHL}P_{HLH}P_{HLL}P_{LHH}P_{LHL}P_{LLH}P_{LLL})}$$

Since

$$P_{GM} = \sqrt[8]{(P_{HHH}P_{HHL}P_{HLH}P_{HLL}P_{LHH}P_{LHL}P_{LLH}P_{LLL})}$$

therefore

$$\ln P_{GM} = <\ln P>$$

If A, B …H = A', B', …H', respectively,

$$\ln P_{HHH} = \ln k + b_1 \ln V_{1H} + b_2 \ln V_{2H} + b_3 \ln V_{3H} \quad \text{A''}$$
$$= <\ln P> + a_1 + a_2 + a_3 + a_{12} + a_{13} + a_{23} + a_{123}$$

$$\ln P_{HHL} = \ln k + b_1 \ln V_{1H} + b_2 \ln V_{2H} + b_3 \ln V_{3L} \quad \text{B''}$$
$$= <\ln P> + a_1 + a_2 - a_3 + a_{12} - a_{13} - a_{23} - a_{123}$$

$$\ln P_{HLH} = \ln k + b_1 \ln V_{1H} + b_2 \ln V_{2L} + b_3 \ln V_{3H} \quad \text{C''}$$
$$= <\ln P> + a_1 - a_2 + a_3 - a_{12} + a_{13} - a_{23} - a_{123}$$

$$\ln P_{HLL} = \ln k + b_1 \ln V_{1H} + b_2 \ln V_{2L} + b_3 \ln V_{3L} \quad \text{D''}$$
$$= <\ln P> + a_1 - a_2 - a_3 - a_{12} - a_{13} + a_{23} + a_{123}$$

$$\ln P_{LHH} = \ln k + b_1 \ln V_{1L} + b_2 \ln V_{2H} + b_3 \ln V_{3H} \quad \text{E''}$$
$$= <\ln P> - a_1 + a_2 + a_3 - a_{12} - a_{13} + a_{23} - a_{123}$$

$$\ln P_{LHL} = \ln k + b_1 \ln V_{1L} + b_2 \ln V_{2H} + b_3 \ln V_{3L} \quad \text{F''}$$
$$< \ln P > - a_1 + a_2 - a_3 - a_{12} + a_{13} - a_{23} + a_{123}$$

$$\ln P_{LLH} = \ln k + b_1 \ln V_{1L} + b_2 \ln V_{2L} + b_3 \ln V_{3H} \quad \text{G''}$$
$$= <\ln P> - a_1 - a_2 + a_3 + a_{12} - a_{13} - a_{23} + a_{123}$$

$$\ln P_{LLL} = \ln k + b_1 \ln V_{1L} + b_2 \ln V_{2L} + b_3 \ln V_{3L} \quad \text{H''}$$
$$< \ln P > - a_1 - a_2 - a_3 + a_{12} + a_{13} + a_{23} - a_{123}$$

Sum A'', B'', C'', D'', E'', F'', G'', H'',

$$8 \ln \sqrt[8]{P_{HHH} P_{HHL} P_{HLH} P_{HLL} P_{LHH} P_{LHL} P_{LLH} P_{LLL}}$$

$$= 8 \ln k + 4b_1 \ln V_{1H} + 4b_1 \ln V_{1L} + 4b_2 \ln V_{2H} + 4b_2 \ln V_{2L} + 4b_3 \ln V_{3H} + 4b_3 \ln V_{3L}$$

$$= 8 <\ln P>$$

sum (A'', B'', C'', D'') – sum (E'', F'',G'',H'')

$$\ln \frac{\sqrt[4]{P_{HHH} P_{HHL} P_{HLH} P_{HLL}}}{\sqrt[4]{P_{LHH} P_{LHL} P_{LLH} P_{LLL}}} = b_1 \ln \frac{V_{1H}}{V_{1L}} = 2a_1$$

sum (A'', B'',E'', F'') – sum (C'', D'',G'',H'')

$$\ln \frac{\sqrt[4]{P_{HHH} P_{HHL} P_{LHH} P_{LHL}}}{\sqrt[4]{P_{HLH} P_{HLL} P_{LLH} P_{LLL}}} = b_2 \ln \frac{V_{2H}}{V_{2L}} = 2a_2$$

sum (A'',C'',E'',G'') – sum (B'',D'',F'',H'')

$$\ln\frac{\sqrt[4]{P_{HHH}P_{HLH}P_{LHH}P_{LLH}}}{\sqrt[4]{P_{HHL}P_{HLL}P_{LHL}P_{LLL}}} = b_3 \ln\frac{V_{3H}}{V_{3L}} = 2a_3$$

sum (A'',B'',G'',H'') – sum (C'',D'',E'',F'')

$$\ln\frac{\sqrt[4]{P_{HHH}P_{HHL}P_{LLH}P_{LLL}}}{\sqrt[4]{P_{HLH}P_{HLL}P_{LHH}P_{LHL}}} = 0 = 2a_{12}$$

sum (A'',C'',F'',H'') – sum (B'',D'',E'',G'')

$$\ln\frac{\sqrt[4]{P_{HHL}P_{HLH}P_{LHL}P_{LLL}}}{\sqrt[4]{P_{HHL}P_{HLL}P_{LHH}P_{LLH}}} = 0 = 2a_{13}$$

sum (A'',D'',E'',H'') – sum (B'',C'',F'',G'')

$$\ln\frac{\sqrt[4]{P_{HHH}P_{HLL}P_{LHH}P_{LLL}}}{\sqrt[4]{P_{HHL}P_{HLH}P_{LHL}P_{LLH}}} = 0 = 2a_{23}$$

sum (A'',D'',F'',G'') – sum (B'',C'',E'',H'')

$$\ln\frac{\sqrt[4]{P_{HHH}P_{HLL}P_{LHL}P_{LLH}}}{\sqrt[4]{P_{HHL}P_{HLH}P_{LHH}P_{LLL}}} = 0 = 2a_{123}$$

Therefore

$$2a_i = \ln\left[\frac{P_H}{P_L}\right] \qquad 7.C.5$$

where P_H and P_L are the geometric means of a property of all samples with the variable, at its high (H) and low (H) level, respectively.

Eq. 7.C.2 and 7.C.4 would be equivalent when the effect of interaction factors ($a_{n,m}$) is negligible. In this case, Eq. 7.C.4 can be simplified as

$$\ln P = <\ln P> \pm a_1 \pm a_2 \pm a_3$$

References

Abou Neel EA, Palmer G, Knowles JC, Salih V, Young AM. Chemical, modulus and cell attachment studies of reactive calcium phosphate filler-containing fast photo-curing, surface-degrading, polymeric bone adhesives. Acta Biomaterilia 2010;6(7):2695-2703.

Agrawal CM, Athanasiou KA. Technique to control pH in vicinity of biodegrading PLA-PGA implants. Journal of Biomedical Materials Research 1997;38(2):105-114.

Allcock HR. Recent developments in polyphosphazene materials science. Current Opinion in Solid State & Materials Science 2006;10(5-6):231-240.

Ambard AJ, Mueninghoff L. Calcium phosphate cement: review of mechanical and biological properties. Journal of Prosthodontics 2006;15(5):321-328.

An YH, Woolf SK, Friedman RJ. Pre-clinical in vivo evaluation of orthropaedic bioabsorbable devices. Biomaterials 2000;21(24):2635-2652.

Andacht T, Hu W, Ivarie R. Rapid and improved method for windowing eggs accessing the stage X chicken embryo. Molecular Reproduction and Development 2004;69(1):31-34.

Andrews JM, BSAC Working PS. BSAC standardized disc susceptibility testing method (version 7). Journal of Antimicrobial Chemotherapy 2008;62(2):256-278.

Apelt D, Theiss F, El-Warrak AO, Zlinszky K, Bettschart-Wolfisberger R, Bohner M, Matter S, Auer JA, von Rechenberg B. In vivo behavior of

three different injectable hydraulic calcium phosphate cements. Biomaterials 2004;25(7-8):1439-1451.

Arifin DY, Lee LY, Wang CH. Mathematical modeling and simulation of drug release from microspheres: Implications to drug delivery systems. Advanced Drug Delivery Reviews 2006;58(12-13):1274-1325.

Arkfeld DG, Rubenstein E. Quest for the Holy Grail to cure arthritis and osteoporosis: Emphasis on bone drug delivery systems. Advanced Drug Delivery Reviews 2005;57(7):939-944.

Atkins PW. Part 1: Equilibrium. In: Atkins PW (ed.),Physical Chemistry. Oxford: Oxford University Press,1994;9-311.

Baroli B. From natural bone grafts to tissue engineering therapeutics: Brainstorming on pharmaceutical formulative requirements and challenges. Journal of Pharmaceutical Sciences 2009;98(4):1317-1375.

Barrere F, van Blitterswijk CA, de Groot K. Bone regeneration: molecular and cellular interactions with calcium phosphate ceramics. International Journal of Nanomedicine 2006;1(3):317-332.

Barriga A, az-de-Rada P, Barroso JL, Alfonso M, Lamata M, Hernaez S, Beguiristain JL, San-Julian M, Villas C. Frozen cancellous bone allografts: positive cultures of implanted grafts in posterior fusions of the spine. European Spine Journal 2004;13(2):152-156.

Bergsma JE, Debruijn WC, Rozema FR, Bos RRM, Boering G. Late degradation tissue-response to poly(l-lactide) bone plates and screws. Biomaterials 1995;16(1):25-31.

Betz RR. Limitations of autograft and allograft: New synthetic solutions.

Orthopedics 2002;25(5S):S561-S570.

Betz VM, Betz OB, Harris MB, Vrahas MS, Evans CH. Bone tissue engineering and repair by gene therapy. Frontiers in Bioscience 2008;13:833-841.

Bohner M. Calcium orthophosphates in medicine: from ceramics to calcium phosphate cements. Injury 2000;31(S4):D37-D47.

Bohner M. Physical and chemical aspects of calcium phosphates used in spinal surgery. European Spine Journal 2001;10(S2):S114-S121.

Bohner M. Reactivity of calcium phosphate cements. Journal of Materials Chemistry 2007;17:3980-3986.

Bohner M, Gbureck U, Barralet JE. Technological issues for the development of more efficient calcium phosphate bone cements: A critical assessment. Biomaterials 2005;26(33):6423-6429.

Bohner M, Lemaitre J, VanLanduyt P, Zambelli PY, Merkle HP, Gander B. Gentamicin-loaded hydraulic calcium phosphate bone cement as antibiotic delivery system. Journal of Pharmaceutical Sciences 1997;86(2):565-572.

Bonadio J. Tissue engineering via local gene delivery: Update and future prospects for enhancing the technology. Advanced Drug Delivery Reviews 2000;44(2-3):185-194.

Bonadio J, Smiley E, Patil P, Goldstein S. Localized, direct plasmid gene delivery in vivo: prolonged therapy results in reproducible tissue regeneration. Nature Medicine 1999;5:753-759.

Cai ZY, Yang DA, Zhang N, Ji CG, Zhu L, Zhang T. Poly(propylene fumarate)/(calcium sulphate/beta-tricalcium phosphate) composites: Preparation, characterization and in vitro degradation. Acta Biomaterialia 2009;5(2):628-635.

Carr MG, Corish J, Corrigan OI. Drug delivery from a liquid crystalline base across Visking and human stratum corneum. International Journal of Pharmaceutics 1997;157(1):35-42.

Carter NP, Ormerod MG. Introduction to the principles of flow cytometry.In: Ormerod MG (ed.), Flow Cytometry: A Practical Approach. Oxford:Oxford University Press,2000;1-22.

Choe JM, Ogan K, Bennet S. Antibacterial mesh sling: A prospective outcome analysis. Urology 2000;55(4):515-520.

Chung I, Xie D, Puckett AD, Mays JW. Syntheses and evaluation of novel biodegradable amino acid based anhydride polymer resins and composites. European Polymer Journal 2003;39(3):497-503.

Colombo P, Bettini R, Santi P, Peppas NA, Airrabeelli R. Swellable matrices for controlled drug delivery: gel-layer behaviour, mechanisms and optimal performance. Pharmaceutical Science & Technology Today 2000;3(6):198-204.

Crowe JH, Crowe LM. Factors affecting the stability of dry liposomes. Biochimica et Biophysica Acta 1988;939(2):327-334.

Dejong ES, DeBerardino TM, Brooks DE, Nelson BJ, Campbell AA, Bottoni CR, Pusateri AE, Walton RS, Guymon CH, McManus AT. Antimicrobial efficacy of external fixator pins coated with a lipid stabilized

hydroxyapatite/chlorhexidine complex to prevent pin tract infection in a goat model. Journal of Trauma-Injury Infection and Critical Care 2001;50(6):1008-1013.

del Valle EMM, Galan MA, Carbonell RG. Drug delivery technologies: the way forward in the new decade. Industrial & Engineering Chemistry Research 2009;48(5):2475-2486.

Doll B, Aleef M, Hollinger JO. Overview of fracture repair. In Pietrzak Ws (ed). Musculoskeletal Tissue Regeneration: Biological Materials and Methods. New York: Springer, 2008:39-61.

Dorozhkin SV. Calcium orthophosphate cements for biomedical application. Journal of Materials Science 2008;43(9):3028-3057.

Dusseault J, Tam SK, Menard M, Polizu S, Jourdan G, Yahia L, Halle JP. Evaluation of alginate purification methods: Effect on polyphenol, endotoxin, and protein contamination. Journal of Biomedical Materials Research Part A 2006;76A(2):243-251.

Ekholm EC, Hietaniemi K, Maatta A, Vuorio E, Paavolainen P, Penttinen RPK. Extended expression of cartilage components in experimental pseudoarthrosis. Connective Tissue Research 1995;31(3):211-218.

Elliott JC. General chemistry of the calcium orthophosphate. Structure and Chemistry of the Apatites and Other Calcium Orthophosphates (Studies in Inorganic Chemistry). New York:Elsevier, 1994;1-61.

Endo M, Kuroda S, Kondo H, Maruoka Y, Ohya K, Kasugai S. Bone regeneration by modified gene-activated matrix: Effectiveness in segmental tibial defects in rats. Tissue Engineering 2006;12(3):489-497.

Fritz JS, Gjerde DT. Principles of ion chromatographic seperations. Ion Chromatography. 4th ed. Weinheim: WILEY-VCH verlag GrmbH & Co. KGaA,2009;105-130.

Silver FH, Cowin SS. Microscopic and macroscopic structure of tissues. Mechanosensing and Mechanochemical Transduction in Extracellular Matrix: Biological, Chemical, Engineering, and Physiological Aspects. New York: Springer, 2006;76-119.

Favre D, Provost N, Blouin V, Blacho G, Cherel Y, Salvetti A, Moullier P. Immediate and long-term safety of recombinant adeno-associated virus injection into the nonhuman primate muscle. Molecular Therapy 2001;4(6):559-566.

Ferraro JR, Nakamoto K, Brown CW. Basic theory. Introductory Raman Spectroscopy. 2nd ed. Boston:Academic Press,2003;1-94.

Ferraro JR, Nakamoto K, Brown CW. Instrumentation and experimental techniques. Introductory Raman Spectroscopy. 2nd ed. Boston:Academic Press, 2003;95-146.

Garcia AJ, Reyes CD. Bio-adhesive surfaces to promote osteoblast differentiation and bone formation. Journal of Dental Research 2005;84(5):407-413.

Gerhart TN, Roux RD, Horowitz G, Miller RL, Hanff P, Hayes WC. Antibiotic release from an experimental biodegradable bone cement. Journal of Orthopaedic Research 1998;6(4):585-592.

Glimcher MJ. Mechanism of calcification - role of collagen fibrils and collagen phosphoprotein complexes in vitro and in vivo. Anatomical Record 1989;224(2):139-153.

Goraltchouk A, Freier T, Shoichet MS. Synthesis of degradable poly(l-lactide-co-ethylene glycol) porous tubes by liquid-liquid centrifugal casting for use as nerve guidance channels. Biomaterials 2005;26(36):7555-7563.

Groessnerschreiber B, Krukowski M, Lyons C, Osdoby P. Osteoclast recruitment in response to human bone-matrix is age-related. Mechanisms of Ageing and Development 1992;62(2):143-154.

Grover LM, Gbureck U, Young AM, Wright AJ, Barralet JE. Temperature dependent setting kinetics and mechanical properties of beta-TCP-pyrophosphoric acid bone cement. Journal of Materials Chemistry 2005;15:4955-4962.

Gunatillake PA, Adhikari R. Biodegradable synthetic polymers for tissue engineering. European Cells and Materials 2003;5:1-16.

Han B, Ma PW, Zhang LL, Yin YJ, Yao KD, Zhang FJ, Zhang YD, Li XL, Nie W. Beta-TCP/MCPM-based premixed calcium phosphate cements. Acta Biomaterialia 2009;5(8):3165-3177.

Harris LG, Mead L, Muller-Oberlander E, Richards RG. Bacteria and cell cytocompatibility studies on coated medical grade titanium surfaces. Journal of Biomedical Materials Research Part A 2006;78(1):50-58.

He S, Timmer MD, Yaszemski MJ, Yasko AW, Engel PS, Mikos AG. Synthesis of biodegradable poly(propylene fumarate) networks with poly(propylene fumarate)-diacrylate macromers as crosslinking agents and

characterisation of their degradation products. Polymer 2001;42(3):1251-1260.

Herrero-Vanrell R, Molina-Martinez IT. PLA and PLGA microparticles for intravitreal drug delivery: an overview. Journal of Drug Delivery Science and Technology 2007;17(1):11-17.

Heyde M, Partridge KA, Oreffo ROC, Howdle SM, Shakesheff KM, Garnett MC. Gene therapy used for tissue engineering applications. Journal of Pharmacy and Pharmacology 2007;59(3):329-350.

Ho SM, Young AM. Synthesis, polymerisation and degradation of poly(lactide-co-propylene glycol) dimethacrylate adhesives. European Polymer Journal 2006;42(8):1775-1785.

Hofmann MP, Mohammed AR, Perrie Y, Gbureck U, Barralet JE. High-strength resorbable brushite bone cement with controlled drug-releasing capabilities. Acta Biomaterialia 2009;5(1):43-49.

Hou HL, Zhang XL, Tang TT, Dai KR, Ge RW. Enhancement of bone formation by genetically-engineered bone marrow stromal cells expressing BMP-2, VEGF and angiopoietin-1. Biotechnology Letters 2009;31(8):1183-1189.

Hou QP, De Bank PA, Shakesheff KM. Injectable scaffolds for tissue regeneration. Journal of Materials Chemistry 2004;14:1915-1923.

Huang YC, Simmons C, Kaigler D, Rice KG, Mooney DJ. Bone regeneration in a rat cranial defect with delivery of PEI-condensed plasmid DNA encoding for bone morphogenetic protein-4 (BMP-4). Gene Therapy 2005;12:418-426.

Hubbell JA. Synthetic biodegradable polymers for tissue engineering and drug delivery. Current Opinion in Solid State & Materials Science 1998;3(3):246-251.

Hwang SJ, Davis ME. Cationic polymers for gene delivery: Designs for overcoming barriers to systemic administration. Current Opinion in Molecular Therapeutics 2001;3(2):183-191.

Iczhowski KA, Omara-Opyene AL, Klosel R. Metafectene is superior to lipofectamine in the transfection of G(s)alpha prostate cancer cells. Molecular Biotechnology 2004;28(2):97-103.

Iisaka K. Effect of filler particle-size on dynamic mechanical-properties of poly(methyl methacrylate). Kobunshi Ronbunshu 1976;33(5):427-431.

Itaka K, Ohba S, Miyata K, Kawaguchi H, Nakamura K, Takato T, Chung UI, Kataoka K. Bone regeneration by regulated in vivo gene transfer using biocompatible polyplex nanomicelles. Molecular Therapy 2007;15(9):1655-1662.

Jang JH, Houchin TL, Shea LD. Gene delivery from polymer scaffolds for tissue engineering. Expert Review of Medical Devices 2004;1(1):127-138.

Kang SH, Zirbes EL, Kole R. Delivery of antisense oligonucleotides and plasmid DNA with various carrier agents. Antisense & Nucleic Acid Drug Development 1999;9(6):497-505.

Keller TS, Mao Z, Spengler DM. Young's Modulus, bending strength, and tissue physical-properties of human compact-bone. Journal of Orthopaedic Research 1990;8(4):592-603.

Kim BS, Hrkach JS, Langer R. Biodegradable photo-crosslinked poly(ether-ester) networks for lubricious coatings. Biomaterials 2000;21(3):259-265.

Kim HK, Shim WS, Kim SE, Lee KH, Kang E, Kim JH, Kim K, Kwon IC, Lee DS. Injectable in situ-forming pH/thermo-sensitive hydrogel for bone tissue engineering. Tissue Engineering Part A 2009;15(4):923-933.

Kim HW, Knowles JC, Kim HE. Development of hydroxyapatite bone scaffold for controlled drug release via poly(epsilon-caprolactone) and hydroxyapatite hybrid coatings. Journal of Biomedical Materials Research Part B-Applied Biomaterials 2004;70B(2):240-249.

Kishimoto KN, Watanabe Y. Bone formation by BMP gene transfection. Electroporation and Sonoporation in Developmental Biology 2009;I:263-270.

Kokubo T. Biomaterials research in Japan. Journal of the Royal Society Interface 2009;6(S3):S267-S268.

Korrenhof MJ, Timmer JG. Stability of total parenteral nutrition supplied as 'all-in-one' for children with chemotherapy-linked hyperhydration. Pharmacy World and Science 1992;14(2):50-54.

Larsson S, Bauer TW. Use of injectable calcium phosphate cement for fracture fixation: A review. Clinical Orthopaedics and Related Research 2000; (395) 23-32.

Lee DY, Spangberg LSW, Bok YB, Lee CY, Kum KY. The sustaining effect of three polymers on the release of chlorhexidine from a controlled release drug device for root canal disinfection. Oral Surgery Oral Medicine Oral Pathology Oral Radiology and Endodontics 2005;100(1):105-111.

Lee SY, Regnault WF, Antonucci JM, Skrtic D. Effect of particle size of an amorphous calcium phosphate filler on the mechanical strength and ion release of polymeric composites. Journal of Biomedical Materials Research Part B-Applied Biomaterials 2007;80B(1):11-17.

Lee YJ, Park SJ, Lee WK, Ko JS, Kim HM. MG63 osteoblastic cell adhesion to the hydrophobic surface precoated with recombinant osteopontin fragments. Biomaterials 2003;24(6):1059-1066.

Leung D, Spratt DA, Pratten J, Gulabivala K, Mordan NJ, Young AM. Chlorhexidine-releasing methacrylate dental composite materials. Biomaterials 2005;26(34):7145-7153.

Lewis G. Alternative acrylic bone cement formulations for cemented arthroplasties: Present status, key issues, and future prospects. Journal of Biomedical Materials Research Part B-Applied Biomaterials 2008;84B(2):301-319.

Lin M, Wang HT, Meng S, Zhong W, Li ZL, Cai R, Chen Z, Zhou XY, Du QG. Structure and release behavior of PMMA/silica composite drug delivery system. Journal of Pharmaceutical Sciences 2007;96(6):1518-1526.

Linhart W, Peters F, Lehmann W, Schwarz K, Schilling AF, Amling M, Rueger JM, Epple M. Biologically and chemically optimized composites of carbonated apatite and polyglycolide as bone substitution materials. Journal of Biomedical Materials Research 2001;54(2):162-171.

Liu F, Huang L. Development of non-viral vectors for systemic gene delivery. Journal of Controlled Release 2002;78(1-3):259-266.

Luo D, Saltzman WM. Synthetic DNA delivery systems. Nature Biotechnology 2000;18:33-37.

Lv HT, Zhang SB, Wang B, Cui SH, Yan J. Toxicity of cationic lipids and cationic polymers in gene delivery. Journal of Controlled Release 2006;114(1):100-109.

Mabilleau G, Moreau MF, Filmon R, Basle MF, Chappard D. Biodegradability of poly (2-hydroxyethyl methacrylate) in the presence of the J774.2 macrophage cell line. Biomaterials 2004;25(21):5155-5162.

Maki DG, Stolz SM, Wheeler S, Mermel LA. Prevention of central venous catheter-related bloodstream infection by use of an antiseptic-impregnated catheter - A randomized, controlled trial. Annals of Internal Medicine 1997;127(6):4257-4266.

Malafaya PB, Silva GA, Baran ET, Reis RL. Drug delivery therapies I - General trends and its importance on bone tissue engineering applications. Current Opinion in Solid State & Materials Science 2002;6(4):283-295.

Mandal S, Berendt AR, Peacock SJ. Staphylococcus aureus bone and joint infection. Journal of Infection 2002;44:143-151.

McCalden RW, McGeough JA, CourtBrown CM. Age-related changes in the compressive strength of cancellous bone - The relative importance of changes in density and trabecular architecture. Journal of Bone and Joint Surgery-American Volume 1997;79A:421-427.

McCann S, Byrne JL, Rovira M, Shaw P, Ribaud P, Sica S, Volin L, Olavarria E, Mackinnon S, Trabasso P. Outbreaks of infectious diseases in

stem cell transplant units: a silent cause of death for patients and transplant programmes. Bone Marrow Transplantation 2004;33(5):519-529.

Mehdawi I, Abou Neel EA, Valappil SP, Palmer G, Salih V, Pratten J, Spratt DA, Young AM. Development of remineralizing, antibacterial dental materials. Acta Biomaterilia 2009;5(7):2525-2539.

Menard K. An introduction to dynamic mechanical analysis. Dynamic Mechanical. Analysis: A Practical Introduction. 2nd ed. Boca Raton: CRC. Press, 2007;1-14.

Menard K. Basic reheological concepts. Dynamic Mechanical. Analysis: A Practical Introduction. 2nd ed. Boca Raton: CRC. Press, 2007a;15-36.

Menard K. Dynamic Testing and Instrumentation. Dynamic Mechanical. Analysis: A Practical Introduction. 2nd ed. Boca Raton: CRC. Press,2007b;71-94.

Mourino V, Boccaccini AR. Bone tissue engineering therapeutics: controlled drug delivery in three-dimensional scaffolds. Journal of the Royal Society. Interface 2010;7(43):209-227.

Muggli DS, Burkoth AK, Keyser SA, Lee HR, Anseth KS. Reaction behavior of biodegradable, photo-cross-linkable polyanhydrides. Macromolecules 1998;31(13):4120-4125.

Muller M, Stangl R. Norian SRS augmentation in revision of acetabular cup of total hip arthroplasty. A follow up of six patients. Unfallchirurg 2006;109(4):335-338.

Nair LS, Laurencin CT. Biodegradable polymers as biomaterials. Progress in Polymer Science 2007;32(8-9):762-798.

Nair SP, Williams RJ, Henderson B. Advances in our understanding of the bone and joint pathology caused by Staphylococcus aureus infection. Rheumatology 2000;39(8):821-834.

Nandi SK, Mukherjee P, Roy S, Kundu B, De DK, Basu D. Local antibiotic delivery systems for the treatment of osteomyelitis - A review. Materials Science & Engineering C-Materials for Biological Applications 2009;29(8):2478-2485.

Nascimento AP, Tanomaru JMG, Matoba F, Watanabe E, Tanomaru M, Ito IY. Maximum inhibitory dilution of mouthwashes containing chlorhexidine and polyhexamethylene biguanide against salivary staphylococcus aureus. Journal of Applied Oral Science 2008;16(5):336-339.

Nerurkar MJ, Zentner GM, Rytting JH. Effect of chloride on the release of chlorhexidine salts from methyl-methacrylate - 2-hydroxyethyl methacrylate copolymer reservoir devices. Journal of Controlled Release 1995;33(3):357-363.

Nuss KMR, von Rechenberg B. Biocompatibility issues with modern implants in bone - a review for clinical orthopedics. Open Orthopaedics Journal 2008;2:66-78.

Nussenbaum B, Krebsbach PH. The role of gene therapy for craniofacial and dental tissue engineering. Advanced Drug Delivery Reviews 2006;58(4):577-591.

O'Brien J, Wilson I, Orton T, Pognan F. Investigation of the Alamar Blue (resazurin) fluorescent dye for the accesment of mammalian cell cytotoxicity. FEBS Journal 2000;267(17):5421-5426.

Ohura K, Hamanishi C, Tanaka S, Matsuda N. Healing of segmental bone defects in rats induced by a beta-TCP-MCPM cement combined with rhBMP-2. Journal of Biomedical Materials Research 1999;44(2):168-175.

Oliveira AC, Ferraz MP, Monteiro FJ, Simoes S. Cationic liposome-DNA complexes as gene delivery vectors: Development and behaviour towards bone-like cells. Acta Biomaterialia 2009;5(6):2142-2151.

Olszta MJ, Cheng XG, Jee SS, Kumar R, Kim YY, Kaufman MJ, Douglas EP, Gower LB. Bone structure and formation: A new perspective. Materials Science & Engineering R-Reports 2007;58(3-5):77-116.

Oriowo OM. AlamarBlue bioassay for cellular investigation of UV-induced crystalline lens damage. Ophthalmic and Psychological Optics 2003;23(4):307-314.

Ormerod MG. Fluorescence and fluorochores. In: Ormerod MG (ed.), Flow Cytometry: A Practical Approach. Oxford:Oxford University Press,2000; 23-34.

Otsuka M, Nakahigashi Y, Matsuda Y, Fox JL, Higuchi WI, Sugiyama Y. A novel skeletal drug delivery system using self-setting calcium phosphate cement VIII: The relationship between in vitro and in vivo drug release from indomethacin-containing cement. Journal of Controlled Release 1997;43(2-3):115-122.

Pagoria D, Lee A, Geurtsen W. The effect of camphorquinone (CQ) mand CQ-related photosensitizers on the generation of reactive oxygen species and the production of oxidative DNA damage. Biomaterials 2005;26(19):4091-4099.

Papisov MI. Biodegradable polyacetal polymers and methods for their formation and use. United States Patent 5863990 1999.

Park JH, Ye ML, Park K. Biodegradable polymers for micro encapsulation of drugs. Molecules 2005;10(1):146-161.

Patil SD, Rhodes DG, Burgess DJ. DNA-based therapeutics and DNA delivery systems: A comprehensive review. Aaps Journal 2005;7(1):E61-E77.

Peter SJ, Kim P, Yasko AW, Yaszemski MJ, Mikos AG. Crosslinking characteristics of an injectable poly(propylene fumarate)/beta-tricalcium phosphate paste and mechanical properties of the crosslinked composite for use as a biodegradable bone cement. Journal of Biomedical Materials Research 1999;44(3):314-321.

Peter SJ, Miller ST, Zhu GM, Yasko AW, Mikos AG. In vivo degradation of a poly(propylene fumarate) beta-tricalcium phosphate injectable composite scaffold. Journal of Biomedical Materials Research 1998;41(1):1-7.

Price N, Bendall SP, Frondoza C, Jinnah RH, Hungerford DS. Human osteoblast-like cells (MG63) proliferate on a bioactive glass surface. Journal of Biomedical Materials Research 1997;37(3):394-400.

Quick DJ, Anseth KS. DNA delivery from photocrosslinked PEG hydrogels: encapsulation efficiency, release profiles, and DNA quality. Journal of Controlled Release 2004;96(2):341-351.

Quick DJ, Macdonald KK, Anseth KS. Delivering DNA from photocrosslinked, surface eroding polyanhydrides. Journal of Controlled Release 2004;97(2):333-343.

Raper SE, Chirmule N, Lee FS, Wivel NA, Bagg A, Gao GP, Wilson JM, Batshaw ML. Fatal systemic inflammatory response syndrome in a ornithine transcarbamylase deficient patient following adenoviral gene transfer. Molecular Genetics and Metabolism 2003;80(1-2):148-158.

Ratier A, Gibson IR, Best SM, Freche M, Lacout JL, Rodriguez F. Setting characteristics and mechanical behaviour of a calcium phosphate bone cement containing tetracycline. Biomaterials 2001;22(9):897-901.

Riggs PD, Braden M, Patel M. Chlorhexidine release from room temperature polymerising methacrylate systems. Biomaterials 2000;21(4):345-351.

Ripamonti U. Osteoinduction in porous hydroxyapatite implanted in heterotopic sites of different animal models. Biomaterials 1996;17(1):31-35.

Ritger PL, Nikolaos A, Peppas NA. A simple equation for description of solute release I. Fickian and non-Fickian release from non-swellable devices in the form of slabs, spheres, cylinders or discs. Journal of Controlled Release 1987a;5(1):23-36.

Ritger PL, Nikolaos A, Peppas NA. A simple equation for description of solute release II. Fickian and anomalous release from swellable devices. Journal of Controlled Release 1987b;5(1):37-42.

Rizzi SC, Ehrbar M, Halstenberg S, Raeber GP, Schmoekel HG, Hagenmuller H, Muller R, Weber FE, Hubbell JA. Recombinant protein-co-PEG networks as cell-adhesive and proteolytically degradable hydrogel matrixes. Part II: Biofunctional characteristics. Biomacromolecules 2006;7(11):3019-3029.

Ruhe PQ, Hedberg EL, Padron NT, Spauwen PHM, Jansen JA, Mikos AG. rhBMP-2 release from injectable poly(DL-lactic-co-glycolic acid)/calcium-phosphate cement composites. Journal of Bone and Joint Surgery-American Volume 2003;85A:75-81.

Sabir MI, Xu XX, Li L. A review on biodegradable polymeric materials for bone tissue engineering applications. Journal of Materials Science 2009;44(21):5713-5724.

Salvay DM, Shea LD. Inductive tissue engineering with protein and DNA-releasing scaffolds. Molecular Biosystems 2006;2:36-48.

Sawhney AS, Pathak CP, Hubbell JA. Bioerodible hydrogels based on photopolymerized poly(ethylene glycol)-co-poly(alpha-hydroxy acid) diacrylate macromers. Macromolecules 1993;26(4):581-587.

Schindeler A, McDonald MM, Bokko P, Little DG. Bone remodeling during fracture repair: The cellular picture. Seminars in Cell & Developmental Biology 2008;19(5):459-466.

Shen JY, Pan XY, Lim CH, Chan-Park MB, Zhu X, Beuerman RW. Synthesis, characterization, and in vitro degradation of a biodegradable photo-cross-linked film from liquid poly(epsilon-caprolactone-co-lactide-co-glycolide) diacrylate. Biomacromolecules 2007;8(2):376-385.

Sideridou I, Tserki V, Papanastasiou G. Effect of chemical structure on degree of conversion in light-cured dimethacrylate-based dental resins. Biomaterials 2002;23(8):1819-1829.

Sideridou I, Tserki V, Papanastasiou G. Study of water sorption, solubility and modulus of elasticity of light-cured dimethacrylate-based dental resins. Biomaterials 2003;24(4):655-665.

Soboleski MR, Oaks J, Halford WP. Green fluorescent protein is a quantitative reporter of gene expression in individual eukaryotic cells. Faseb Journal 2005;19(3):440-442.

Takechi M, Miyamoto Y, Ishikawa K, Nagayama M, Kon M, Asaoka K, Suzuki K. Effects of added antibiotics on the basic properties of anti-washout-type fast-setting calcium phosphate cement. Journal of Biomedical Materials Research 1998;39(2):308-316.

Tang Y, Singh J. Controlled delivery of aspirin: Effect of aspirin on polymer degradation and in vitro release from PLGA based phase sensitive systems. International Journal of Pharmaceutics 2008;357(1-2):119-125.

Taton TA. Nanotechnology - Boning up on biology. Nature 2001;412:491-492.

Teixeira S, Ferraz MP, Monteiro FJ. Biocompatibility of highly macroporous ceramic scaffolds: cell adhesion and morphology studies. Journal of Materials Science-Materials in Medicine 2008;19(2):855-859.

Temenoff JS, Mikos AG. Injectable biodegradable materials for orthopedic tissue engineering. Biomaterials 2000;21(23):2405-2412.

Truong-Le VL, Walsh SM, Schweibert E, Mao HQ, Guggino WB, August JT, Leong KW. Gene transfer by DNA-gelatin nanospheres. Archives of Biochemistry and Biophysics 1999;361(1):47-56.

Vaibhav B, Nilesh P, Vikram S, Anshul C. Bone morphogenic protein and its application in trauma cases: A current concept update. Injury-International Journal of the Care of the Injured 2007;38(11):1227-1235.

Valdes TI, Kreutzer D, Moussy F. The chick chorioallantoic membrane as a novel in vivo model for the testing of biomaterials. Journal of Biomedical Materials Research 2002;62(2):273-282.

Vargas A, Zeisser-Labouebe M, Lange N, Gurny R, Delie F. The chick embryo and its chorioallantoic membrane (CAM) for the in vivo evaluation of drug delivery systems. Advanced Drug Delivery Reviews 2007;59(11):1162-1176.

Verettas DAJ, Galanis B, Kazakos K, Hatziyiannakis A, Kotsios E. Fractures of the proximal part of the femur in patients under 50 years of age. Injury-International Journal of the Care of the Injured 2002;33(1):41-45.

Walton M, Cotton NJ. Long-term in vivo degradation of poly-l-lactide (PLLA) in bone. Journal of Biomaterials Applications 2007;21(4):395-411.

Wang HN, Li YB, Zuo Y, Li JH, Ma SS, Cheng L. Biocompatibility and osteogenesis of biomimetic nano-hydroxyapatite/polyamide composite scaffolds for bone tissue engineering. Biomaterials 2007;28(22):3338-3348.

Witt RK, Cizek EP. Effect of filler particle size on resins. Industrial and Engineering Chemistry 1954;46(8):1635-1639.

Woo BH, Fink BF, Page R, Schrier JA, Jo YW, Jiang G, DeLuca M, Vasconez HC, Deluca PP. Enhancement of bone growth by sustained delivery of recombinant human bone morphogenetic protein-2 in a polymeric matrix. Pharmaceutical Research 2003;20(2):334.

Xia WZ, Cook WD. Exotherm control in the thermal polymerization of nona-ethylene glycol dimethacrylate (NEGDM) using a dual radical initiator system. Polymer 2003;44(1):79-88.

Xie D, Park JG, Zhao J, Turner CH. Novel injectable and in situ curable glycolide/lactide based biodegradable polymer resins and composites. Journal of Biomaterials Applications 2007;22(1):33-54.

Xu HHK, Carey LE, Simon CG, Takagi S, Chow LC. Premixed calcium phosphate cements: Synthesis, physical properties, and cell cytotoxicity. Dental Materials 2007;23(4):433-441.

Yadava P, Gibbs M, Castro C, Hughes JA. Effect of lyophilization and freeze-thawing on the stability of siRNA-liposome complexes. Aaps Pharmscitech 2008;9(2):335-341.

Yaszemski MJ, Payne RG, Hayes WC, Langer R, Mikos AG. The in vitro mechanical strength and in vivo bone ingrowth of a degrading polymeric composite biomaterial. Polymers in Medicine and Pharmacy 1995;394:21-24.

Yaszemski MJ, Payne RG, Hayes WC, Langer R, Mikos AG. Evolution of bone transplantation: Molecular, cellular and tissue strategies to engineer human bone. Biomaterials 1996;17(2):175-185.

Young AM, Ho SM, Abou Neel EA, Ahmed I, Barralet JE, Knowles JC, Nazhat SN. Chemical characterization of a degradable polymeric bone adhesive containing hydrolysable fillers and interpretation of anomalous mechanical properties. Acta Biomaterialia 2009;5(6):2072-2083.

Young AM, Ho SM. Drug release from injectable biodegradable polymeric adhesives for bone repair. Journal of Controlled Release 2008;127(2):162-172.

Young AM, Ng PYJ, Gbureck U, Nazhat SN, Barralet JE, Hofmann MP. Characterization of chlorhexidine-releasing, fast-setting, brushite bone cements. Acta Biomaterialia 2008;4(4):1081-1088.

Zhao X, Olsen I, Li HY, Gellynck K, Buxton PG, Knowles JC, Salih V, Young AM. Reactive calcium-phosphate-containing poly(ester-co-ether) methacrylate bone adhesives: Chemical, mechanical and biological considerations. Acta Biomaterilia 2010;6(3):845-855.

Zilberman M, Elsner JJ. Antibiotic-eluting medical devices for various applications. Journal of Controlled Release 2008;130(3):202-215.

List of publications and presentations

Publications

1. *Injectable Biodegradable Poly (ester-co-ether) Methacrylate Monomers for Bone Tissue Engineering and Drug Delivery Applications*, **X Zhao**, SM Ho, AM Young, *Tissue Engineering*, 13 (6), 1372 (2007).

2. *Injectable Degradable Polymeric Adhesives Containing Reactive Calcium Phosphate Filler Particles,* E Abou Neel, **X Zhao**, SM Ho, JC Knowles, V Salih, AM Young, Conference abstract, Pan European Federation of the International Association for Dental Research (Sept. 2008).

3. *Reactive Calcium Phosphate – Containing Poly (ester-co-ether) Methacrylate Bone Adhesives: Chemical, Mechanical and Biological Considerations*, **X Zhao**, I Olsen, HY Li, K Gellynck, PG Buxton, JC Knowles, V Salih, AM Young, *Acta Biomaterialia*, 6 (3), 845-855 (2010).

4. *In vitro Studies on the Influence of Surface Modification of Ni-Ti Alloy on Human Bone Cells*, W Chrzanowski, E Abou Neel, D Armitage, **X Zhao**, JC Knowles, V Salih, *Journal of Biomedical Materials Research: Part A*, 93 (4), 1596-1608 (2010).

5. *Reactive Calcium Phosphate – Containing Poly (ester-co-ether) Methacrylate Bone Adhesives: Setting, Degradation and Drug Release Considerations,* **X Zhao**, I Olsen, J Pratten, JC Knowles, AM Young, submitted to *Journal of Mateirals Science: Materials in Medicine*.

Presentations

1. Oral presentation, 17th Interdisciplinary Research Conference on Biomaterials, Oxford, UK, Apr. 2007.

2. Poster presentation, 8th World Biomaterials Congress, Amsterdam, the Netherlands, May 2008.

3. Oral presentation, 22nd European Biomaterials Conference, Lausanne, Switzerland, Sept. 2009.